

A Thesis Submitted for the Degree of PhD at the University of Warwick

Permanent WRAP URL:

<http://wrap.warwick.ac.uk/176512>

Copyright and reuse:

This thesis is made available online and is protected by original copyright.

Please scroll down to view the document itself.

Please refer to the repository record for this item for information to help you to cite it.

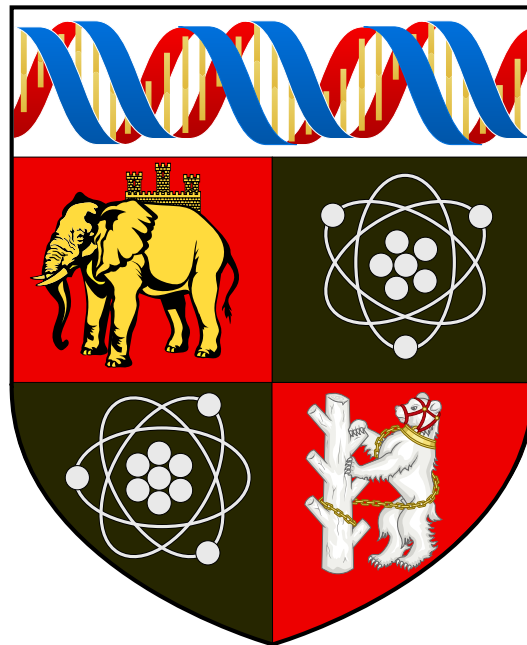
Our policy information is available from the repository home page.

For more information, please contact the WRAP Team at: wrap@warwick.ac.uk

TRANSLATIONAL CONTROL OF LEFT- RIGHT PATTERNING BY A 3'UTR RNA ELEMENT

AGNIESZKA NAGORSKA

A thesis submitted to the University of Warwick for the
degree of Doctor of Philosophy in Medical Sciences.



Warwick Medical School

August 2022

CONTENTS

Contents	i
List of Figures.....	iii
List of Tables	v
Acknowledgements.....	vi
Declaration.....	vii
Abstract.....	viii
List of abbreviations	ix
Chapter 1 Introduction	1
1.1 Overview of zebrafish development.....	2
1.2 Nodal signalling pathway	6
1.3 Characterisation of the proprotein convertases in the Nodal pathway	9
1.4 Left-right asymmetry establishment in vertebrate organisms	11
1.5 <i>Nkx2.5</i> in heart development in zebrafish.....	18
1.6 The Regulation of RNA Activity and Functions	18
1.7 The role of Ybx1 RNA binding protein in translational regulation.....	20
1.8 The RNA motifs and their importance	22
1.9 Justifications for research methods.....	24
Chapter 2 Materials and methods.....	26
2.1 Zebrafish breeding.....	27
2.2 RNA extraction and cDNA synthesis	27
2.3 Primer design and generation of plasmids.....	29
2.4 Quantitative polymerase chain reaction and RT- PCR.....	31
2.5 Immunofluorescence.....	32
2.6 <i>In situ</i> hybridisation (WISH)	35
2.7 Microinjections of zebrafish embryos	37
2.8 <i>In vitro</i> Fluorescent mRNA synthesis.....	38
2.9 RNA immunoprecipitation	40
2.10 Genomic DNA extraction from zebrafish embryos and fin clips	42
2.11 <i>Ybx1</i> ^{<i>sa42</i>} mutant allele.....	42
2.12 Generating CRISPR- Cas9 mutations in zebrafish.....	43
2.13 T7E1 assay to determine efficiency of the gRNAs	45
2.14 Genotyping of the mutant alleles.....	47
2.15 Translation assay	49
2.15.1 Imaging of embryos for translation assay	50
2.15.2 Western Blot analysis of zebrafish embryos	50

2.16 Statistical analysis.....	53
2.17 Imaging of MZ <i>ybx1</i> and control heart embryos at 5 dpf.....	53
2.17.1 Mounting of embryos and sample preparation.....	53
2.17.2 Analysis of blood flow	54
2.18 List of primers:	58
Chapter 3 Validation of <i>FurinA</i> variant <i>XI</i> in zebrafish.....	62
3.1 Introduction.....	63
3.2 Results.....	65
3.3 Discussion.....	81
Chapter 4 Translational control by Ybx1 RNA binding protein.....	86
4.1 Introduction.....	87
4.2 Results.....	89
4.3 Discussion.....	108
Chapter 5 Analysis of the left right asymmetry and cardiac development in <i>ybx1</i> mutant embryos.....	112
5.1 Introduction.....	113
5.2 Results.....	115
5.3 Discussion.....	134
Chapter 6 Conclusions and future directions	139
Chapter 7 References	146

LIST OF FIGURES

- Figure 1.1 Schematic showing germ layer formation in zebrafish embryos.
- Figure 1.2 Overview of zebrafish development.
- Figure 1.3 Nodal signalling pathway in zebrafish.
- Figure 1.4 Human left-right asymmetry disorders.
- Figure 1.5 Left-sided *Nodal* is conserved in vertebrate species.
- Figure 1.6 Mechanism of Nodal inhibition of the left-right asymmetry in zebrafish and mouse.
- Figure 1.7 Proposed mechanism of Ybx1 translational repression in zebrafish.
- Figure 3.1 Schematic of the *furina* transcripts.
- Figure 3.2 Validation of the *furina XI* variant expression in zebrafish embryos.
- Figure 3.3. Analysis of the length of *furina* variant *XI* 3'UTR sequence.
- Figure 3.4. Optimisation of the amplification conditions of the 3'UTR of variant *XI* transcript.
- Figure 3.5 Analysis of the transcript *XI* expression in real-time.
- Figure 3.6. Analysis of the expression of *furina* mRNA in two transcripts.
- Figure 3.7 Generating *furina* protein knockout.
- Figure 3.8 *Furina* Δ 56 bp zygotic mutants show a range of defects at the 5 dpf.
- Figure 3.9 Generating *furina XI* Δ 3'UTR mutation in zebrafish.
- Figure 4.1 Nodal pathway components harbour the YBE motif.
- Figure 4.2 Fluorescent mRNA reporters for *furina* and *lefty1* mRNAs co-localise at the 4-cell stage in zebrafish.
- Figure 4.3 Disruptions of the YBE motif affect localisation at the 4-cell stage embryos.
- Figure 4.4 *Furina* mRNA is enriched in Ybx1 pull down in zebrafish.
- Figure 4.5 *Ybx1^{sa42}* temperature sensitive allele.
- Figure 4.6 Conservation of FurinA protein sequence compared to mammalian FURIN sequences.
- Figure 4.7 FurinA translation and Spaw maturation are elevated in *ybx1* mutant embryos.
- Figure 4.8 Spaw secretion to extracellular space is increased in *ybx1* mutants.

Figure 4.9 Relative fluorescence levels are very similar between wild-type and *ybx1* mutant embryos.

Figure 5.1 Mutant *ybx1* embryos have abnormal left-right expression.

Figure 5.2 *Ybx1* mutant embryos exhibit heart looping defects.

Figure 5.3 *Ybx1* mutant embryos show organ positioning defects.

Figure 5.4 The expression of the heart markers *BMP4* and *notch1b* is normal in *ybx1* mutant embryos.

Figure 5.5 The total area of the heart is bigger in *MZybx1* mutant embryos at the 5 dpf.

Figure 5.6 The atrioventricular canal is enlarged in *MZybx1* mutant embryos.

Figure 5.7 Proportion of the *MZybx1* mutant embryos has retrograde blood flow.

Figure 5.8 Analysis of the direction of the blood flow in *MZybx1* mutant embryos at 5 dpf.

LIST OF TABLES

Table 2-1 cDNA synthesis step 1	28
Table 2-2 cDNA synthesis step 2	28
Table 2-3 Preparation of Gibson assembly reagent	29
Table 2-4 Phusion PCR reaction	30
Table 2-5 PCR conditions for Phusion polymerase	31
Table 2-6 RT-PCR	32
Table 2-7 List of antibodies for immunofluorescence experiment	33
Table 2-8 Preparation of WISH probes.....	35
Table 2-9 rNTP capping mix.....	38
Table 2-10 Fluorescent mRNA transcription reaction	38
Table 2-11 Oligo assembly for the gRNAs.....	43
Table 2-12 Oligo assembly thermocycler conditions.....	44
Table 2-13 gRNA in vitro transcription protocol.....	44
Table 2-14 <i>furina</i> Δ 56 gRNA sequences	46
Table 2-15 <i>furina</i> Δ 3'UTR gRNA sequences	47
Table 2-16 PCR mastermix for genotyping	48
Table 2-17 Thermocycler conditions set up for genotyping	48
Table 2-18 List of primers.....	58

ACKNOWLEDGEMENTS

I would like to thank my supervisor Professor Karuna Sampath for giving me advice and support throughout my PhD. My scientific career began as a research technician in the Sampath laboratory, and I am very grateful to Karuna for her encouragement and for giving me the opportunity to begin my studies and progress further as a scientist. I would also like to thank Warwick Medical School for the sponsorship that allowed me to pursue a PhD program and the Medical and Life Sciences research fund for giving me an award that enabled me to purchase consumables during my studies.

I also thank the Sampath and Balasubramanian laboratories for creating an enjoyable work environment and providing a lot of assistance. I really liked participating in laboratory parties and celebrating birthdays, papers, and successful grant applications.

Most of all I would like to thank Alan Wemyss for his continuous support and love during my studies. Alan gave me a lot of advice that was very useful and appreciated. I would also like to thank my mum, my dad, and my brother for taking interest in my work and asking me a lot of questions about zebrafish research.

DECLARATION

This thesis is submitted to the University of Warwick in support of my application for the degree of Doctor of Philosophy. It has been composed by myself and has not been submitted in any previous application for any degree

ABSTRACT

Heart development is a dynamic process that occurs rapidly in zebrafish embryos. Within 48 hpf heart looping is complete with the formation of two distinct chambers. During the next 5 days of development, endocardial cushions begin differentiating into mature heart valves that help to regulate the blood flow in zebrafish. Previous studies in mice and zebrafish have shown that pro-protein convertase FurinA has a role in cardiac morphogenesis. To date, the zebrafish genome has not been well annotated leaving sequences of many transcripts and their isoforms unknown. Here I describe a novel *furina* transcript *X1*, which interestingly has an unusually long 3'UTR sequence. The alternative 3'UTR *furina* isoform is expressed at embryonic stages prior to organ positioning. Computational analysis of the zebrafish transcriptome shows that a short sequence motif 'AGCAC' and a stem loop which we had previously studied in the 3'UTR of Nodal ligand *sqt* and inhibitors *lefty1* and *lefty2*, is present in a variant 3'UTR transcript of *furina*. Reporter localization assays show that the *furina* 3'UTR element behaves similarly to the other 3'UTR motifs identified in the Nodal pathway. It also forms complexes *in vivo* with the RNA-binding protein and translational repressor, Ybx1. Analysis of the *ybx1* mutant embryos revealed that they manifest left-right asymmetry and cardiac morphogenesis defects. I observed that the atrioventricular canal in these mutants is significantly larger than in the wild type controls. In a proportion of *ybx1* mutant embryos, as a result of an enlargement of their atrioventricular canal, there is retrograde blood flow at the 5 dpf. In this work, I show an essential function for the 3'UTR element/Ybx1 regulon in translational repression of FurinA and reveal a new upstream regulatory mechanism that controls embryonic left-right asymmetry and heart development in zebrafish embryos.

LIST OF ABBREVIATIONS

1K	1000-cell stage
Acvr1	Type 1 Activin receptor
Acvr2	Type 2 Activin receptor
ALPM	anterior lateral plate mesoderm
Arg	arginine
AV canal	atrioventricular canal
BMP	Bone morphogenic pathway
Bp	base pair
Ca	calcium
CDS	coding region sequence of a gene
<i>C. elegans</i>	<i>Caenorhabditis elegans</i>
CRISPR	Clustered regularly Interspaced Short Palindromic Repeats
CSD	cold shock domain
Cyc	Cyclops
DFS	dorsal forerunner cells
DLE	dorsal localisation element
DNA	deoxyribonucleic acid
Dpf	days post fertilization
EGFP	enhanced green fluorescent protein
eIF4G	eukaryotic initiation factor 4 complex

FGF	Fibroblast growth factor
G1	growth
G2	growth and preparation for mitosis
GFP	green fluorescent protein
Gln	glutamine
gRNA	guide RNA
Hp _f	hours post fertilization
KV	Kupffer's vesicle
L _{ft}	Lefty
LPM	lateral plate mesoderm
LRO	left-right organiser
Lys	lysine
M	mitosis
MBT	midblastula transition
miRNA	micro RNA
MiR-430	microRNA 430
<i>Mybx1</i>	maternal <i>ybx1</i> mutant embryos
MZT	maternal to zygotic transition
MZ <i>ybx1</i>	maternal-zygotic <i>ybx1</i> mutant embryos
<i>oep</i>	<i>one-eyed pinhead</i>
PABP	PolyA binding protein
Paip2	PABP-interacting protein 2

PCR	polymerase chain reaction
Pg	picograms
<i>Pybx1</i>	paternal or zygotic <i>ybx1</i> mutants
PIV	particle image velocimetry
RBP	RNA-binding protein
RNA	ribonucleic acid
RNA seq	RNA sequencing
RT	reverse transcriptase
S	DNA synthesis
Ser	serine
sfGFP	superfolder green fluorescent protein
Spaw	Southpaw
SPCs	subtilisin-like proprotein convertase
Sqt	Squint
Som	somite
TGF- β	Transforming growth factor β
UTR	untranslated region
WISH	Whole mount <i>in situ</i> hybridization
WT	wild type
YBE	Ybx1 binding element
Ybx1	Y-box binding protein 1
ZGA	zygotic genome activation

CHAPTER 1

INTRODUCTION

1.1 OVERVIEW OF ZEBRAFISH DEVELOPMENT

During the zebrafish development a single, fertilised egg gives rise to a complex living organism. Starting with a 1-cell stage zygote, the initial cell divisions occur very rapidly, with the cells dividing approximately every 15-30 minutes. These early cell divisions are fast paced because they do not require transcription and are solely reliant on the maternally contributed RNAs and proteins. Furthermore, they skip the growth (G1) and growth and preparation for mitosis (G2) gap phases and only use mitosis (M) and DNA synthesis (S) phases consecutively during the cell divisions (Jukam, Shariati and Skotheim, 2017).

At the 3 hpf, the embryo undergoes mid blastula transition (MBT). This marks a point in development where the cell divisions lengthen and lose synchrony. MBT is triggered as the cell's ratio of nuclear to cytoplasmic volume reaches a critical threshold. The cell cycles become longer, transcription is activated, and cells gain motility. At this stage with the increase in length of the interphase of the cell cycle, the amount of transcription gradually increases per cell. These key processes are important to prepare the embryo for the onset of gastrulation (Kane and Kimmel, 1993; Wagner *et al.*, 2004; Vastenhouw, Cao and Lipshitz, 2019). The maternal to zygotic genome transition (MZT) represents another key event during embryonic development. About one quarter of maternal transcripts are degraded and for the first time, the embryo gains the ability to control gene expression and cell differentiation (Jukam, Shariati and Skotheim, 2017). The microRNA miR-430 has been identified as a key regulator of MZT. It is expressed at the start of the zygotic genome activation (ZGA) and has an important role in facilitating the degradation of a large proportion of maternal mRNAs (Giraldez *et al.*, 2006). Along with the reduction in the number of maternal mRNAs and proteins, global transcription of the zygotic genome is activated. These events completely remodel the embryonic gene expression landscape and allow cells to acquire distinct fates. When transcription is blocked in embryos, even though their cells continue to divide, they fail to undergo gastrulation (Lee, Bonneau and Giraldez, 2014). ZGA has been shown to occur gradually during the

development of the zebrafish, with the first zygotic transcripts being detected as early as the 64-cell stage and by the 512-cell stage approximately 600 transcripts can be detected (Jukam, Shariati and Skotheim, 2017).

MZT is also required to induce other genetic regulatory events in the embryo, such as the establishment of heterochromatin. The clearance of Smarca2 protein by miR-430 is necessary for the formation of heterochromatin. In the genome, heterochromatin is marked by methylation of histone 3 lysine 9 (H3K9me3) and it is found on the repetitive sequences in the genome. This process is important in genome organisation and it promotes genome stability and transcriptional repression (Laue *et al.*, 2019).

Following MZT zebrafish embryos undergo gastrulation, which is characterised by the formation of three germ layers from the pool of blastoderm progenitors: mesoderm, endoderm, and ectoderm. Throughout gastrulation cells migrate and as a result embryos gradually elongate at the anterior-posterior axis, which generates the early body plan. One of the contributing factors is the Cadherins, which modulate cell to cell adhesion. With the formation of three germ layers, the cells acquire different fates that later will contribute to the formation of various organs (Montero *et al.*, 2005; Williams and Solnica-Krezel, 2020). The three layers are apparent at 6 hpf and they all have distinct functions, as shown in Figure 1.1. The mesoderm, which is a middle layer, gives rise to deep tissues such as the circulatory system, cartilage, kidneys, connective tissues, and muscles. The inner layer, or endoderm, is located at the blastoderm-yolk margin and is partially intermingled with the mesoderm. Endodermal progenitor cells will later form visceral organs such as the liver, pancreas, and digestive tract. Finally, the outer layer, the ectoderm, will form the epidermis, central nervous system and neural crest derived tissues (Schier and Talbot, 2005; Brown *et al.*, 2008; Kiecker, Bates and Bell, 2016)

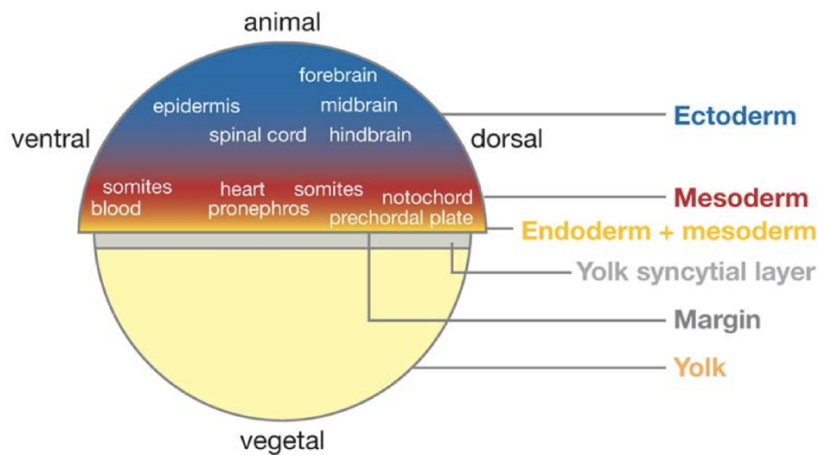


Figure 1.1 Schematic showing germ layer formation in zebrafish embryos.

Ectoderm is shown in blue with corresponding cell fates, mesoderm in red and yellow and endoderm in yellow. Schematic adapted from (Schier and Talbot, 2005)

Following gastrulation, the embryo begins to take the shape of a larva, as shown in Figure 1.2. From 10 to 24 hpf it undergoes a process called segmentation. During segmentation, the formation of somites in a trunk and a tail and a rapid extension of the body length occurs. At the 17-somite (som) stage, the embryo starts weak contractions involving individual myotomes and axons from developing primary motoneurons (Singleman and Holtzman, 2014). As the embryo develops, these contractions become more frequent and stronger. At 24 hpf the embryonic pharyngeal arches become visible, marking the pharyngula period of development. Pharyngeal arches will later become gills. Notochord development is complete, and the embryo starts forming pigment. The circulatory system also develops at this stage and the early embryonic heart starts beating (Kimmel *et al.*, 1995).

At 48 hpf to 72 hpf the embryos hatch, escaping the chorion and becoming free-swimming larvae. Although the timings of hatching will vary, morphogenesis of most organs will be almost finished at this point regardless. The formation of gills, jaw and fins also occurs around this time. The larvae continue to grow into juveniles and

gradually develop the features of adult fish. At around three months the fish reach sexual maturity and can be crossed to obtain eggs (Singleman and Holtzman, 2014).

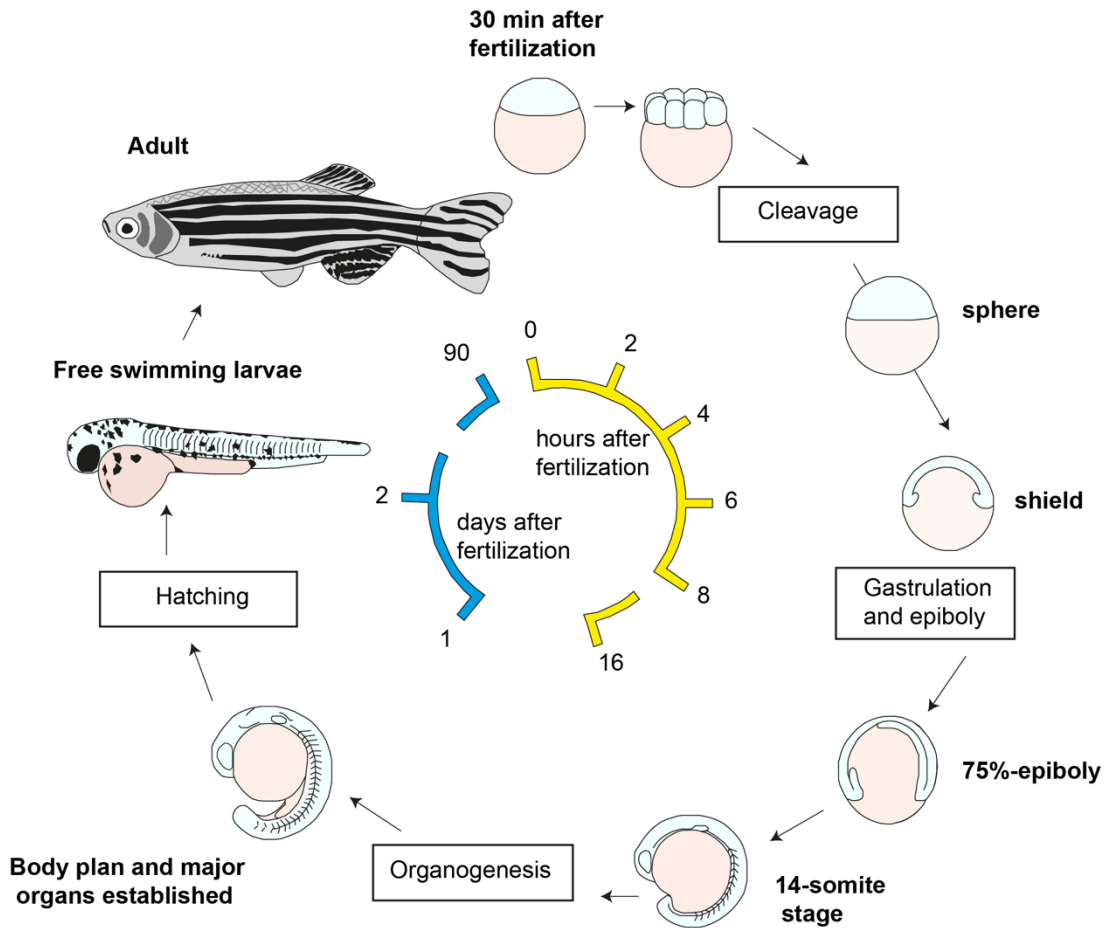


Figure 1.2 Overview of zebrafish development.

Key stages in embryogenesis of zebrafish, from 1-cell stage embryo just after fertilization to a mature adult fish. Important events such as cleavage, gastrulation and epiboly, organogenesis and hatching are highlighted.

1.2 NODAL SIGNALLING PATHWAY

The Nodal factors belong to the secreted transforming growth factor β (TGF- β) superfamily, which has a critical role in many aspects of embryonic development. These roles include embryonic axis organisation, embryonic body patterning via mesoderm, and endoderm specification. Additionally, Nodal also maintains the expression of stem cell pluripotency genes such as *Oct4* and *Nanog*. Consistently with other TGF- β family members, Nodal is expressed as a precursor that must be cleaved at the Arg-X-X-Arg cleavage site by the proprotein convertases, to be then diffused in its mature form to the extracellular space. This is an essential step in activating the signalling pathway (Hill, 2018).

The Nodal signalling pathway has been extensively studied in a range of research models such as chicks, frogs, zebrafish, and mice, and is very well conserved across many vertebrate species. Although the general roles and mechanisms of the pathway are very similar across species, the number of nodal-related homologs varies (Tian and Meng, 2006). In humans, mice, and chicks there is only one Nodal ligand, however, as shown in Figure 1.3, in zebrafish there are three ligands: *squint* (*nodal related-1*), *cyclops* (*nodal related-2*), and *southpaw* (*nodal related-3*). *Squint* (*sqt*) and *cyclops* (*cyc*) exhibit overlapping expression during the blastula stages and are required for mesendoderm induction and embryonic axis formation (Wang *et al.*, 2016). In contrast, *southpaw* (*spaw*) is expressed during late somitogenesis in the lateral plate mesoderm (LPM) and left diencephalon. Additionally, it is a crucial factor in the establishment of left-right asymmetry and correct positioning of the visceral organs (Long, Ahmad and Rebagliati, 2003; Sampath and Robertson, 2016).

Nodal ligands are diffusible and following cleavage at the prodomain by the convertases Furin and Pace4, the mature domains are secreted to the extracellular space, where they co-localise with Vg1 protein. Studies in zebrafish have shown that Nodal ligands form heterodimers with Vg1 and then bind to the receptors. This

interaction is necessary for the Nodal endogenous activity. Additionally, this mechanism has been shown to be conserved in both mice and zebrafish (Tanaka *et al.*, 2007; Montague and Schier, 2017).

The Nodal pathway is activated upon binding of the ligand heterodimers with the Activin receptors, Type 2 receptor (Acvr2a or Acvr2b) phosphorylates Type 1 receptor (Acvr1b), which then phosphorylates cytoplasmic intracellular transducers Smad2 and Smad3, at the C terminus on two serines (Shen, 2007). Phosphorylated Smad2 and Smad3 form a trimer complex with Smad4. This complex enters the nucleus to initiate transcription of Nodal targets. FoxH1, Mixer and p53 transcription factors facilitate the expression of Nodal targets. The Nodal pathway is also regulated through small cysteine-rich membrane EGF-CFC co-receptors, which have a role in promoting binding to the Activin receptor complex (Constam, 2009; Schier, 2009). Without the EGF-CFC co-receptor, Nodal ligands are unable to perform their function. Zebrafish *MZoep* mutant embryos lack the majority of the mesendoderm structures. They display anterior-posterior axis defects and abnormal head and trunk development. They phenotypically resemble *sqt* and *cyclops* double mutants and are unresponsive to overexpression of these ligands (Feldman *et al.*, 1998; Dougan *et al.*, 2003). Mammalian studies suggested that EGF-CFC has a role in Nodal trafficking and recruiting it to endosomes. There is evidence that suggests that the strength of Nodal signalling is dependent on the endocytic uptake. EGF-CFC has a role in modulating this process via promoting internalisation, both at the cell surface and within endosomes (Gritsman *et al.*, 1999; Constam, 2009).

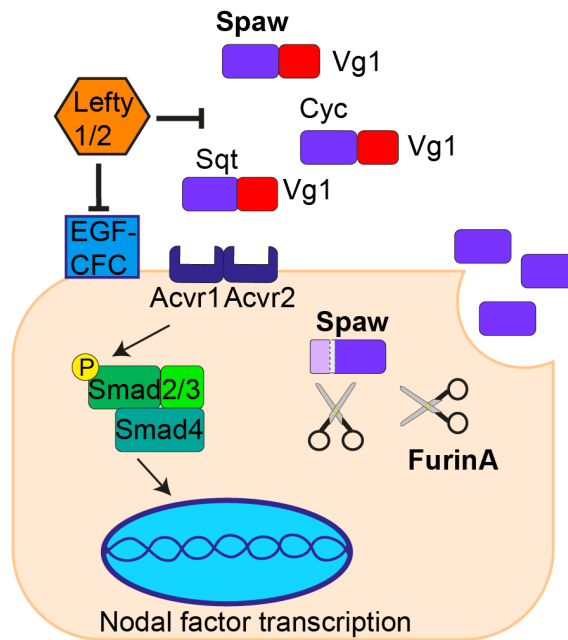


Figure 1.3 Nodal signalling pathway in zebrafish.

Schematic showing ligands: Spaw, Cyc and Sqt in a heterodimer with Vg1. Lefty 1 and Lefty 2 inhibitors, Acvr1 and Acvr2 receptors, EGF-CFC co-receptors, FurinA proprotein convertase. Intracellular transduces Smad2/3 and 4 are shown in heterotrimer.

The Nodal pathway also consists of two homologous inhibitors, *lefty1* and *lefty2*, which help to regulate it. At the early developmental stages in zebrafish, both Nodal inhibitor genes are expressed at the blastoderm margin together with *sqt* and *cyc*. Although Lefty1 and Lefty2 translation is suppressed due to the activity of the microRNA: mir430. This is referred to as a temporal window that enables the timely expression of Nodal Signalling (Meno *et al.*, 1998; van Boxtel *et al.*, 2015; Hill, 2018). However, between the sphere and 50%-epiboly stages, *lefty1* and *lefty2* mRNA levels rapidly increase and overcome the activity of miR-430. At this point, Lefty1/2 translation is initiated. Lefty1/2 has two modes of regulating the Nodal pathway, as it can inhibit Nodal activity either by directly binding to the ligands or interacting with the EGF-CFC coreceptors and blocking ligands from binding (Chen and Shen, 2004; van Boxtel *et al.*, 2015). Furthermore, during somitogenesis Lefty1 is expressed at the

midline of the zebrafish embryo to restrict Spaw protein activity to the left side of the LPM. Loss of *lefty1* expression in the midline, abolish special control of *spaw* and consequently causes bilateral *spaw* expression (Lenhart *et al.*, 2011).

1.3 CHARACTERISATION OF THE PROPROTEIN CONVERTASES IN THE NODAL PATHWAY

Key components of the Nodal pathway are the proprotein convertases, which activate ligands and thus modulate the signalling of Nodal. The two main convertases are FURIN and PACE4, they belong to the subtilisin superfamily (SPCs) and share sequence similarity in the catalytic domain of the protein. Interestingly the sequences of other proprotein convertases can be between 54-70% identical to FURIN (Thomas, 2002). Additionally, their characteristics include a P domain, which is essential for the enzymatic activity of the convertases and a cytoplasmic domain. The function of the cytoplasmic domain is to localize the protein to the trans-Golgi network and the endosomal system, which is where they primarily reside. Additionally, FURIN is also found at the cell surface. This localisation allows them to fulfil their role of endoproteolytic cleavage of inactive precursor proteins via recognition of the Arg-Gln-Arg-Arg residue according to mammalian studies (Izidoro *et al.*, 2009).

Regarding the mode of action of FURIN, there are two conflicting reports. In mice, studies propose that proprotein convertases FURIN and PACE4 are present in the extracellular fluid of the embryonic ectoderm, and FURIN is also present in the visceral endoderm. Both proteases are primarily secreted from these areas into the embryonic region. FURIN and PACE4 are required to induce Nodal signalling and their expression is important for maintaining extraembryonic lineages and embryonic patterning. Additionally, in this study, Beck suggests that the proteolytic processing of NODAL occurs after secretion, in the extracellular fluid. Moreover, in tissue culture, Furin has been shown to activate NODAL in a complex with coreceptor CRIPTO (Beck *et al.*, 2002). CRIPTO can also recruit the proprotein convertases and

controls Nodal signalling trafficking by binding to NODAL and directing it to the cell surface. Therefore the proprotein convertases contribute to the embryonic patterning in a non-cell autonomous manner and cleave a substrate bound to a receptor (Mesnard *et al.*, 2011).

In contrast, studies in zebrafish have shown that FurinA cleaves the Nodal ligand Spaw intracellularly and is required for facilitating its long-range activity in the LPM. FurinA is required cell autonomously for maturation of Spaw. Once Spaw is processed, it is secreted to the extracellular space and forms a diffusion gradient. Then mature Spaw gradually diffuses to the adjacent cells and binds to the receptors. This triggers further production of intracellular Spaw, which creates a feedback loop. The speed and levels of Spaw maturation are dependent on the amount of FurinA available. In support of this hypothesis, maternal-zygotic *furina* mutants do not have any *spaw* expression in the LPM (Tessadori *et al.*, 2015).

In zebrafish there are two *furin* paralogs, *furina* and *furinb*. These have been shown to have a sequence similarity of approximately 69.5%, with the conservation of key SPC domains and partially redundant functions. Both genes in zebrafish are co-orthologs to a single mammalian *Furin* gene and are ubiquitously expressed during embryonic development. Both *furina* and *furinb* play an important role in craniofacial development and the deletion of these genes has caused various jaw defects in zebrafish larvae (Walker *et al.*, 2006; Murata and Kinoshita, 2015). Maternal-zygotic (MZ) *furina* mutant embryos also exhibit left-right asymmetry and heart defects, such as heart jogging, dextral looping and trabeculation defects. Additionally, most MZ mutants are not viable and do not survive past day eight of development due to a lack of inflation of the swim bladder (Tessadori *et al.*, 2015; Zhou *et al.*, 2021). Medaka *furin* mutants have cardiac oedema, enlarged blood vessels, and fluid accumulation in their yolk sac. These embryos are not able to survive after hatching (Murata and Kinoshita, 2015). Similarly, in mice deletion of *Furin* causes embryonic lethality around E10.5 due to severe cardiovascular defects. The hearts of these embryos do not undergo the ventral closure and axial rotation required for heart looping. They also

exhibit impairment of large vessel formation and defects in yolk sac vasculature (Roebroek *et al.*, 1998). Conditional deletion of *Furin* in endothelial cells in mice did not reduce the severity of this phenotype and also resulted in embryonic lethality. This was due to ventricular septal defects and heart valve malformations (WooJin *et al.*, 2012). This leads to the conclusion that even though FURIN protein shares some similarities with other proprotein convertases, it is indispensable in the early development of many vertebrate species. It has a range of functions due to its broad activity and involvement in major pathways.

FURIN has been shown to be a key regulator of Notch and TGF- β signalling pathways, including the Nodal and Bone morphogenic pathway (BMP) (Constam and Robertson, 2000; Zhou *et al.*, 2021). In the *Xenopus* embryos, *furin* effectively cleaves BMP4, similarly to other ligands it recognises the Arg-Ser-Lys-Arg residue and facilitates proteolytic maturation. Consistent with early studies, *furin* transcripts are present in the oocyte and embryos, across various developmental stages. Additionally, Furin expression overlaps with the expression of BMP-4. Furin is a key proprotein convertase required for BMP-4 maturation and contributes to embryonic patterning (Cui *et al.*, 1998). Recent work in zebrafish has also shown that FurinA is expressed in the heart and specifically at the atrioventricular canal on day three of development. This expression is overlapping with Notch1B, which also requires activation by a proprotein convertase. FurinA has been shown to cleave Notch1B and this key interaction is required for correct heart looping and trabeculation in zebrafish larvae (Zhou *et al.*, 2021).

1.4 LEFT-RIGHT ASYMMETRY ESTABLISHMENT IN VERTEBRATE ORGANISMS

In vertebrates, asymmetric organ placement is referred to as *situs solitus*, and alterations to this arrangement may affect organ efficacy and function. Complete inversion of organs does not produce any symptoms, however, bilateral organ

distribution also called heterotaxy may have more serious consequences on organ function. Such disorders include asplenia and polysplenia. These disorders are rare (stats 1:10000) and vary in the extent of severity, and which organs are affected. Heterotaxy may also alter the structure of the heart and lobes of the lungs. In Figure 1.4 all the potential c disorders are listed and they include complete absence or multiple spleens, mispositioned liver and stomach, and heart disorders (Deng, Xia and Deng, 2014; Blum and Ott, 2018).

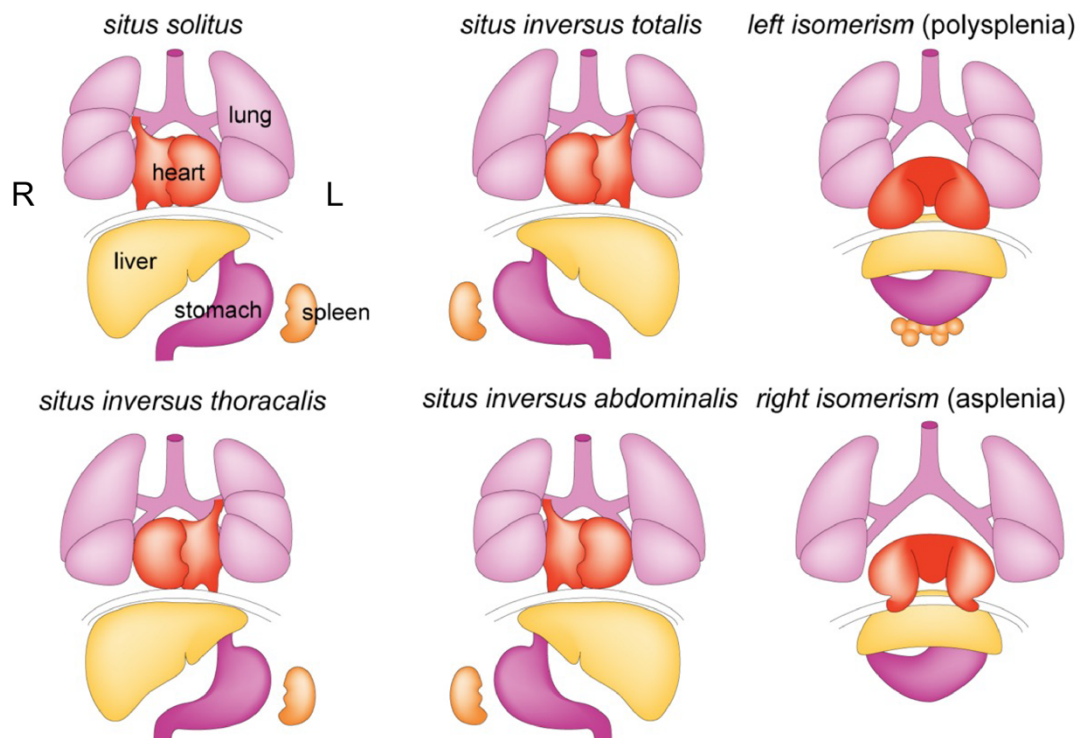


Figure 1.4 Human left-right asymmetry disorders.

On the top left, there is *situs solitus*, which is a normal left-right body asymmetry. After there are five different left-right asymmetry defects that affect the heart, liver, lungs, stomach, and spleen. R indicates the right side and L is the left side of the body. Schematic adapted from (Kloesel, DiNardo and Body, 2016).

In all vertebrate species, the left-right axis is specified during early embryogenesis. The left-right organizer (LRO) is a key structure in this process. LRO is a ciliated epithelium, that may have a dome or spherical shape depending on the species. In

humans, rodents, amphibians, and fish motile cilia are utilized to break the left-right asymmetry(Gros *et al.*, 2009). Figure 1.5 shows the LRO and left sided *nodal* expression mechanisms. Interestingly in birds, there are no motile cilia in the LRO structure. In chick embryos, this structure is called Hensen’s node and during somitogenesis *nodal* ortholog *cnr1* is expressed on the left side of the embryo. This is due to the counterclockwise rotation of the Hensen’s node during gastrulation, causing leftward expression of *cnr1*. Additionally, notochord emerges from the right side and causes further displacement of the *cnr1* to the left side of the embryo (Cui, Little and Rongish, 2009; Gros *et al.*, 2009).

In other species, a similar mechanism is observed, where *nodal* genes are asymmetrically expressed in the left LPM. This is referred to as the Nodal cascade and is broadly conserved between species. Nodal cascade involves the Nodal ligand, inhibitors of Nodal pathway Lefty and Pitx2, which encodes the homeobox transcription factor (Schweickert *et al.*, 2017).

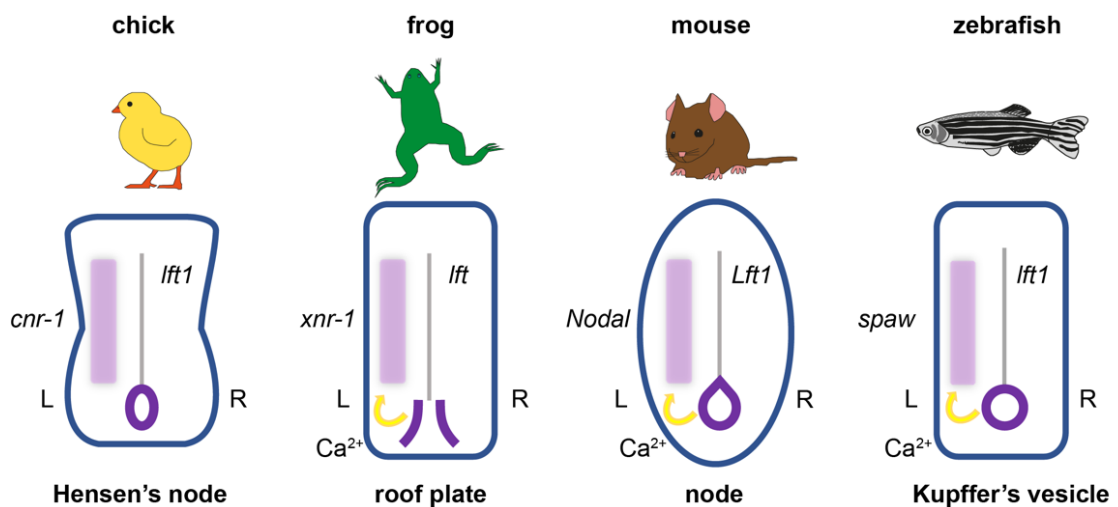


Figure 1.5 Left-sided *Nodal* is conserved in vertebrate species.

Schematic of chick, frog, mouse, and zebrafish embryos with a left-sided expression of *Nodal* gene shown in light purple and *lefty1* in the midline in grey. Dark purple structures are the LROs for corresponding organisms. Yellow arrows show calcium flow.

Motile cilia in the early embryos have an important role in the establishment of left-right asymmetry. There are numerous studies about the events leading up to the breaking of the symmetry events. In mice, these events occur at stage E7.5 and they involve the activity of cilia. There are two types of cilia in the node cavity: motile and immotile. Motile cilia contain a doublet microtubule with dynein arms that allows them to generate clockwise rotational movements that direct the leftward fluid flow. This process facilitates the expression of *Nodal* on the left side (Shiratori and Hamada, 2006). On the edge of the node, there are also immotile cilia, which have an equally vital role in the establishment of the left-right asymmetry. They do not have dynein arms and their role is to sense the flow through the PKD111- PKD2 complex with the Ca^{2+} channel. The PKD111-PKD2 complex is localised in the periphery of the immotile cilia and ventral cell body. PKD2 channel opens in cilia to allow Ca^{2+} ions to enter the cell body and initiate the Ca^{2+} flux in LRO cells. Experiments where calcium flow was inhibited in the LRO revealed the embryos with left-right asymmetry defects. Additionally, to the regulation of left-sided *Nodal* by ciliary movements, there is also regulation by *Cerl2*, which is initially expressed symmetrically at the node, and it has a *Nodal* inhibitory role. Once the leftward flow is initiated the *Cerl2* on the left side is degraded and becomes exclusively expressed on the right side of the LRO thus allowing *Nodal* expression to proceed on the left side of the LPM. (Field *et al.*, 2011; Dasgupta and Amack, 2016; Shinohara and Hamada, 2017).

The role of PKD2 protein is well conserved in vertebrate species. It is localised to LRO in mice, frogs and fish. In Figure 1.5 LRO for each species is shown, in mouse LRO is called a node, in fish Kupffer's vesicle and frogs, there is a gastrocoel roof plate. The formation of KV begins when dorsal forerunner cells (DFS) migrate to the vegetal pole of the embryo during late gastrulation and start forming clusters, this is maintained by the positive feedback loop from the Fibroblast growth factor (FGF) pathways by *Canopy1*. *This gene* promotes the Cadherin1 mediated DFS clustering, so they can eventually differentiate into the ciliated epithelial cells that form the KV. At the 6-som stage, there is a visible KV structure with functional rotating monocilia. (Matsui *et al.*, 2011; Matsui and Bessho, 2012).

Studies in zebrafish uncovered that the flashes of Ca^{2+} , also referred to as the intra-ciliary calcium oscillations, and Pkd2 protein have a key role in the establishment of the left-right asymmetry. They proposed a model where the LRO initiates Pkd2 dependent calcium oscillations on the left side of the epithelium. These oscillations are then transduced and transmitted into the cytosol and result in the formation of the secondary calcium wave, which surrounds the left side of the LRO and gradually induces a Nodal signalling cascade (Yuan *et al.*, 2015). This mechanism is an event that leads up to the breaking of the symmetry in the embryo. As previous studies have shown that once the ciliary movement is triggered and there is an enrichment of the Ca^{2+} on the left side of the embryo, a positive feedback loop is created by phosphorylation of Ca^{2+} /CaM-dependent protein kinase II. As result, there is an influx of Ca^{2+} from those cells to the LPM. This is also directing the expression of Spaw to the left side of the embryo and extends it from anterior to posterior (Francescato *et al.*, 2010).

As previously mentioned, Nodal ligands in zebrafish form heterodimers with Vg1; this mechanism is also conserved in mice. Interestingly *vg1* zebrafish mutants have a reduction of *spaw* expression in LPM and heart looping defects. Studies have shown that Vg1 and Spaw interact and that Spaw is required for Vg1 maturation. After translation Spaw forms a heterodimer with inactivated Vg1 and that in turn causes Vg1 processing. Spaw expression on the left side is also guarded by two forms of inhibition. The first mode is by CERL2 ortholog Dand5, which is expressed around the Kupffer's vesicle. Once the calcium flow is initiated, Dand5 is degraded on the left side of the embryo, allowing Spaw expression as shown in Figure 1.6 (Montague, Gagnon and Schier, 2018). The second mode of inhibition is by Lefty1, which is expressed at the midline in the embryo, preventing the Spaw to cross the barrier from the left LPM. During the left-right asymmetry establishment *lefty1* is expressed in notochord in the embryo and prevents ectopic Nodal expression in the right LPM (Lenhart *et al.*, 2011; Smith *et al.*, 2011). Zebrafish mutants lacking the Dand5 or Lefty1 expression, show bilateral expression of *spaw* during somitogenesis and as a result exhibit left-right asymmetry defects (Montague, Gagnon and Schier, 2018). In Figure 1.6 it is shown that during somitogenesis BMP pathway is required for activation of *lefty1* at the midline in both mouse and zebrafish embryos (Kishigami *et al.*, 2004; Smith *et al.*, 2011). Additionally, studies have demonstrated inhibition of

the BMP pathway diminishes *lefty1* expression at the midline and without the inhibitor, *spaw* is expressed bilaterally in embryos (Furtado *et al.*, 2008). There have been some discrepancies regarding, which BMP pathway genes are directly involved in triggering *lefty1* expression. In mice, due to the requirement of some BMP genes in early embryonic development, it has been challenging to study, which exact genes are required to induce Lefty1 expression at the midline. This is due to the severity and early embryonic lethality of some BMP genes, for example, *Bmpr1a* mutant mice do not form mesoderm structures and die before the establishment of left-right asymmetry is initiated (Smith *et al.*, 2011).

In zebrafish, receptors *bmpr1a* and *bmpr2a* were shown to be directly implicated in activating *lefty1* expression at the midline (Monteiro *et al.*, 2008; Smith *et al.*, 2011). Furthermore, *bmpr2a* and *bmpr2b* heterodimers mediate the expression of *spaw* on the left side of the LPM and activate *lefty2* and *bmp4* in the left heart field. Zebrafish *bmpr2a* and *bmpr2b* mutants show bilateral *spaw* at 18 somites and visceral organ positioning defects (Monteiro *et al.*, 2008). Bmp 4 is also important in this mechanism, as and contributes to *lefty1* midline expression via binding to the *bmpr2a* and *bmpr2b* receptors in both mice and zebrafish. Surprisingly *bmp4* mutants show mild or no left-right asymmetry defects phenotype (Chocron *et al.*, 2007; Lenhart *et al.*, 2011).

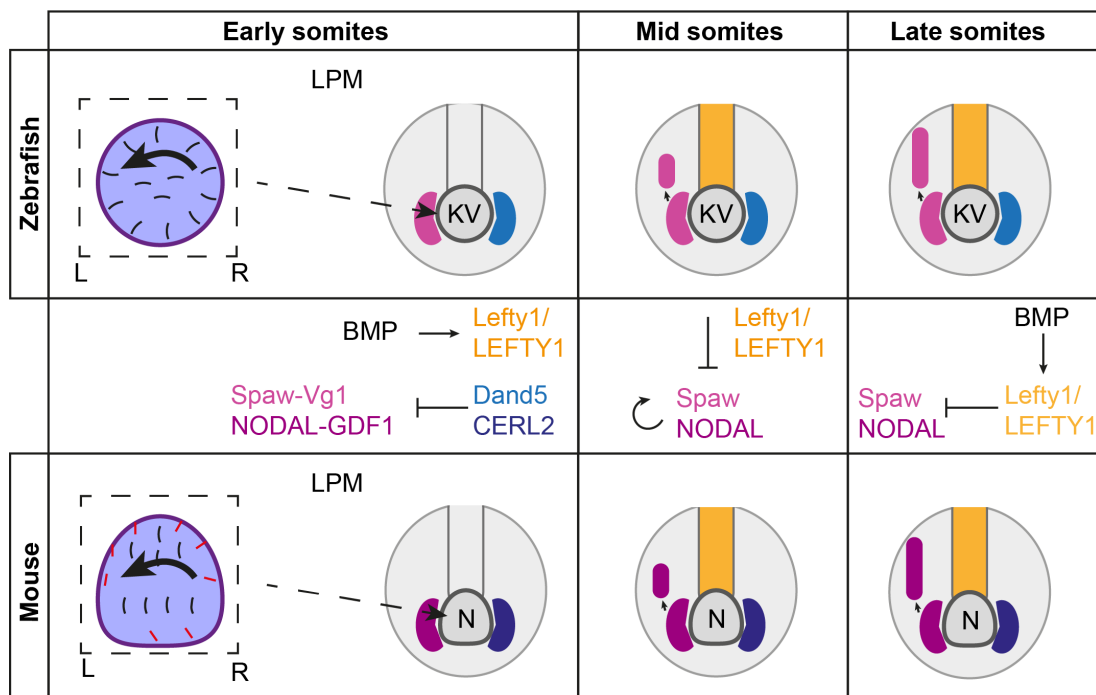


Figure 1.6 Mechanism of Nodal inhibition of the left-right asymmetry in zebrafish and mouse.

Schematic showing distinct modes of inhibition of NODAL/Spaw during early, mid and late somitogenesis. Zebrafish KV or Kupffer's vesicle and mouse node are shown in purple. Motile cilia rotating in a leftward direction (black), in mouse sensory cilia (red). During early somitogenesis CERL2/Dand 5 (blue) facilitates the timely and leftward expression of NODAL/Spaw (pink) and the BMP pathway induces midline Lefty1/LEFTY1 expression. At around the 12- to 14- somite stage Lefty1/LEFTY1 is expressed at the midline and NODAL/Spaw (pink) propagates itself. At the late somitogenesis the NODAL/Spaw (pink) signal extends across the LPM and Lefty1/LEFTY1 (yellow) prevents it from crossing to the right side of the embryo. BMP maintains the Lefty1/LEFTY1 midline expression.

Leftward expression of *spaw* is necessary for the correct expression of its downstream effector *pitx2*. Similarly, to *spaw*, *pitx2* is expressed in the left LPM and although it contributes to the establishment of the laterality, it is dispensable for visceral organ positioning. In zebrafish *pitx2* mutant fish survive to adulthood and show eye and tooth defects (Ji, Buel and Amack, 2016). In other species, however *pitx2* plays an important role in the establishment of the left-right patterning. In chick and frog embryos abnormal expression of *pitx2* results in abnormal looping of the heart and gut laterality defects (Logan *et al.*, 1998; Ryan *et al.*, 1998). Furthermore, in mice *Pitx2* is a vital target of the *ActRIIB* gene, and upon *Pitx2* knock out mice show tooth malformations, a range of cardiac phenotypes such as failure of septation of the heart chambers and hypoplasia of ventricles. These mice also have left-right axis defects such as right pulmonary isomerism, which means instead of four lobes in the right lung, there is a variable number (Lin *et al.*, 1999).

1.5 NKX2.5 IN HEART DEVELOPMENT IN ZEBRAFISH

During vertebrate embryonic development, the heart is the first organ to form. At the 1-to-3-som stage, the transcription factor *nkx2.5* is induced in the zebrafish embryos through the BMP pathway. Interestingly, *nkx2.5* is required for cardiogenic differentiation in a range of species from flies to humans. The importance of *NKX2.5* in cardiac specification is illustrated by the fact that mutations to this gene alone account for 1-4% of congenital heart disorders in humans. These disorders may involve atrial septal defects or positioning of outflow vessels. Similarly, in mice it is required for the development of normal heart chambers, myocardium and the outflow tract (Prall *et al.*, 2007; Bakkers, 2011). Studies in zebrafish have demonstrated that mutant *swirl* and *bmp2b* embryos showed a lack of *nkx2.5* expression (Kishimoto *et al.*, 1997). Interestingly, in mice *Nkx 2.5* directly represses *Furin* expression in the heart. The same study also showed that *Furin* is required for the maturation of cardiac progenitor cells and the formation of the atrioventricular canal, where it is mainly expressed (Dupays *et al.*, 2019).

1.6 THE REGULATION OF RNA ACTIVITY AND FUNCTIONS

The appropriate regulation of the mRNAs is vital in the expression of different proteins. The RNA biogenesis is initiated in the nucleus, where transcription of the DNA by RNA polymerase II takes place. To be translated, the newly synthesized mRNAs must leave the nucleus and enter the cytoplasm. Studies in *Drosophila* identified some of these export factors, examples include p15, NXF1, and UAP56. Translation, however, does not happen immediately instead the mRNA must be transported and localised to the right place for the protein to be synthesized. The 3'UTRs on the RNA strand has a key function in the localisation. In a way 3'UTRs encode a postcode, navigating the RNA to the right location, along with the

cytoskeleton machinery such as actin filaments and microtubules. This process is also facilitated by the dynein and kinesin motor proteins (Shav-Tal and Singer, 2005).

Structural aspects of the RNA also utilize important biological functions. As an example, the mRNA cap, which is located at the 5' end and normally is highly methylated has a key role in RNA biogenesis. The mRNA cap is required to maintain the RNA stability, for example, its presence blocks the 5'-3' exonuclease from carrying out degradation. In the mammalian systems, the 5' cap predominantly comprises 7-methylguanosine linked by a 5' to 5' triphosphate bridge and methylated at the ribose O-2, in short, annotated as m⁷G(5')ppp(5')Xm (Bentley, 2014). Interestingly, this was considered to be a cap structure in all the mRNAs. However, due to advances in biochemical research methods, it is known not to be the case and other variations of the 5' cap exist depending on different factors, such as the cell type. Furthermore, a eukaryotic initiation factor 4F (eIF4F) complex enhances translation, this complex consists of eIF4E, which binds directly to the 5' cap, scaffold protein eIF4G and eIF4A helicase. The eIF4F complex also recruits the translation initiator eIF3, which recruits tRNA and 40s ribosomal subunit and begins protein synthesis (Galloway and Cowling, 2019).

In contrast, the 3' end nearly all eukaryotic mRNAs contain a long stretch of adenine (A) nucleotides called a poly A-tail. Polyadenylation occurs co-transcriptionally and facilitates the transport of the mRNAs to the cytoplasm. Normally around 200bp of stretches of A residues are added to mammalian mRNAs. PolyA tails interact with the 5' cap to promote translation, stabilise the RNAs and protect them from degradation. The removal of the polyA tail will have the opposite effect on the transcript. The evolutionarily conserved poly(A)-binding protein (PABP) binds the 3' end of the mRNA at the poly(A) stretch and interacts with the eIF4F complex to stimulate translation. In contrast, another important protein called PABP-interacting protein 2 (Paip2) causes translational repression by displacing PABP and eIF4G from the poly(A) tail. Therefore, to summarise there are different modes of action of the mRNAs and mechanisms that control their biogenesis (Svitkin *et al.*, 2009; Passmore and Collier, 2022).

1.7 THE ROLE OF YBX1 RNA BINDING PROTEIN IN TRANSLATIONAL REGULATION

RNA binding proteins (RBPs) have important regulatory roles in all organisms, normally ubiquitously expressed they modulate transcript expression via subcellular localisation, translation, and degradation in a timely manner. All of these processes are essential for cellular function (McKee and Silver, 2007). RBPs have also been implicated in various diseases. The Y-Box1 (YBX1) protein expression is upregulated to different extents and has been implicated in the aggressiveness of malignant cancers of the breast, colon, prostate and lung. Additionally, the N terminus domain interacts with the tumour suppressor p53 and mediates its transcription. Interestingly YBX1 can also bind single DNA, damaged DNA and RNA strands with variable specificity, which explains its broad range of targets and functions (Prabhu *et al.*, 2015).

The YBX1 protein sequence is very well conserved between species, mammalian YBX1 cold shock domain (CSD) interestingly shares 40% homology with the *E. coli*. In fish, there is only Ybx1, but in humans, there are YBX1, YBX2 and YBX3 each with different functions. YBX1 is ubiquitous and more broadly expressed in somatic cells. It is involved in the regulation of transcription and translation and in maintaining the stability of various DNAs and mRNAs. YBX2 is found in the germ cells and its key role is to regulate germline mRNAs. Finally, YBX3 is exclusively present during embryonic development and is not found in the adult tissues. It has been shown to have a regulatory role in growth factor promoter GM-CSF (Lyabin, Eliseeva and Ovchinnikov, 2014; Prabhu *et al.*, 2015).

One of the most interesting characteristics of the YBX1 protein is its high affinity for binding nucleic acids. YBX1 was first discovered and named due to its ability to bind the Y-box CTGATTGGCCAA DNA motifs, however, the range of sequences it can bind and interact with is much broader. To regulate transcription, YBX1 has been found to bind the single stranded motifs such as GGGG and single or double stranded

CACC and CATC. Overall, it has a high affinity for GC rich elements. (Suresh, Tsutsumi and Venkatesh, 2018) Studies in zebrafish also identified that YBX1 is a global translational repressor that binds different targets with variable specificity, from the 3'UTR motif DLE in early embryos, to a range of targets to allow zygotic genome activation (Gilligan *et al.*, 2011; Kumari *et al.*, 2013; Sun *et al.*, 2018).

The mechanisms of action of YBX1 also vary. Mammalian studies demonstrated that of the key ones is its ability to compete for binding with the eIF4F complexes and PABP as shown in Figure 1.6 A. *In vitro* studies have suggested that when YBX1 is present in excess it competes and displaces PABP, which is bound to the Poly(A) tail and the eIF4G from the 5' cap. It competes with both of these proteins and prevents them from binding, causing translational repression (Svitkin *et al.*, 2009; Lyabin *et al.*, 2011). In zebrafish, studies have shown that Ybx1 binds 4EBP, suggesting that this may prevent eIF4E association in the complex with eIF4G and therefore also prevent the recruitment of ribosomes. In Figure 1.6 it is shown that as a result of binding with Ybx1, the eIF4F complex is disrupted and the translation of mRNA is repressed (Kumari *et al.*, 2013; Sampath and Robertson, 2016).

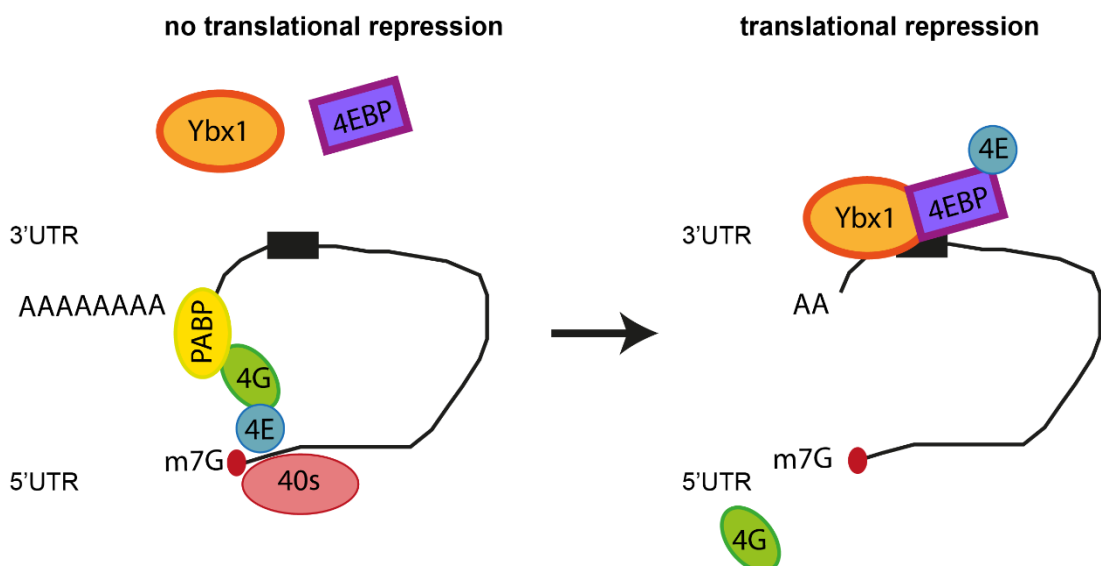


Figure 1.7 Proposed mechanism of Ybx1 translational repression in zebrafish.

When Ybx1 (in orange) is not bound to mRNA or 4EBP there is no translational repression. But when Ybx1 binds to the 3'UTR of the transcript and 4EBP shown in purple it disrupts translation initiation complex assembly and blocks mRNA translation.

Consistent with the ubiquitous expression of YBX1 and its regulation of a number of genetic pathways, the mouse *Ybx1* mutant embryos exhibit neural tube closure and exhibit embryonic lethality. Another allele shows that *Ybx1* mutants have multiple organ malfunctions and growth retardation. They develop up to stage E13.5, but shortly afterwards they die and they do not survive until adulthood (Lu, Books and Ley, 2005). On the other hand, both male and female *Ybx2* mutant mice are viable, but in combination with the *Ybx3* mutation, they are infertile (Li *et al.*, 2021). In fish, *ybx1* mutant embryos do not survive past gastrulation, they show an expanded yolk syncytial layer and cellular malformation (Kumari *et al.*, 2013). Other mutant zebrafish alleles also describe deficient egg activation and abolition of MZT (Sun *et al.*, 2018).

1.8 THE RNA MOTIFS AND THEIR IMPORTANCE

Studies focusing on motifs in mRNAs have been emerging across different research model organisms. These motifs have a key role in the localisation of the mRNA as well as a regulatory function. Some motifs are recognised by the RBPs, and they function as a binding site. For example, CLIP-seq datasets from mammalian HEK293 cells identified various RNA motifs in the 3'UTR. In this study, they identified general RNA motifs that many RBPs preferentially bind to such as UGAU or AAUAAA. They also showed more specific examples, such as that the IGF2BP RBP family recognises CWWCATCA and TGCACTAT motifs to carry out their roles in the translation and transport of mRNAs (Li *et al.*, 2017).

In neurons, there are reports of the mRNAs localising to axons, dendrites, and growth cones. A recent study in mice describes the unique motifs UCUCMCWSUSAKCKC, AWMAAARRWARRAAARCHYKRAAGUG and CWCCAGUC in *Mbpa-201*, *Eif4ebp2*, and *Fmr1* mRNAs that are sufficient to cause localisation in myelin sheaths (Yergert *et al.*, 2021). Moreover, the neuronal Hu RBP family in humans consists of HuR, HuB, HuC and HuD. All these proteins have the Hur recognition motif that preferentially binds to the 3'UTRs of the RNAs with 'AU' and 'U' rich sequences. Those interactions are a part of cellular response to changes in physiological conditions and can enhance both RNA stability and translation (Lopez de Silanes *et al.*, 2004). Therefore, there is huge diversity within the RNA motifs, they can vary in length and sequence homology.

Another example is the AU-rich motifs in the 3'UTR, which belong to the very popular ARE *cis*- regulatory elements group. They form complexes with many RBPs. One of the key interacting RBPs is the AU-rich element binding/degradation factor1 (AUF) that binds to AU rich motifs in the mRNAs and promotes their decay (Choi, Yoon and Chang, 2016). Other studies in *C. elegans* described associations of conserved Lin-41 with an NHL domain that binds to the stem loops on target mRNAs. The shape of the stem loops determines the binding efficiency in the complex as the *in vitro* and *in vivo* studies have shown that the triple loop is complementary to the pocket in the NHL domain and thereby facilitates either degradation or translational repression (Kumari *et al.*, 2018).

Indeed, there are many examples across different species of mRNAs motifs. Most can reside in the coding region or more often in the 3'UTR of the RNA. They have a variable number of nucleotides. Interestingly different mRNA motifs can carry out various functions. There are specific motifs, which attract concrete RBP binders or there are general mRNA motifs that can bind many different RBPs. These motifs are utilised depending on what is required by the cellular environment and can perform functions such as RNA degradation, repression, and transport.

1.9 JUSTIFICATIONS FOR RESEARCH METHODS

Zebrafish is an established research model organism, which gained popularity for studying interactions of different RNAs and proteins as well as their early development. The key advantage of using zebrafish embryos for research is the vast supply of eggs in a short period of time. These eggs are produced externally of a mother, which makes them easily accessible in contrast to mammalian research organisms such as mice. Zebrafish eggs are transparent and develop rapidly forming major internal organs within the 72 hpf. Additionally, the zebrafish genome shares approximately 70% similarity with the human genome and 71.4% of human genes have at least 1 corresponding ortholog in zebrafish. This broad conservation makes the zebrafish research model versatile, as it can be used to study the function of genes, and drug toxicity or entirely as a disease model (Howe *et al.*, 2013).

One of the key components of this work determining the mechanism of translational control of FurinA proprotein convertase. A vast supply of biological material allows us to study in detail the mRNA and RNA binding proteins interactions. Numerous complex biochemical assays can be performed in a relatively short period of time such as RNA immunoprecipitation, protein extraction etc. Many laboratories have taken advantage of this and generated RNA sequencing (RNA-seq) libraries and gene expression atlas resources to shed light on the various gene expression patterns. There are also more straightforward techniques such as microinjections that allow to quickly determine the behaviour of specific mRNAs and proteins *in vivo*.

As previously mentioned, zebrafish embryos are transparent until 48 hpf, afterwards they gradually start forming small speckles of pigment (Kimmel *et al.*, 1995). The formation of pigment during larvae stages can be easily suppressed by adding a chemical to water in a petri dish. This simple manipulation makes zebrafish a fantastic model for staining methods such as in situ hybridization and immunofluorescence as well as live imaging. Complex processes such as heart development and vasculature

formation can be observed and imaged at high resolution. In this work, I take advantage of an attribute in zebrafish and present multiple stainings of heart and live imaging that allow a better understanding of cardiac development.

Zebrafish develop fast and only require three months to reach sexual maturity. This allowed multiple laboratories over the years to generate genetic screens that led to the characterization of many phenotypes. These screens contributed to a better understanding of the function of genes and processes such as embryonic body axis formation, organ development and cellular specification. The new technology of genome editing CRISPR-Cas9 has also been successfully used in zebrafish to uncover novel functions of different genes, promoters and non-coding regions (Uribe-Salazar *et al.*, 2022). In this thesis, I present the CRISPR mutants that I generated in the laboratory, and I also use the existing mutant fine line, which will help in identifying novel regulatory functions of the RBP Ybx1 and *furina* mRNA.

Research aims:

- To analyse the differences between *furina* transcript 1 and the computationally predicted variant *XI*
- To examine the relationship between RBP Ybx1 and *furina*
- To analyse heart morphogenesis in *ybx1* mutant embryos

CHAPTER 2
MATERIALS AND METHODS

2.1 ZEBRAFISH BREEDING

Zebrafish crosses were set up a night before the experiment by the fish facility staff in accordance with home office regulations. Male and female fish were kept apart with a divider in a breeding tank and just prior to egg collection, the water in the tank was changed and the separators were removed. Once the fish finished mating, eggs were collected in a petri dish and kept in 0.3X Danieau's solution (17 mM NaCl, 2 mM KCl, 0.12 mM MgSO₄, 1.8 mM, Ca(NO₃)₂, 1.5 mM HEPES, pH 7.6). They were then either used for experiments or kept at 28 °C until they reached the desired stage of development.

2.2 RNA EXTRACTION AND cDNA SYNTHESIS

Embryos were kept in an incubator at 28 °C and following the first cleavage stage, all of the unfertilised and low-quality eggs were removed. Once the embryos reached a desired developmental cell stage, they were counted and collected into 1.5 mL Eppendorf tubes. All residual Danieau's solution was removed from the tube with a p1000 Gilson pipette. TriZol reagent was then added to homogenise the embryos. The volume of the reagent used was dependent on the number of embryos, i.e. per 10 embryos, 100 µL of TriZol is required. Embryos were homogenised with a thin needle syringe (1 mL) and either immediately used for experiments or stored at -80 °C. To purify the total RNA from the embryonic lysate in TriZol, 200 µL of chloroform (1/5 of the volume of TriZol) was added to the thawed sample, vigorously mixed, and spun down in a cold centrifuge at 4 °C for 15 min at the 12000 ×g. After centrifugation, the sample formed three phases: aqueous, interphase and organic phase. The aqueous phase was carefully removed and transferred into a fresh Eppendorf. An equal volume of 96% ethanol in DEPC water was then added to the sample and gently mixed using a pipette. An RNA miniprep kit from NEB (cat: T2010) was used to purify the RNA starting from step 4, PART 2: RNA binding and elution in the online protocol. Total RNA was eluted in 100 µL and run on a 1.5% agarose gel to determine the integrity

of the sample. Its concentration was then measured using a nanodrop. Samples were aliquoted and stored long term at -80 °C.

For the cDNA synthesis, 500 ng to 1 µg of total RNA was used with a ThermoFisher kit (cat 18091050). In a 200 µL PCR tube total RNA was added to 1 µL of dNTPs mix (10 mM each) and 200 ng of random hexamer primer. The total volume was then adjusted to 13 µL with nuclease free water. Samples were prepared in duplicate per each RNA. This ensured that one was available for a no reverse transcriptase control. Samples were then incubated in a thermocycler, as given in Table 2-1.

TABLE 2-1 CDNA SYNTHESIS STEP 1

Temperature	time
65 °C	5 min
4 °C	hold

Samples were removed from the thermocycler, spun down in microcentrifuge and kept on ice. Next 4 µL of 5× first strand buffer, 1 µL of 0.1 M DTT, 1 µL RNase inhibitor Promega (cat: N2111) 1 µL of superscript III reverse transcriptase were added to each sample. For the no reverse transcriptase control, 1 µL of nuclease free water was added instead of the enzyme. The reactions were mixed gently with a pipette and spun down in a microcentrifuge. They were then returned to the thermocycler and run using the conditions given in Table 2-2. Samples were removed from the thermocycler and stored at -20 °C.

TABLE 2-2 CDNA SYNTHESIS STEP 2

Temperature	time
25 °C	5 min
60 °C	60 min

70 °C	15 min
4 °C	hold

2.3 PRIMER DESIGN AND GENERATION OF PLASMIDS

Furina plasmid was a gift from Jeroen Bakkers laboratory. Plasmids were cloned in a pCS2+ vector and contained the protein coding sequence only. Using the ensembl and UCSC databases, primers were designed to clone the 5'UTR and 3'UTR of the *furina* sequence and were inserted into the vector using the Gibson assembly cloning method. The non-coding sequences of *furina* were amplified from a cDNA library from 1 K-cell stage zebrafish embryos generated with random hexamer primer in the TU background. The 50 μ L PCR reaction contained the following: 5 \times GC buffer, 10 mM dNTPs, 10 μ M each primer (both forward and reverse), cDNA and a high-fidelity polymerase from NEB (cat: M0530S) of Phusion. The thermocycler was set up according to the manufacturer's recommendation except for the extension step, which was longer than advised (1 kb per 1 min). Both the insert and the vector were amplified, run on an agarose gel, and the correct DNA bands were isolated using the Qiagen gel extraction kit (cat: 28706). Samples were then digested overnight at 37 °C with Dpn1 enzyme from NEB (cat: R0176S), purified and used for Gibson assembly reaction. The ingredients of the 2 \times Gibson assembly master mix are given in Table 2-3.

TABLE 2-3 PREPARATION OF GIBSON ASSEMBLY REAGENT

Reagent	volume
5 \times isothermal buffer	100 μ L
Taq ligase (40 U/ μ L)	50 μ L
T5 exonuclease (1 U/ μ L)	2 μ L

Phusion polymerase (2 U/ μ L)	6.25 μ L
ddH ₂ O	91.75 μ L

Prior to the reaction, a vector was diluted to 10% with water. Then 0.5 μ L of the diluted vector was added to 2 μ L of insert and 2.5 μ L of the Gibson assembly master mix. The mixture was then incubated at 50 °C for 1 h in the thermocycler. Following incubation, the entire reaction was transformed in XL-1 blue competent cells and spread on an LBA amp plate and incubated overnight at 37 °C. The next day single colonies were extracted to 2 mL LB amp cultures, again incubated overnight at 37 °C, and then plasmids were purified using a Qiagen miniprep kit (cat: 27115). Purified plasmids were sent for sequencing and only samples with the correct sequence were kept for the experiments.

The GFP sequence was inserted in full length *spaw* and *furina* vector after the cleavage site according to literature methods (Tessadori et al; 2015). Primers with 25 bp overhangs were designed to amplify the GFP sequence and allow ligation into the *furina* and *spaw* vector. The GFP sequence was amplified from existing plasmid stocks. PCR and Gibson assembly reactions were performed as described above.

TABLE 2-4 PHUSION PCR REACTION

Reagent	Volume μ L
5 \times GC buffer	10
10 mM dNTPs	1
10 μ M primer Fwd	2.5
10 μ M primer Rev	2.5
cDNA	1
Phusion polymerase	0.5

water	32.5
-------	------

TABLE 2-5 PCR CONDITIONS FOR PHUSION POLYMERASE

Step	Temperature	Time
First denaturation	98 °C	1 min
35 cycles	98 °C	20 s
	60 °C	30 s
	72 °C	1 min per 1 kb
Final extension	72 °C	3 min
Hold	12 °C	∞

Furina mutation constructs were generated using the site directed mutagenesis method. Primers (40 bp) overlapping the site of the mutation were designed and amplified using the high-fidelity polymerase Phusion and they targeted the 3'UTR YBE element. Similarly, to what was found in the literature, mutations either caused complete deletion of the YBE motif or caused disruption to the stem and changes in sequence (Gilligan, Kumari *et al.* 2011).

2.4 QUANTITATIVE POLYMERASE CHAIN REACTION AND RT- PCR

Zebrafish embryos from stages 1 K, 50% epiboly 10 som, 18 som and ovaries were collected, and 50 embryos were used per stage, RNA was initially homogenised in TriZol reagent and then extracted using Monarch NEB RNA miniprep kit. RNAs were eluted in DEPC water and then were run on 1.5% agarose gel. The concentration of the samples was measured on a nanodrop. The RNAs were then reverse transcribed with superscript III using the protocol described in section 1.2. Each cDNA was

amplified using GAPDH, *furina* and *furina XI* primers in a standard 20 μ L PCR reaction that is given in Table 2-6.

TABLE 2-6 RT-PCR

Reagent	Volume
water	12.9 μ L
5 \times go taq buffer	4 μ L
dNTPs (10 mM)	0.4 μ L
primer fwd (10 μ M)	0.6 μ L
primer rev (10 μ M)	0.6 μ L
cDNA template	1 μ L
Taq polymerase	0.5 μ L

The quantitative PCR was performed with commercially available NEB 2 \times LUNA qPCR master mix (cat no. M3003L). The manufacturer's recommendation was followed for the reaction conditions and the primer compatibility was tested by generating a standard curve and primer efficiency calculation.

2.5 IMMUNOFLUORESCENCE

To study the atrioventricular canal length in zebrafish, prior to fixing embryos were treated with stock 25 \times tricaine solution until the heartbeat stopped. This ensured that both chambers were in a diastole (relaxed) phase and the heartbeat was in the sample phase among mutant and wild type control samples. For analysis of the heart looping, zebrafish larvae were fixed at 55 hpf in 4% paraformaldehyde solution in DEPC treated PBS. Samples were incubated in the 4 $^{\circ}$ C cold room overnight and the next day they were washed 3 times for 5 mins with PBS with 0.1% Tween (PBS-T).

Samples were gradually dehydrated in methanol. The first wash was 25% methanol in PBS-T for 5 minutes and subsequent washes were: 50% methanol in PBS-T, 75% methanol in PBS-T and finally 100% methanol. Following dehydration, samples were stored at -20 °C. On the day of the experiment, they were gradually rehydrated with increasing amounts of PBS-T in solutions: 25% PBS-T in methanol, 50% PBS-T in methanol, 75% PBS-T in methanol and finally washed twice in 100% PBS-T solution. Embryos were washed with each solution for at least 5 minutes on a gently rotating nutator. Next PBS-T was replaced with water and samples were kept on ice for 5 minutes. To allow permeabilization of fixed larvae, they were next soaked in acetone and kept at -20 °C for 20 minutes. Then the acetone was completely removed, and samples were washed with water twice for 5 minutes. The samples were then blocked in 10% BSA solution in PBS-T for 1 h on a rotating nutator. Following heart antibodies were obtained from Developmental Studies Hybridoma Bank and solutions were prepared as given in Table 2-7.

TABLE 2-7 LIST OF ANTIBODIES FOR IMMUNOFLUORESCENCE EXPERIMENT

Name	Antigen	Host species
ZN-8	CD166 antigen homolog A (neurolin)	mouse
MF-20	Myosin heavy chain, sarcomere (MHC)	mouse
S-46	Myosin heavy chain, slow developmental (sd-MyHC), stains the atrium of the heart	mouse

An antibody solution containing ZN-8 antibody at a concentration of 3 µg/ml, in 1% BSA in PBS-T was prepared to stain the atrioventricular canal of zebrafish larvae. The antibody solution was added to the samples for overnight incubation at 4 °C for 16 hours. The samples were then washed in PBS-T at least 6 times for 10 minutes and then a secondary antibody solution containing anti-mouse Alexa 488 conjugated antibody 1:2500 in 1% BSA in PBS-T. Samples were covered with aluminium foil to prevent bleaching of the fluorescence and incubated at 4 °C overnight. The next day, samples were washed extensively with PBS-T, frequently changing the solution and

preventing exposure to light. They were left washing for 2 days in a 4 °C cold room on a nutator.

For double immunostaining of the heart chambers with antibodies MF20 and S46, the incubations were performed sequentially. Firstly, larvae were incubated with an antibody solution containing 4 µg/ml S-46 antibody in 1% BSA/PBS-T at 4 °C overnight to stain the atrium. The next day embryos were washed with PBS-T and then they were incubated overnight with the Alexa 488 anti-mouse secondary conjugated antibody 1:2500 in 1% BSA/PBS-T solution. The samples were then extensively washed with PBS-T and then incubation with MF-20 for staining of the ventricle was performed using 2.5 µg/ml of antibody in a 1% BSA/PBS-T solution. Similarly, to the previous antibody, incubation was done overnight at 4 °C and embryos were then washed with PBS-T and stored overnight in a secondary antibody solution of 1:2500 anti-mouse Alexa 546 conjugated antibody in 1% BSA/PBS-T. 15 hours later samples were washed with PBS-T, frequently changing buffer and shielding samples from light.

To prepare samples for imaging they were washed in solutions containing increasing amounts of glycerol for 10 minutes per wash at room temperature. The composition of the glycerol solution used was: 25% glycerol in PBS-T, 50% glycerol in PBS-T, 75% glycerol in PBS-T and finally 100% glycerol. To prevent bleaching of fluorescence antifade solution was added to each sample and then they were stored at 4 °C. To image the samples, they were first carefully mounted in 100% glycerol on a slide ensuring the best angle to visualise the heart. Z-stacks containing the entire larvae heart were generated with 1 µm step size on a confocal Andor Revolution XD microscope with an Andor iXon 888 camera.

2.6 *IN SITU* HYBRIDISATION (WISH)

Similar to the immunofluorescence protocol, embryos were collected at the required stages and then fixed in 4% PFA overnight at 4 °C. The next day PFA was washed out 4 times with PBS-T in DEPC water for 5 minutes per wash. Embryos were then manually dechlorinated using tweezers and then gradually dehydrated in 25%, 50% and 75% methanol in DEPC PBS-T solutions and finally washed twice with 100% methanol and stored at -20 °C.

Prior to antisense probe synthesis, all template vectors were linearised according to the enzyme specifications and column purified. An *in vitro* transcription reaction was then prepared for the DIG labelled probes (Roche cat no: 11277065910) using the reaction mixture given in Table 2-8.

TABLE 2-8 PREPARATION OF WISH PROBES

Reagent	volume
DEPC water	up to 50 µL
5× transcription buffer	10 µL
100 mM DTT	5 µL
RNase inhibitor	1 µL
10× DIG labelling mix	5 µL
Linearised template	1 µg
SP6/T7/T3 polymerase	2 µL

The reaction was first incubated at 37 °C for 2 h, after which 1 µL of the Turbo DNase was added to the sample to degrade any remaining DNA template. After the transcription reaction, samples were taken out of the incubator and 15 µL of 7.5 M

ammonium acetate and 75 μ L of DEPC water were added. To begin the RNA purification next equal volumes of the phenol-chloroform (sigma cat no: 77617) were added to the sample in the fume hood and the sample was mixed vigorously. The samples were then placed in a tabletop centrifuge and spun down for 5 minutes at 12000 \times g. The bottom organic phase was then removed from the sample and discarded into the appropriate hazardous waste bottle and 150 μ L of chloroform was added to the sample. The sample was again shaken vigorously and spun down in the centrifuge. The bottom phase was once again removed and discarded and 150 μ L of cold isopropanol was added to allow precipitation of the probe overnight at -20 $^{\circ}$ C. The next day, the sample was spun down at 12000 \times g for 30 min at 4 $^{\circ}$ C in a centrifuge and the supernatant was discarded. The RNA pellet was washed twice with ethanol and eluted in nuclease free water. Probes were run on an agarose gel to check the integrity of the sample and then diluted in the hybridisation buffer with pH 6-6.5 containing 60% Formamide, 5 \times SSC, 1 mg/ml torula RNA, 100 μ g/ml heparin, 1 \times Denhardt's solution, 0.1% CHAPS, 10 mM EDTA, 0.1% Tween-20. Samples were diluted at the 10 \times (10 ng per 1 μ L) and 1 \times (1 ng per 1 μ L) concentrations and stored at -20 $^{\circ}$ C.

To begin the WISH experiment embryos were rehydrated in 75%, 50%, and 25% methanol /PBS-T solution and then washed extensively in PBS-T. Next, they were digested in 10 μ g/ml proteinase K in PBS-T for 3 minutes if they were 55 hpf. For embryos that were 24 hpf, proteinase K digestion was reduced to 1 minute. If embryos were younger than 24 hpf, the digestion step was skipped. The next samples were washed 5 more times in PBS-T. The hybridisation buffer was pre-warmed to 65 $^{\circ}$ C, the wash buffer was completely removed from the samples and 200 μ L of hybridisation buffer was added. Samples were then incubated for 4 h in a 65 $^{\circ}$ C water bath. Previously diluted probes (1 \times) were then warmed up at 65 $^{\circ}$ C, spun down, added to the samples, and incubated overnight. The next day the following buffers were pre warmed to 65 $^{\circ}$ C and once probes were removed from the samples washing steps were performed at 65 $^{\circ}$ C water bath: 2 \times 30 min 50% formamide, 1 \times SSC, 0.1% Tween, 1 \times 15 min 2 \times SSC 0.1% Tween, 2 \times 30 min 0.2 SSC, 0.1% Tween. Samples were then washed twice for 5 minutes at room temperature with 1x MAB containing 0.1 M

maleic acid and 0.15 M sodium chloride and 0.1% Tween. Samples were blocked for 1 h to prevent non-specific results with 1× MAB, 2% blocking reagent (Roche cat no 11112589001) 10% FEBS and 0.1 % Tween and then the blocking solution was removed, and samples were incubated overnight at 4 °C with 1 in 4000 of DIG FAB fragments antibody (Roche cat no. 11093274910) in the blocking solution.

The following day samples were washed 6-8 times for 10 minutes in 1× MAB and then washed once for 10 minutes in NTMT buffer containing 1 M Tris-HCL pH 9.5: 4 mL, 1 M MgCl₂: 2mL, 5M NaCl: 0.8 mL, Tween 20: 40 µL. In the meantime, BM purple (Roche cat no 11442074001) was pre-warmed to room temperature. Eppendorf tubes containing samples were next wrapped in aluminium foil to shield them from light and developed in 500 µL of BM purple at room temperature. Samples were checked carefully every 30 minutes to 1 hour to determine when sufficient staining has developed. After the staining of embryos was complete kept in the *in situ* stop solution and then put in gradually in increasing amounts of glycerol 25%, 50% 75% and 100% in PBS-T. Samples were stored at 4 °C and then using a sandwich slide imaged on the stereo microscope with a Nikon DS-Fi2 colour camera.

2.7 MICROINJECTIONS OF ZEBRAFISH EMBRYOS

Embryos were collected from the breeding tanks that were set up a night before 20 minutes after fertilisation and mounted on the 1.5% agarose mould in a neat column. 0.58 mm glass filament needle was trimmed at the sharp edge on a slight angle with tweezers. It was filled with the sample and the injection time was adjusted to the diameter of the drop. Drop diameter was measured on a glass slide and it was immobilised in mineral oil. A drop of 0.12 mm in diameter indicated a 1 nl droplet. The RNA sample was then injected into the middle of the embryo, ensuring from time to time that the needle has not been clogged. After injection embryos were collected on a petri dish in 0.3× Danieau's media and places in 28.5°C incubator.

2.8 *IN VITRO* FLUORESCENT mRNA SYNTHESIS

Plasmids of interest were linearized using Not1 enzyme and column purified with a Qiagen PCR purification kit (Cat 28104) prior to the transcription reaction. The rNTP capping mix was prepared in advance and aliquoted in a -80 °C freezer:

TABLE 2-9 RNTP CAPPING MIX

Reagent	volume	concentration
ATP (100 mM)	2 μ L	10 mM
CTP (100 mM)	2 μ L	10 mM
UTP (100 mM)	1.8 μ L	9 mM
GTP (100 mM)	0.5 μ L	2.5 mM
⁷ mG(5')pppG cap (40 mM) (Ambion cat no: AM8048)	3.75 μ L	7.5 mM
DEPC water	10 μ L	-

Next the transcription reaction was prepared shielding the reaction from light:

TABLE 2-10 FLUORESCENT mRNA TRANSCRIPTION REACTION

Reagent	volume
DEPC water	Up to 50 μ L
5 \times transcription buffer	10 μ L
100 mM DTT	5 μ L

rNTP capping mix	5 μ L
Alexa fluorophore 488-5- UTP (1 mM) (Fisher scientific cat no: 10103672)	5 μ L
Linearised DNA template	500 ng
RNasin inhibitor	1 μ L
RNA polymerase (SP6/ T7/ T3) (Promega cat no: P1085)	2 μ L

The sample containing the reaction master mix was wrapped in aluminium foil to protect it from exposure to light and incubated at 37 °C incubator for 2.5 hours. Following transcription samples were treated for 30 minutes with 2.5 μ L of Turbo DNase I enzyme and then unincorporated nucleotides were removed using Bio-Rad P30 minispin column (cat no: 732-6250) according to the manufacturer's instructions. Next phenol-chloroform purification was performed using the same protocol described under the WISH heading. The fluorescent RNAs were precipitated overnight in isopropanol and eluted the next day in DEPC treated water. To determine the efficiency of the fluorophore incorporation samples were run on two types of agarose gel, one standard agarose containing gel stain and one without. If the RNA band was visible on agarose gel with no gel stain it indicated successful incorporation of the fluorophore and the sample was further measured in the nanodrop on the UV setting absorbance 260 nm and 482 nm. Incorporation of the fluorophore was then calculated as described in the manual for item 10103672 from Molecular Probes:

$$A_{base} = A_{260} - (A_{dye} \times CF_{260}) \quad \text{Eq. 1}$$

CF is a correction factor that was provided in a manual for each fluorophore.

To calculate base: dye ratio:

$$\text{Base: dye} = (A_{\text{base}} \times \epsilon_{\text{dye}}) / (A_{\text{dye}} \times \epsilon_{\text{base}}) \quad \text{Eq. 2}$$

ϵ_{dye} is the extinction coefficient provided by the company for each fluorescent dye and ϵ_{base} is the average extinction coefficient for nucleotides.

Embryos were injected at 1 cell stage with approximately 10-40 pg of the fluorescent RNA depending on the base to dye ratio of the RNA. Embryos were next put in the 28°C incubator, dechorionated using protease at previously optimised conditions, washed with fish facility system water, and mounted in an agarose mould for imaging. Embryos were oriented at animal view and the imaged at 4-cell stage using Nikon ECLIPSE Ni, Nikon, ECLIPSE Ni microscope with a HAMAMATSU digital camera C11440, ORCA-Flash4.OLT.

Z-stacks of 10 um each were captured of an entire embryo and maximum intensity projections were analysed in ImageJ software.

2.9 RNA IMMUNOPRECIPITATION

The immunoprecipitation protocol was based on the previously published protocol in Kumari *et al* 2013 and Zaucker *et al* 2018 with Ybx1 antibody (Sigma 4F12). Zebrafish embryos were collected at required stages: 50% epiboly, 10 som and 18 som and counted to ensure there were at least 300 embryos per stage. Embryos were fixed in 1% formaldehyde solution for 20 minutes and then quickly washed with DEPC PBS. Next embryos were lysed in RIPA buffer (50 mM Tris-Cl pH 7.5, 1% NP-40, 1% sodium deoxycholate, 0.1% SDS, 1 mM EDTA, 1 M NaCl, 1 M urea, protease inhibitor). with protease inhibitor added fresh and then homogenised with a thin needle syringe. Following homogenisation samples were spun down at the tabletop centrifuge set to 4 °C at maximum speed for 5 minutes. The supernatant was removed

to a fresh Eppendorf 1.5 mL tube and samples were flash frozen in liquid nitrogen and kept in a -80 °C freezer until the day of the experiment. Protein G magnetic beads from Biorad (cat no: 161-4021) were washed once with 300 µL of RIPA buffer, put on a magnetic stand and then the supernatant was discarded. Magnetic beads were conjugated with the Ybx1 antibody (Sigma 4F12) and simultaneously separate samples conjugating beads with the mouse IgG control (cat no. sc2025) were also prepared and incubated for 2 h at 4 °C on the rotating nutator. 50 µL of the beads were added to 300 µL of RIPA buffer and 10 µL (1 µg) of the Ybx1 antibody. The embryonic lysate was precleared with 50 µL of washed magnetic beads and 100 µg per 1 mL of Torula RNA to reduce non-specific binding and incubated at 4 °C for 2 h. Next conjugated beads-antibody samples were magnetised and washed once with RIPA buffer and then incubated with 20 units of RNAsin inhibitor on ice. Samples were then magnetised again, and the supernatant was discarded and replaced with the precleared lysate. The lysate from each stage of embryonic development was split equally into conjugated beads with either Ybx1 antibody or mouse IgG. 10% of the cleared lysate for each stage was saved and flash frozen in liquid nitrogen to later serve as input. Lysate/antibody solutions were incubated at 4 °C overnight on a rotating nutator and the next day samples were magnetised on a stand, the supernatant was discarded, and they were washed at least 8 times for 20 minutes with 300 µL of RIPA buffer. All washes were performed in a 4 °C cold room to prevent the degradation of protein and RNAs. RIPA buffer was then discarded, and samples were eluted in 100 µL of buffer containing 50 mM Tris-Cl (pH 7), 5 mM of the EDTA, 10 mM of DTT and 1% SDS. Beads were mixed vigorously in elution buffer and then samples were reverse cross-linked in 72 °C heatblock for 30 minutes. Finally, samples were magnetised and split 50 µL each for protein extraction with 4× lammeli buffer and 50 µL for the RNA extraction with TriZol reagent and then subsequent cDNA synthesis according to the protocol described under the second heading. 10% of input that was earlier frozen has also been split equally for protein extraction and RNA extraction together with the immunoprecipitation samples. Protein samples were added to 12.5 µL of 4× lemmler buffer and boiled for 5 minutes at 95 °C. Samples were then stored in a -20 °C freezer long term. Western blot was next run to determine if Ybx1 protein pull down was successful and cDNA libraries generated from the reaction were used for quantitative PCR to determine interacting RNAs in a complex with Ybx1.

2.10 GENOMIC DNA EXTRACTION FROM ZEBRAFISH EMBRYOS AND FIN CLIPS

Single embryos were collected at 24 hpf in the strips of 8 PCR tubes. Residual egg water was removed with a pipette. Lysis buffer (10 mM Tris pH 8.3, 50 mM KCl) was mixed with proteinase K. 10 µL of the 10 mg/ml of proteinase K was added fresh to 1ml of the lysis buffer and vortexed. 30 µL of the lysis buffer master mix was used per embryo and next they were incubated in a thermocycler at 55 °C for 4 h and then proteinase K was heat inactivated at 95 °C for 5 minutes. Next samples were vortexed and spun down using a microtube centrifuge and 1 µL was used for genotyping PCR.

Genomic DNA from adult fish was extracted from fin biopsies, which were performed by a trained technician in accordance with animal welfare regulations. The UK Home office license numbers: PPL 70/7836 and P782A73C4.

Similarly, to the DNA extraction from embryos, lysis buffer was mixed with proteinase K. 100 µL of lysis buffer was added per fin clip and samples were incubated at 55 °C for 12 hours and then heat inactivated at 95 °C

2.11 *YBX1*^{SA42} MUTANT ALLELE

The temperature sensitive mutant allele has been previously generated as described in Kumari *et.al* 2013. The *ybx1*^{sa42} allele contains the V83F amino acid substitution in the crucial cold shock domain of the protein. *Ybx1*^{sa42} fish line was grown in the laboratory to homozygosity. The mutation is activated when embryos are exposed to 22 °C temperature and stops at 28 °C. For analysis of the left-right asymmetry defects and heart morphogenesis homozygous fish and the wild type sibling or heterozygous controls were mated and the embryos were collected at the 1 cell stage and kept at 28 °C until 70% epiboly. At 70% epiboly the embryos were temperature shifted to 22 °C

and kept until the 21-som stage. At the 21-som stage embryos were put back to 28 °C and grown until 55 hpf.

2.12 GENERATING CRISPR- CAS9 MUTATIONS IN ZEBRAFISH

All potential target sites for genome editing in zebrafish have been sequenced to identify any genetic variations and nucleotide substitutions, especially in the non-coding regions of the gene. The gRNAs were designed using CHOP CHOP software (Thyme *et. al* 2016), selection of the guides was determined by their proximity to the target site, the number of mismatches, predicted efficiency and self-complementarity. Best candidates were then put into the forward oligonucleotide sequence containing a T7 promoter, according to the protocol from Gaurav Varshney, Shawn Burgess Lab 2015. The forward and reverse oligo were bound together using the oligo assembly protocol:

TABLE 2-11 OLIGO ASSEMBLY FOR THE gRNAS

Reagent	Volume
5× buffer	5 µL
10 mM dNTP	0.5 µL
Oligo 1 (10 µM)	1 µL
Oligo 2 (10 µM)	1 µL
Phusion polymerase	0.5 µL
Water (nuclease free)	17 µL

PCR conditions:

TABLE 2-12 OLIGO ASSEMBLY THERMOCYCLER CONDITIONS

Temperature	Time
98 °C	2 min
50 °C	10 min
72 °C	10 min
12 °C	hold

Samples were then run on a 2.5% agarose gel and used as a template for *in vitro* transcription. Next the gRNAs were synthesized using the HiScribe kit from NEB (cat: E2040S) according to the manufacturer's instructions and purified using the Monarch RNA clean up kit 50µg (cat: T2040L).

To synthesize the Cas9 globin mRNA, the pT3TS Cas9 plasmid (addgene 46757, Jao et. al. 2013) was digested with the XbaI enzyme for 2 hours at 37 °C and then purified using the Qiagen PCR purification kit (Cat 28104). The next sample was run on a 1% agarose gel to ensure it has been completely linearised and its concentration was measured on the nanodrop. The linearised template was then used as a template for a capped mRNA *in vitro* transcription reaction with an mMACHINE kit from Ambion (cat AM1340).

TABLE 2-13 gRNA IN VITRO TRANSCRIPTION PROTOCOL

Reagents	Volume
10× Reaction buffer	2 µL
2× NTP/CAP	10 µL
Linearised template	1 µg
T7 polymerase	1.5 µL
RNasin inhibitor	0.5 µL

Nuclease free water	up to 20 μ L
---------------------	------------------

The reaction was incubated for 2 hours at 37 °C, after 2 hours 1 μ L of the Turbo DNase enzyme was added and the reaction was incubated for further 30 minutes. Following incubation sample was purified using an RNA clean up kit 50 μ g (cat: T2040L).

The pCS2 Cas9 nanos 3'UTR plasmid (addgene: 62542, Moreno-Mateos et al. 2015) was linearised using Not1 enzyme for 2h and following linearisation the sample was purified, and the RNA was synthesized using the same protocol as the Cas9 globin mRNA.

The dosage of the gRNAs was tested by microinjections into the zebrafish embryos. The starting dose was 250 pg of Cas9 globin with 50 pg of the gRNA. Following injections unfertilised and abnormal embryos were discarded and the remaining embryos were kept in the 28.5 °C incubator and grown until 24 hpf.

2.13 T7E1 ASSAY TO DETERMINE EFFICIENCY OF THE gRNAs

Injected single embryos were lysed with proteinase K and used as a template for a PCR reaction. Once the region of interest amplified with a single sharp band, T7E1 endonuclease (cat: M0302L) was used to cleave the mismatched DNA within the gene and recognise which gRNAs have effectively generated mutations. The first 4 μ L of the PCR reaction was combined with 1 μ L of buffer 2 10 \times NEB and 5 μ L of nuclease free water. The reaction was put in the thermocycler at the following program for the PCR product to reanneal and form heteroduplexes:

95 °C – 10 min

95 °C to 85 °C, -2 °C/s

85 °C to 25 °C, -0.1 C/s

4 °C- hold

The next reaction was removed from the thermocycler and the enzyme mix containing 8.75 µL of nuclease free water, 1 µL of buffer 2 10× NEB and 0.25 µL of the T7E1 enzyme (10 U/µL) was added per reaction. The sample was then incubated at 37 °C for further 30 minutes.

To check the cleaving of the PCR products, samples were run on a 3% agarose gel. The PCR sample untreated with the T7E1 endonuclease was run alongside cleaved samples to allow comparison and determine the efficiency of the gRNAs. Cleaved samples indicated, which gRNAs have successfully produced mutation and these PCR products were sent for sequencing to confirm the mutations.

Furina loci:

Chr7 alt: 13987475-14207606

Designed gRNAs targeted the sequence of the start codon and a signal peptide of *furina*, they were injected together into 1 cell stage zebrafish embryo and produced in a 56 bp deletion and a knockout of a protein. This deletion resulted in removal of the start codon and also knocked the protein out of frame.

TABLE 2-14 *FURINA* Δ56 gRNA SEQUENCES

Name	gRNA sequence (5' to 3')
<i>Furina</i> ATG gRNA1 F	ATTGACGCTCGGTACACTAC

<i>Furina</i> ATG gRNA2 R	GACACACATAGGAGAACCA
------------------------------	---------------------

The next set of gRNAs were targeting the 3'UTR of *furina* computationally predicted variant *XI*, which covered the YBE motif and created a 1.3 kb deletion.

TABLE 2-15 *FURINA* Δ3'UTR gRNA SEQUENCES

Name	gRNA sequence (5'to 3')
CHOP CHOP g1 R	GTATTCAGACGAACCCAGAAAGG
gRNA4 R8 3'UTR F	CGTCACTGGCAAATCACGACGG

Microinjections with the selected gRNAs and Cas9 mRNA were repeated at the lower dosages to determine, the appropriate amount of gRNAs/Cas9 mix to generate deletions and at the same time reduce toxicity to the embryos. Finally, to grow microinjected embryos into adulthood, zebrafish embryos were injected into the yolk at 20 minutes post fertilisation with the optimised amount of gRNAs and Cas9 nanos 3'UTR mRNA. The first injection set with *furina* ATG gRNA1 F, *furina* ATG gRNA2, 25 pg each and 100 pg Cas9 nanos 3'UTR generated deletion resulting in the knock out the FurinA protein and the second injection set with the 25 pg of each gRNA: CHOP CHOP g1 R, gRNA4 R8 3'UTR F and Cas9 nanos 3'UTR mRNA made a deletion in the 3'UTR. Injected embryos were grown into adulthood.

2.14 GENOTYPING OF THE MUTANT ALLELES

To genotype the mutant alleles generic taq polymerase PCR protocol was adapted. Following genomic DNA extraction PCR master mix was prepared:

TABLE 2-16 PCR MASTERMIX FOR GENOTYPING

Reagent	Volume
water	12.9 μ L
5 \times go taq buffer	4 μ L
dNTPs (10mM)	0.4 μ L
primer fwd 5' to 3' (10 μ M)	0.6 μ L
primer rev 3' to 5' (10 μ M)	0.6 μ L
Genomic DNA	1 μ L
Taq polymerase (10U)	0.5 μ L

With thermocycler set to the following protocol:

TABLE 2-17 THERMOCYCLER CONDITIONS SET UP FOR GENOTYPING

temperature	time
95 $^{\circ}$ C	5 min
95 $^{\circ}$ C	30s
55 $^{\circ}$ C	30s
72 $^{\circ}$ C	1 min per 1kb
go to step 2	34 times
72 $^{\circ}$ C	3 min
12 $^{\circ}$ C	hold

***Ybx1^{sa42}* genotyping**

Genotyping of the *ybx1^{sa42}* allele was performed according to the protocol generated by Kumari et. al. 2013. Samples were amplified with forward 5' to 3' primer: #4137 V83Fr: GAGTCAAAC TAAGCTACGACTAAAAGC and the reverse 3' to 5' primer:

YbxV83F-Fw II: TTGGGGACAGTGAAATGGTT. 5 µL of the total PCR reaction was then digested in 0.2 µL enzyme Alu I (NEB cat no R0137R), 2 µL of 10x cutsmart buffer and 12.8 µL of nuclease free water. Samples were incubated at 37°C overnight and digested bands were resolved on 2.5% agarose. The wild type band was 384 bp and the mutant bands were 294 bp and 90 bp.

***Furina* ATG Δ56bp allele**

To identify the *furina* Δ56bp allele forward 5' to 3' primer *furina* variant X1 exon 2F: CAGGTGATTCTGAAGTACATC and the reverse 3' to 5' primer *furina* variant X1 exon 2R: CATTCCCATGGTTCACAAAGC were used. PCR reaction was then run on a 3% agarose gel, the wild type band size was 318 bp and the mutant band was 262 bp.

***Furina* Δ3'UTR allele**

To identify the *furina* 3'UTR deletion forward 5' to 3' primer: *furina* 3'UTR F: CCTTCTCTAGCATCTACTGCACTGTTG and the reverse 3' to 5' primer: *furina* R4 every 500bp R: CATCTCTCTCACAGTTCCTCTTC were used. The wild type band was 1493 bp and the mutant band was 182 bp. This PCR product is very AT rich, therefore decreased annealing temperature is recommended.

2.15 TRANSLATION ASSAY

Temperature sensitive *ybx1*^{sa42} homozygous mutant fish and wild type sibling control fish were set up in a breeding tank with a divider a night before the experiment. Normally three pairs of fish were set up together per mutation. The next day water in

tanks was replaced and dividers removed. After mating embryos were collected in warm systems water, placed on the injection mould and injected in a yolk with an injection mix containing either 50 pg of capped *spaw* EGFP mRNA or 50 pg of *furina* sfGFP capped mRNA with 20 pg of *mCherry* capped mRNA. After injection embryos were dechorionated with a pronase 2mg/ml mixture in egg water for 2 minutes and then rinsed extensively with 400 ml pre-warmed to 28 °C egg water and placed in a glass dish in a 28 °C incubator. At the 16-cell stage, they were temperature shifted to 22 °C Danieau's media and a 22 °C incubator until the 512-cell stage. Next embryos were temperature shifted to a 28 °C incubator until they reached the 1K cell stage. Next samples were either lysed in RIPA buffer for western blot analysis or mounted in an agarose mould dish Zaucker *et.al.* 2021 for confocal imaging.

2.15.1 Imaging of embryos for translation assay

Before reaching the 1K-cell stage *MZybx1* mutant embryos and wild type controls were positioned laterally in the agarose mould on the glass bottom dish for the confocal imaging as described in Zaucker *et.al.* 2021. *Spaw* EGFP and *furina* sfGFP expression were analysed with 488nm laser and mCherry control mRNA with 561 nm laser. Z-stacks of the entire blastoderm of the embryo were taken with each step size being 1 µm on a confocal Andor Revolution XD microscope with an Andor iXon 888 camera. The imaging of each sample was done at 1K, sphere and 30% epiboly stages of zebrafish development.

2.15.2 Western Blot analysis of zebrafish embryos

For analysis of Furin sfGFP and Spaw GFP expression *Mybx1* mutant embryos were used. Following the temperature shift at the 512-cell stage, all embryos were collected and lysed in RIPA buffer with the proteinase inhibitor in a 1:1 ratio i.e. per 30 embryos in a sample, 30 µL of RIPA buffer was added. The sample concentration was normalised using Bradford assay with a quick start Bradford protein assay kit (Bio-Rad cat: 5000201) according to the manufacturer's protocol and then samples were boiled at 95 °C for 5 min in Laemmli buffer and run on a polyacrylamide gel.

10% polyacrylamide gel was synthesized according to the following protocol:

TABLE 2-18 SEPARATING GEL PROTOCOL

Reagent	Volume
Water	1.9 ml
30% acrylamide/ bis solution (Bio-Rad cat: 1610157)	1.7 ml
1.5 M Tris-HCl (pH 8.8)	1.3 ml
10 % APS	0.05 ml
10 % SDS	0.05 ml
TEMED (Bio-Rad cat: 1610801)	0.002 ml

The reaction was mixed and poured into the secured glass plates leaving approximately 2.5 cm space at the top of the plates. 100% isopropanol was poured into the gap and the separating gel was allowed to dry. Once the gel was set, isopropanol was carefully poured out of the glass plates and stacking gel was prepared fresh:

TABLE 2-19 STACKING GEL PROTOCOL

Reagent	Volume
Water	1.4 ml

30% acrylamide/ bis solution (Bio-Rad cat: 1610157)	0.33 ml
1.0 M Tris-HCl (pH 6.8)	0.25 ml
10 % APS	0.02 ml
10 % SDS	0.02 ml
TEMED (Bio-Rad cat: 1610801)	0.002 ml

The stacking gel was poured onto the top of the glass plates and 10 well comb was inserted carefully avoiding creating any bubbles. The gel was allowed to set for 10 minutes and the next wells were rinsed with the RO water and gel was then placed in the tank, samples were loaded and they were run at 30 mA constant for 2-3 hours.

Once the polyacrylamide gel resolved sufficiently samples, samples were next transferred into the nitrocellulose membrane using the Trans-Blot turbo transfer system (Bio-Rad cat: 1704150). Filter paper sheets, nitrocellulose membrane and a gel were soaked in a 5× Turbo buffer (Bio-Rad cat: 10026938) with 20% ethanol. Three sheets of filter paper, nitrocellulose membrane, gel and another three sheets of filter paper were placed in the Trans-Blot turbo cassette and a program at 25 V constant for 30 minutes was run. Following the transfer, filter paper and gel were discarded, and the membrane was put in 5% milk in TBS-Tween solution for 1 hour. For detection of Spaw EGFP and FurinA sfGFP anti-GFP HRP conjugated antibody (Santa Cruz cat: sc9996) was used at the concentration of 1:2000 in 5% milk in TBS-Tween solution. To ensure an equal amount of protein is loaded per sample on a gel, anti-Actin HRP (Santa Cruz cat: sc4778) conjugated antibody at the concentration of 1:2500 in 5% milk/TBS-Tween solution served as a loading control. Antibody incubations took place in a 4 °C cold room overnight on a rotating nutator. The next day membranes were washed six times with TBS-Tween for 5 minutes and developed using Super Signal West Dura substrate (ThermoFisher Scientific cat: 34075). Membranes were

then put in a plastic wallet and developed at the optimal exposure chemifluorescence on a Bio-Rad ChemiDoc MP imager (cat: 17001402).

2.16 STATISTICAL ANALYSIS

In this thesis all statistical analysis was performed in Microsoft Excel. Student's t-test was used in statistical analysis of the heart looping, qPCR datasets and western blot band and fluorescence intensity measurements. Single factor ANOVA was used for statistical analysis of the size of the heart at the 5 dpf and also width of the atrioventricular canal data at 3 dpf. This method was used to compare the significance of differences in heart morphology between various genotypes of *ybx1* mutant embryos. For all statistical analysis P value > 0.05 were considered non-significant or ns, * represented p value < 0.05 , ** p value < 0.01 , *** p value < 0.001 .

2.17 IMAGING OF MZYBX1 AND CONTROL HEART EMBRYOS AT 5 DPF

2.17.1 Mounting of embryos and sample preparation

MZybx1 and wild type control embryos were crossed simultaneously and grown at 28.5 °C until the 75% epiboly stage. Next, they were temperature shifted at 22 °C until 21 som stage and then returned to the 28 °C and incubated until 5 dpf. At 24 hpf embryos were treated with the phenylthiourea (PTU) at 0.003% concentration in Danieau's solution to prevent pigment formation. Prior to imaging on day 5 embryos were immobilised by adding 25× tricaine solution to Danieau's solution and mounted

in 0.6% low melt agarose on a 3 cm falcon petri dish. Once the agarose set dish was refilled with tricaine in Danieau's solution and the sample was imaged. Movies were taken at 13 frames per second focusing on the atrioventricular canal and heart valves using Nikon ECLIPSE Ni, Nikon, ECLIPSE Ni microscope with a HAMAMATSU digital camera C11440, ORCA-Flash4.OLT. Movies were approximately 30 s-1 minute long.

2.17.2 Analysis of blood flow

To analyse the direction of the blood flow in *ybx1* and control embryos, Particle image velocimetry (PIV) application was used in MATLAB (Thielicke, W. and Sonntag, 2021). Each movie was converted in ImageJ using the function 'find edges' and uploaded to PIV, region of interest was set out to be a junction in the AV canal and frames were analysed. Vectors were next saved and analysed for direction with the following code in MATLAB:

```
clear all
figure
JustRet=1;
WTFileName='/Users/agnieszkanagorska/Desktop/PIVjunction/Wildtype/';
MutantFileName=('Users/agnieszkanagorska/Desktop/PIVjunction/ybx1mutant/');
WTFileList=dir([WTFileName, '*.mat*']);%type name of WT vectors
folder path
if JustRet
    MutantFileList=dir([MutantFileName, '*RET*']);%type name of
mutant files
else
    MutantFileList=dir([MutantFileName, '*.mat*']);
end
for WvM=1:2
```

```

if WvM==1
    FileList=WtFileList;
    FileName=WtFileName;
elseif WvM==2
    FileList=MutantFileList;
    FileName=MutantFileName;
end

for FN=1:length(FileList)
    load([FileName,FileList(FN).name]); %this automates opening
of the PIV file
    for t=1:length(u_original) %run through every time point
        sz=size(u_original{t});
        count=1;
        U=u_original{t,1};
        V=v_original{t,1};

        %this section analyses the data
        count=1;
        Total_U=0;
        Total_V=0;%Here we are initialising arrays that will sum
up all the vectors in the X and Y direction
        for Col=1:sz(1)
            for Row=1:sz(1) %looping through all vectors in
image
                if isnan( U(Row,Col) )==0 && U(Row,Col)<10 &&
U(Row,Col)>-10 V(Row,Col)<10 && V(Row,Col)>-10;
                    Total_U=Total_U+U(Row,Col);%sum up every
vector in x direction
                    count=count+1;
                    Total_V=Total_V-V(Row,Col); %sum up every
vector in y direction
                    Angle(t,count,FN,WvM)=atan(-
V(Row,Col)/U(Row,Col)); % calculating what angle every vector is
facing

```



```

        if U(Row,Col)<0

Angle(t,count, FN,WvM)=pi+Angle(t,count, FN,WvM); %for angles that
are going in negative x direction

        end

        end

        end

        end

        U_over_t(t, FN,WvM)=Total_U/count;%calculating average X
velocity over top left quadrant of image

        V_over_t(t, FN,WvM)=Total_V/count;%calculating average Y
velocity over top left quadrant of image

        end

        end

end

AveWTU=mean(U_over_t(:,: ,1),2);
AveMutU=mean(U_over_t(:,: ,2),2);

AveWTV=mean(V_over_t(:,: ,1),2);
AveMutV=mean(V_over_t(:,: ,2),2);

%%
% Polar plots
for t = [10,30,40] % the values of t are the frames to be analysed
    tChar=num2str(t);

    AngleVecWT=nonzeros(Angle(t,: ,1));
    AngleVecMutant=nonzeros(Angle(t,: ,2));

    figure
    polarhistogram(AngleVecWT,10, 'LineWidth',
1, 'Normalization', 'Probability')

```

```

set(gca, 'fontsize', 24, 'FontWeight', 'bold', 'FontName', 'Helvetica')%, '
GridAlpha', 1, 'RGrid', 'off', 'ThetaGrid', 'off', 'RTickLabel', ''

exportgraphics(gcf, ['/Users/agnieszkanagorska/Desktop/PolarPlotWT', t
Char, '.pdf'], 'ContentType', 'vector')

    figure

        polarhistogram(AngleVecMutant, 10, 'LineWidth',
1, 'Normalization', 'Probability', 'FaceColor', 'r')

set(gca, 'fontsize', 24, 'FontWeight', 'bold', 'FontName', 'Helvetica')%, '
GridAlpha', 1, 'RGrid', 'off', 'ThetaGrid', 'off', 'RTickLabel', ''

    %change RGrid and ThetaGrid on/off depending on if you want grid
lines

    %remove RTickLabel and following if you want number along the
radius

    if JustRet

exportgraphics(gcf, ['/Users/agnieszkanagorska/Desktop/PolarPlotRet',
tChar, '.pdf'], 'ContentType', 'vector')

        else

exportgraphics(gcf, ['/Users/agnieszkanagorska/Desktop/PolarPlotMutan
t', tChar, '.pdf'], 'ContentType', 'vector')

            end

        end

    end

```

2.18 LIST OF PRIMERS:

TABLE 2-18 LIST OF PRIMERS

Name	Sequence
pCS2 3'UTR FurinA F	ATCAGATTAGACCATTAGCATCAAGGGCGAATTC AAGGCCTCTC
pCS2 3'UTR FurinA R	GCAGTAGATGCTAGAGAAGGGTTAAAGAGCACT TTGTG
pCS2 Furin A F	CTTGGTTCTCCTATAGTGTGTCTGATGGATCTCAG GCTTGCCTC
pCS2 Furin A R	GTAACGCGACGCTACGGCATCACTAAGGGCGAAT TCGAATC
Furin 5'UTR F	AGTGATGCCGTAGCGTCGCGTTAC
Furin 5'UTR R	CAGACACACTATAGGAGAACCAAGGCAG
Furin A 3'UTR F	CCCTTCTCTAGCATCTACTGCACTG
Furin 3'UTR R for RT	GCGTTCCTGAAAGACCCATAGATC
Furin A 3' UTR R	GATGCTAATGGTCTAATCTGATTC
Furin CDS GFP R	GCTGCTGTCTGCTGTCTGGCTG
Furin CDS GFP F	TGCAAACCTACGACCTCAATC
Furin superfold GFP R	GAGGTCGTAGGTTTTGCAATGGTGATGATGATGG TG
Furin superfoldGFP F	CAGACAGCAGACAGCAGCGTTAGCAAAGGTGAA G
Furin GFP ov F	CAAAACACAAAGTGCTCTTGTGAGCAAGGGCGA GGAG
Furin GFP ov R	CAGTAGATGCTAGAGAAGGGTACTTGTACAGCT CGTC
Furin gfp F	CCCTTCTCTAGCATCTACTGCACTG
Furin gfp R	AAGAGCACTTTGTGTTTTGATAAAG

sothpaw R	GTCATCAGTCATGCGCATCCTTTC
Southpaw F	AGAAATGTGACAGGAAAGCCAAC
egfp southpaw R	GAAGGTGTTGGCTTTCCTGTCACATTTCTCTTGTA CAGCTCGTCCATGC
egfp Southpaw F	GAAAGGATGCGCATGACTGATGACGTGAGCAAG GGCGAGGAGCTG
Southpaw superfold gfp F	GGATGCGCATGACTGATGACGTTAGCAAAGGTGA AG
Southpaw superfold GFP R	GGCTTTCCTGTCACATTTCTGCTGCCTTTATACAG TTC
FurinA ex15 Intron spanning F	CCTCAATCAGATCTGCACAG
Furin ex16 intron spanning R	CAGCTCATTATTGAGGATAGTG
Furin dDLE F	GAGATTTTAAAGGAATGCTCAGTTTACATGTC
Furin dDLE R	GACATGTAAACTGAGCATTCTTTAAAATCTC
Furin Loop Mutant F	GAGATTTTAAAGGAGCACTTATTAATAATATG CTCAGTTTACATGTC
Furin Loop mutant R	GACATGTAAACTGAGCATATTAGTTTAATAAGTG CTCCTTTAAAATCTC
Furin DLE stem break F	GAGATTTTAAAGGAGCACTTATTTTTGAttaATGCT CAGTTTACATGTC
Furin DLE stem break R	GACATGTAAACTGAGCATTAAATCAAAAATAAGTG CTCCTTTAAAATCTC
Furin Stem Restore F	GAGATTTTAAAGGAGCACTTTAATTTGATTAATG CTCAGTTTACATGTC
Furin Stem Restore R	GACATGTAAACTGAGCATTAAATCAAATTAAGTG CTCCTTTAAAATCTC
Furin A R2 R	GCGTTCCTGAAAGACCCATAGATC
FurinA 500 bp R3	ACACTTTCACACTCATTCACTCATC

FurinA 500 bp R4	CATCTCTCTCACAGTTCCTCTTC
FurinA 500 bp R5	GCCAGTGTCTGCAAAGTTTAG
FurinA 500 bp R6	GATCTCAAGTAGAGCTCTTTTACACC
FurinA 500 bp R7	GGGAGTGAACGGTGCCAAAAC
FurinA 500 bp R8	TGGTCTTTGGTCGTGCCTTTTG
FurinA 500 bp R9	ATGCACCATATATATAGTACAAAAATAGGC
Furin A cDNA R	atcgatGTAAATGACAATGCACCATATATATAGTAC
FurinA cDNA F	GGATCCAGTGATGCCGTAGCGTCGCG
FurinA 3'UTR F	CATGATTCACTTGGGTGTTTGATC
furinA exon 3.4 F	GTGAACCATGGGAATGTATTTGGAG
furinA exon 5.6 R	GATGGTCTTGGTTGTACAAGTACCAC
furina exon15 F	GTG GCT GGA ACC AGT GAC TAT G
furinA variant X1 exon 2 F	CAG GTG ATT CCT GAA GTA CAT C
furinA variant X1 exon2 R	CAT TCC CAT GGT TCA CAA AGC

Gapdh_3'UTR_Fw	CTGACAGTCCGTCTTGAGAAAC
Gapdh_3'UTR_Rev	AGTGATCGTTGAGAGCAATACC
18S qPCR F	TCGCTAGTTGGCATCGTTTATG
18S qPCR R	CGGAGGTTCGAAGACGATCA
Lft exon 2F	CTCTACAAGAAGGCCCCACA
Lft exon 3R	CTCCTCTAGGTTGAGTGTGTAAG
5S rRNA F	ATTGGAGGACCAGCTCGCTC
5S rRNA R	TTCTGGCAGCAACCCAGC

CHAPTER 3
VALIDATION OF *FURINA* VARIANT *XI*
IN ZEBRAFISH

3.1 INTRODUCTION

Furin is a ubiquitously expressed proprotein convertase that has an essential developmental role in vertebrate embryos. Studies across different organisms have found that Furin is implicated in key genetic pathways such as BMP, Notch, and Nodal. Furthermore, it is also known to activate infections, by cleaving viruses and bacteria. This includes the novel SARS-Cov-2 virus (Cui *et al.*, 1998; Tessadori *et al.*, 2015; Bestle *et al.*, 2020; Zhou *et al.*, 2021). Given that Furin is such a versatile proprotein convertase with many crucial functions, understanding how it is regulated is of great importance.

Lately, many studies have emerged about the proteins being regulated by non-coding elements. For example, the CTG nucleotide repeat in the 3'UTR of the myotonic dystrophy protein kinase results in the transcript being stuck in the nucleus and not being exported to the cytoplasm for further processing. Consequently, individuals with this dominantly inherited mutation develop myotonic dystrophy (Davis *et al.*, 1997). Although the role of the FurinA protein in zebrafish has been well studied, the question of how its activity is regulated remains unanswered. Interestingly the zebrafish *Furin* homolog, *furina* has been annotated with two isoforms in the zebrafish genomic databases. These two isoforms only differ in the length of the 3'UTR sequence.

We are interested in the 3'UTR elements in the mRNA sequences with roles during embryonic development. Previous work from the Sampath group showed that transcripts of the Nodal ligand *sqt* in zebrafish consists of an RNA motif in the 3'UTR that controls *sqt* RNA localisation at the 4-cell stage (Gore *et al.*, 2005; Gilligan *et al.*, 2011). This element consists of an AGCAC sequence motif and a three base stem loop structure. Subsequently, it was given the name YBE, due to its interaction with the RNA-binding protein Ybx1. Interestingly, further analysis of the zebrafish transcriptome showed that many Nodal pathway components harbour this element,

including *lefty1* and *lefty2* inhibitors and the novel *furina* isoform (Zaucker *et al.*, 2017).

A closer examination of zebrafish genomic databases such as ensembl, UCSC and RNA-seq datasets revealed that one of the *furina* transcript isoforms has a 275 bp 3'UTR sequence, whereas a second computationally predicted variant *XI* has a 3.5 kb 3'UTR (White *et al.*, 2017). In addition to having an unusually long 3'UTR sequence, variant *XI* also contains the YBE motif. The significance of this divergence of non-coding sequences in the UTR is not clear, as there are not many studies analysing such differences and the available information is limited. In the mouse nervous system, there is evidence of the presence of the long 3'UTR isoforms in some genes. Studies in mouse embryonic stem cell derived neurons and deletion assays suggest that in some cases these long 3'UTRs may have regulatory functions in RNA expression, whereas other targets do not show any phenotype (Bae and Miura, 2021).

In zebrafish, there is not much known about the non-coding roles of the 3'UTR isoforms with long sequences. Studying the role of these sequences is essential for understanding different modes of gene regulation. In this chapter, I analyse and verify the sequence of the *furina* variant *XI* from zebrafish embryos and compare it to the genomic databases. I studied the expression patterns of *furina* variant *XI* and compared them to the *furina* protein sequence. I also show a design of CRISPR-Cas9 deletions to study the function of *furina* and the *furina* non-coding region in zebrafish embryos.

Aims:

- Analysis of the sequence of the alternative transcript *XI*
- Analysis of the overall expression of the *furina* transcript and the variant *XI* and also analysis of the expression patterns.

- Design and generation of the CRISPR-Cas9 mutants in the *furina* and *furina* 3'UTR and preliminary analysis of the phenotype.

3.2 RESULTS

An analysis of the UCSC and ensembl genomic databases has shown that zebrafish *furina* has two transcripts, which have distinct 3'UTR sequences. The *furina* gene is located on zebrafish chromosome 7. As illustrated in the schematic in Figure 3.1, transcript 1 has a 275 bp 3'UTR sequence and the other transcript, the computationally predicted variant *XI*, has an unusually long 3'UTR of 3862 bp. Although the length of the 3'UTR sequences differs considerably between the transcripts, the 5' UTR and protein-coding sequences (CDS) are the same, as shown in the blue and light blue regions of the two transcripts in Figure 3.1. Additionally, the YBE motif is present exclusively in variant *XI*'s 3'UTR sequence.

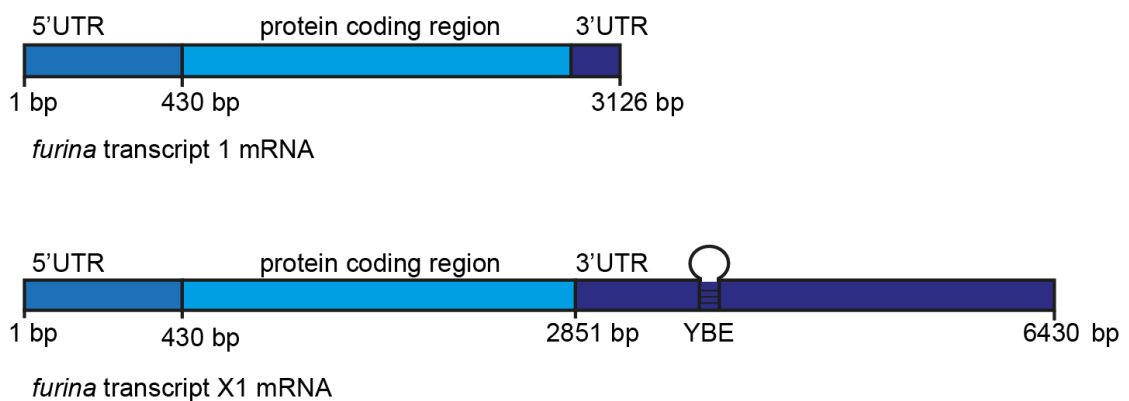


Figure 3.1 Schematic of the *furina* transcripts.

Comparison of length of the non-coding 3'UTR mRNA sequences between two transcripts. The 5'UTR region and the CDS are identical in both transcripts.

As variant *XI* has only been predicted in genetic databases and available RNAseq datasets, it has not been studied experimentally. The schematic in Figure 3.1 is based on these predictions. To date, the expression of variant *XI* has not been analysed during different stages of embryonic zebrafish. To determine the expression of the *furina* transcript *XI*, total mRNA was collected from adult zebrafish ovaries and 50% epiboly, 10 som and 18 som. These stages were selected because in the literature it has been reported that *furina* has a role in the left-right asymmetry establishment during somitogenesis (Tessadori *et al.*, 2015). The YBE motif is located outside of the reference sequence of transcript 3'UTR. This experiment aimed to determine if the computationally predicted variant containing a YBE motif is at all expressed in the zebrafish embryos. The YBE motif has been previously shown to be important in the translational regulation of protein expression, therefore the expression of variant *XI* in zebrafish embryos was of great interest to us (Gilligan *et al.*, 2011; Kumari *et al.*, 2013; Zaucker *et al.*, 2017).

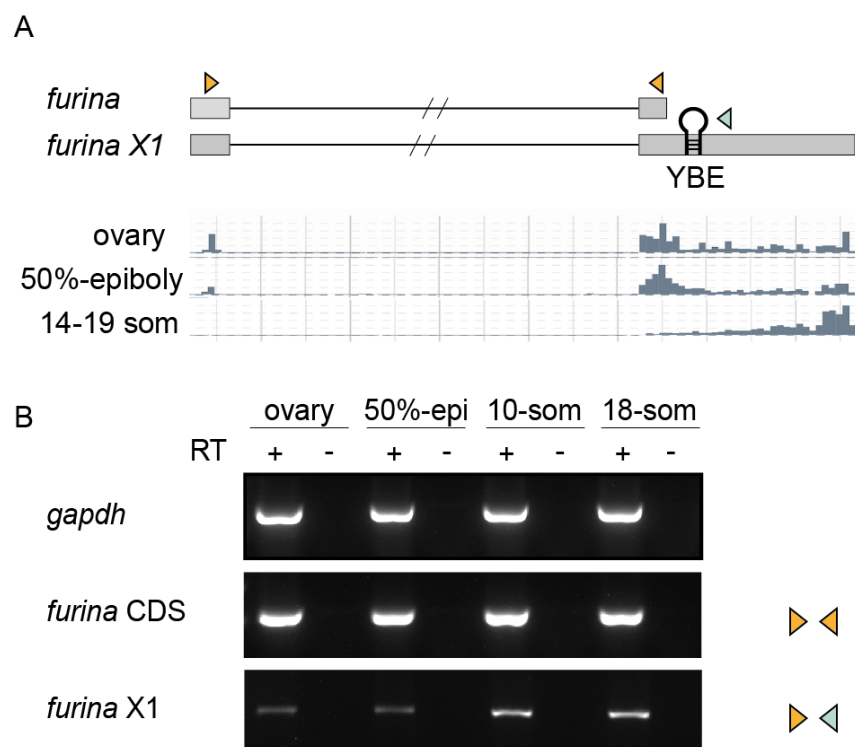


Figure 3.2 Validation of the *furina XI* variant expression in zebrafish embryos.

A) Schematic showing the location of primers used for amplification in both transcripts. The orange set was used to amplify *furina* CDS. The orange forward

primer and the reverse light green primer, shown behind the hairpin YBE motif, were designed to amplify variant *XI* 3'UTR. Expression data, below the schematic of the *furina* transcripts is adapted from ensembl (<https://www.ensembl.org>);

B) PCR amplification of *gapdh* (housekeeping gene control), *furina* coding sequence (orange primers) and variant *XI* 3'UTR (orange and green) using cDNA libraries from adult zebrafish ovary, 50% epiboly, 10-som and 18-som stage. RT indicates usage of reverse transcriptase enzyme, lanes with + indicate samples where RT enzyme was added, - indicates samples where no RT was added and serves as genomic DNA control.

The RT-PCR primers were designed to distinguish the expression of two *furina* isoforms and confirm the expression of variant *XI* with the YBE motif, as illustrated in Figure 3.2 A. In the agarose gel in Figure 3.2 B I observed that across all embryonic stages and in the adult fish ovary both sequences of the CDS and the variant *XI* were amplified. Some studies suggested that embryonic 3'UTRs may have longer sequences than in the adult fish (Li *et al.*, 2012). Therefore, to test if variant *XI* was exclusively expressed in zebrafish embryos, as an additional control, cDNA from the ovary was included in the PCR set. From the amplification in Figure 3.2 B, the first lane of the *furina* CDS and *furina XI* sets shows that variant *XI* is also expressed in the adult fish ovary. However, it is likely to be expressed at lower levels based on the much weaker band intensity of variant *XI* compared to *furina* transcript 1. Furthermore, transcript 1 was strongly expressed in the ovary and throughout embryonic development as shown in *furina* CDS samples. Interestingly, even though the amplification of variant *XI* is weak in the ovary and 50% epiboly sample lanes in 3.2 B, at 10-som and 18-som stages the PCR bands appear much stronger. This agrees with the expression data shown in Figure 3.2 A from ensembl.org and also suggests that variant *XI* expression might be important during the somitogenesis stages of zebrafish development.

Since semi-quantitative PCR experiments have confirmed that variant *XI*'s 3'UTR is expressed in zebrafish embryos, the next question to address was how accurate the online genome browser sequence prediction was. I was particularly interested to see

if the entire predicted sequence is expressed in the embryos. I used the cDNA templates shown in Figure 3.2 B and designed reverse primers at 1 kb intervals to determine the length of the *furina* 3'UTR variant *XI*. A schematic of the experimental design is given in Figure 3.3 A. The final distance between R8 and R9 primers was shorter as it was at the very end of the 3'UTR sequence of variant *XI*.

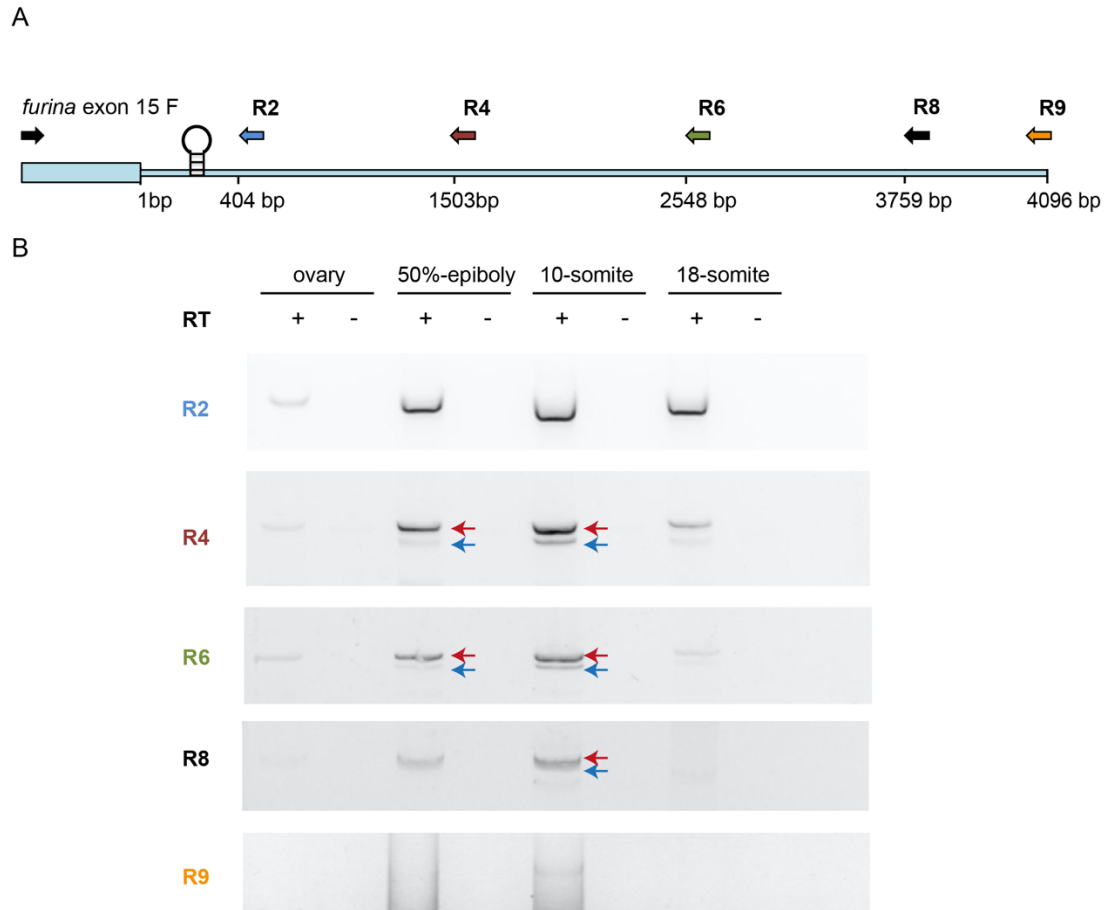


Figure 3.3 Analysis of the length of *furina* variant *XI* 3'UTR sequence.

- A) Schematic of the *furina* variant *XI* 3'UTR and the PCR primers. The same forward primer was used for each amplification and with different reverse primers approximately 1000 bp apart.
- B) Agarose gels showing amplification of variant *XI* 3'UTR from an adult ovary and different embryonic stages of development cDNA libraries: 50% epiboly, 10 som and 18 som. Each PCR set is colour coded with a corresponding reverse primer used in a reaction. RT indicates usage of reverse transcriptase enzyme, in lanes with + RT enzyme was added, - indicates samples were no RT was added

and serves as genomic DNA control. In PCR sets where multiple bands are present in a sample, a red arrow indicates main amplification and a blue arrow shows non-specific PCR product.

Amplification of the entire 3'UTR of variant *XI* was challenging since this 3'UTR sequence contained many small regions of repeats and was very rich in adenine and thymine residues (AT-rich). As shown in Figure 3.3 B, in the primer R8 set, it was possible to amplify the 3'UTR up to 3759 bp with the strongest amplification being at the 10-som stage. Further amplification with primer R9 was not effective and resulted in very smeary bands. Interestingly, a similar pattern was observed as in Figure 3.2 B, that variant *XI* in each PCR set: R2, R4, R6 and R8 has the strongest amplification at the 10-som stage and slightly weaker amplification at other stages based on the PCR band intensities in Figure 3.3 B. To check the sequence integrity from the genomic databases and determine amplification of the right target, the PCR bands were extracted and sent for sequencing. The PCR sequences perfectly matched the computationally predicted variant *XI*. In Figure 3.3 B there are also smaller bands marked with blue arrows under the main amplifications, these were particularly visible in PCR sets: R4 and R6. They were also purified and sent for sequencing; however, the results came back showing scrambled sequences that could not be matched to the variant *XI*. This led to the conclusion that most likely they were a random PCR artefact and not part of the *furina* variant *XI* transcript.

To determine if in Figure 3.3 the additional bands in different PCR sets were a result of the poor efficiency of a reaction, an additional forward primer was designed. In 3.3 B I observed that the R2 PCR is more efficient and amplifies better compared to other reactions. Therefore, I decided to design a new forward primer that was closer to reverse primers R4, R6 and R8, as indicated in the schematic in Figure 3.4 A. Amplifications were repeated with a new forward primer. Consequently, the overall efficiency of the PCR reaction appeared to increase, and the resulting amplifications were much stronger across all of the developmental stages, as shown in Figure 3.4 B. Finally, all gel bands were sequenced, and the results confirmed that they were variant *XI* PCR products.

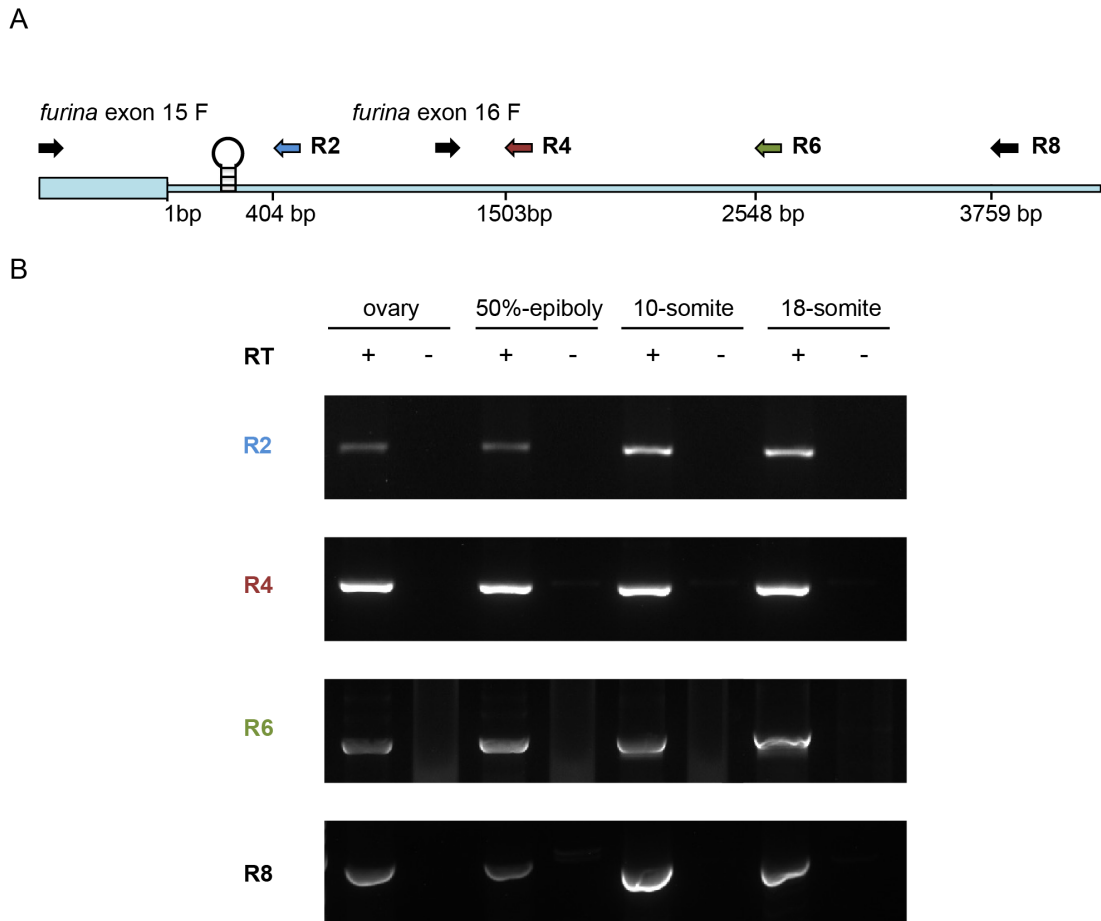


Figure 3.4 Optimisation of the amplification conditions of the 3'UTR of variant *XI* transcript.

- A) Schematic of the variant *XI* 3'UTR with the primers used for amplification, the new primer is called *furina* exon 16 F.
- B) PCR amplifications with *furina* exon 16 F primer and reverse R4, R6 and R8 primers. The cDNA libraries from an adult ovary and 50%-epiboly, 10-som and 18-som embryonic stages. RT is a reverse transcriptase enzyme, lanes with + indicate samples where RT enzyme was added, - indicates samples where no RT was added and serves as genomic DNA control

Since previous results in Figures 3.2, 3.3 and 3.4 from semi-quantitative PCR reactions have shown that variant *XI* is clearly expressed in the zebrafish embryos, I next wanted to study in more detail the expression levels of this variant. In Figures

3.2, 3.3 and 3.4 I consistently observed that variant *XI* expression appeared to be stronger during the somitogenesis stages. To quantitate the levels of expression, I used real-time PCR. This type of PCR is more accurate because it yields a CT value that provides a quantitative measure of expression patterns of transcripts. The oligonucleotides of comparable efficiencies were designed and tested to distinguish between *furina* transcript 1 and variant *XI* (see methods Chapter 2, qPCR section). The cDNA libraries from the adult fish ovary, 1K (1000-cell stage), 50%-epiboly, 10-som and 18-som served as a template for amplification. After the PCR reaction, given CT values per duplicate of the sample were normalised to the ribosomal 18S housekeeping gene control CT value. 18S is a standard real-time PCR control as it is expressed at the same level throughout zebrafish development (Drummond *et al.*, 2013). This process ensures that there is no variation in results due to different concentrations of cDNA used per sample and gives a more accurate representation of transcript expression at different developmental stages in zebrafish embryos.

The normalised results in Figure 3.5 show that in the ovary and at the 1K (1000-cell), 50%-epiboly and 18-som stages there was no significant difference in expression levels between both transcripts. However, at the 10-som stage, I observed that variant *XI* was significantly upregulated when compared to the *furina* CDS control. This is consistent with what I previously observed in Figure 3.2 in the semi-quantitative PCRs results. This result also suggests that the variant *XI* is likely to have a function in zebrafish development during somitogenesis and it might be useful to study the expression pattern during these stages in more detail.

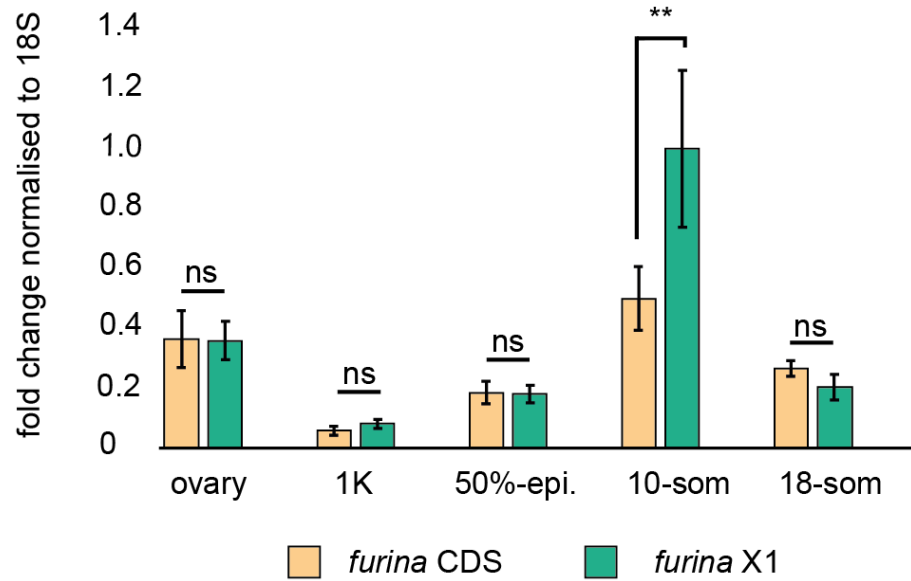


Figure 3.5 Analysis of the transcript *XI* expression in real-time.

Fold change in expression of *furina* CDS and *furina XI* normalised to 18S ribosomal RNA in the ovary, at the 1K(1000-cell), 50%-epiboly, 10-som and 18-som stage. ** $p < 0.01$ unpaired two-tailed student's t-test.

As a first step to understanding the potential role of variant *XI* 3'UTR in zebrafish, the whole mount *in situ* hybridization (WISH) at the stages of interest was performed. I wanted to analyse if there are differential expression patterns between both transcripts. Previous studies from different groups have shown that *furina* mRNA is expressed ubiquitously during zebrafish development (Walker *et al.*, 2006; Tessadori *et al.*, 2015). Therefore to separate the overall *furina* expression and exclusively detect variant *XI* mRNA, two distinct probes were designed. The sequence of the first one consisted only of the *furina* CDS and the second probe was variant *XI* 3'UTR as illustrated in the schematic in Figure 3.6 A. A variant *XI* probe was synthesized using the PCR product amplified with the R8 oligonucleotide.

In the literature, it has been reported that *furina* is maternally contributed and it is also present at the earlier developmental stages in zebrafish embryos. I wanted to have a broader idea of the *furina* isoforms' expression patterns, therefore in this analysis set, embryos at the 4-cell stage of development were also included (Tessadori *et al.*, 2015).

Furthermore according to the expression atlas of *furina*, and also the semi-quantitative RT-PCR and real-time PCR experiments shown in Figures 3.2 and 3.5, during gastrulation the *furina* transcript expression is low and then it starts to increase again approximately 8 hours post fertilisation (White *et al.*, 2017). For this reason in addition to 4-cell stage embryos, I also selected the bud, 10-som and 18-som stages to study *furina* expression patterns.

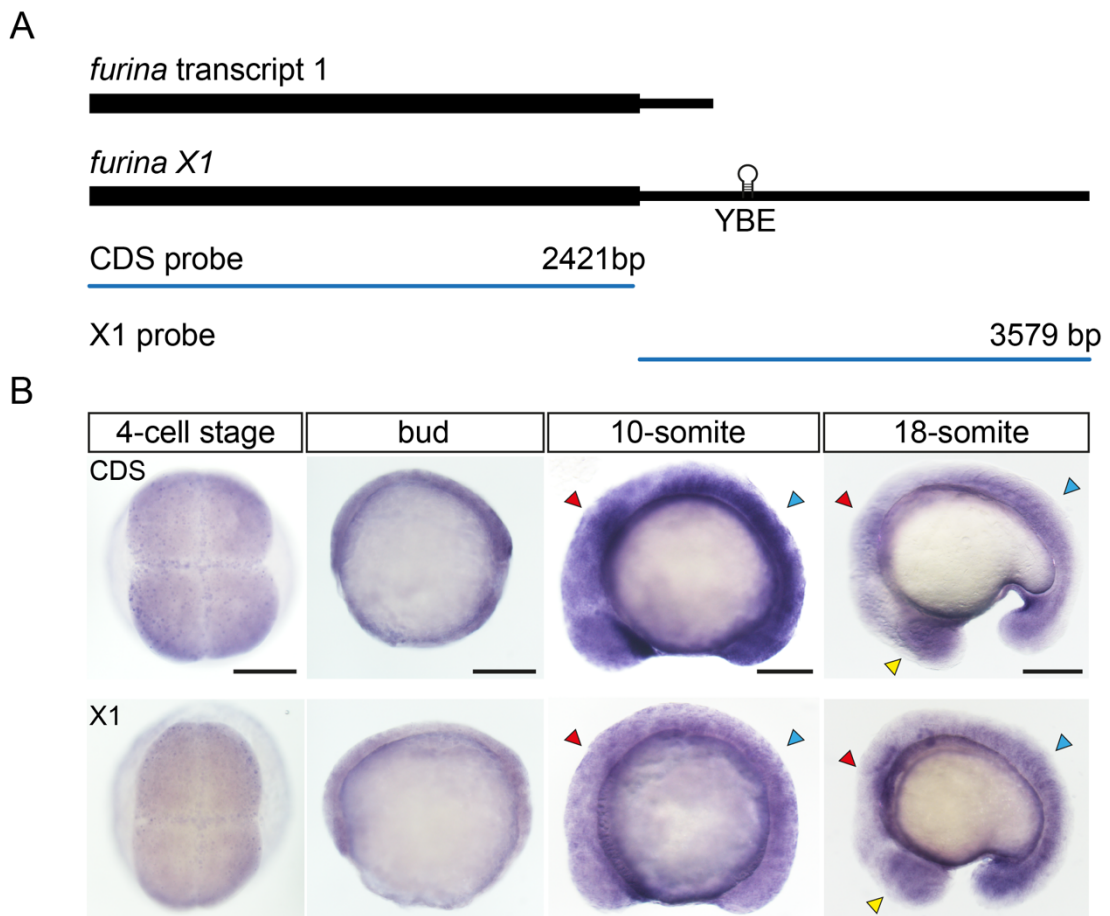


Figure 3.6 Analysis of the expression of *furina* mRNA in two transcripts.

A) Schematic of the sequences of *furina* transcripts and corresponding probes, CDS probe is used to distinguish *furina* transcript 1 and X1 probe detects *furina* variant X1.

B) Images of the WISH with either *furina* CDS probe at the top panel and variant X1 at the bottom panel. Animal pole view is shown at the 4-cell stage, and lateral view at the bud, 10-som, and 18-som stages of zebrafish development. Arrows highlight areas

of enrichment for *furina* expression. The red arrow points to the hindbrain, the blue arrow to somites and the yellow arrow to the eyes. Scale bars are 100 μm .

As expected and previously reported in the literature, in the top panel of Figure 3.6 B, the *furina* CDS probe was ubiquitously expressed at all stages of zebrafish development (Walker *et al.*, 2006; Tessadori *et al.*, 2015). The endogenous expression pattern of variant *XI* is very similar to *furina* transcript 1 as shown in the bottom panel of Figure 3.6 B. I did not detect any differential expression patterns between the two isoforms and concluded that overall they are broadly expressed. There is no difference between the expression patterns of both transcripts at the 4-cell stage, bud, 10 and 18 som. Interestingly, at the 10- and 18-som stages, I noticed that there were certain areas of enrichment, such as the hindbrain and somites that are pointed to by arrows in Figure 3.6 B. I also observed additional enrichment of both *furina* transcripts in the eyes of the embryos at 18 som. Furthermore, it is worth noting that the *XI* probe appears to be expressed at a lower level, based on the intensity of the staining. However, it is not possible to conclude anything other than the expression pattern from this experiment as the efficacy of the probes is most likely not comparable due to the *XI* probe being 1.3 kb larger than the WT probe.

After the expression patterns of *furina* variant *XI* were established, the next question was what is the function of this isoform? To answer this question CRISPR-Cas9 mutants were generated in fish at two different loci. The first mutation was designed to delete the *furina* start codon and a proportion of a signal peptide, effectively disrupting the function of the protein. The second mutation was targeting variant *XI* 3'UTR and removed the majority of the sequence. Previous publications about the *furina* protein truncation mutants have reported the phenotype. Therefore, the rationale for this experiment was to compare both mutants and uncover potentially novel functions of the 3'UTR of variant *XI* (Walker *et al.*, 2006; Tessadori *et al.*, 2015; Zhou *et al.*, 2021). CRISPR-Cas9 technology is a robust method for generating mutations in tissue culture as well as animal models such as fish, mice and flies. It is highly popular in research laboratories because it is fairly simple, quick and inexpensive. There are different variations of genome editing with the Cas9 enzyme,

however for this study Cas9 from *S. pyogenes* was used. To generate mutations in zebrafish embryos Cas9 mRNA or protein has to be injected together with a guide RNA (gRNA). This is a single-stranded sequence that contains a complementary region to the target and allows the Cas9 to bind and generate mutations in the required region (Ran *et al.*, 2013; Thyme *et al.*, 2016).

The strategy for generating a *furina* knockdown fish line was to use two Guide RNA (gRNAs) to create a deletion that would remove a start codon and a large proportion of signal peptide. Pro-FurinA protein self cleaves at the signal peptide to be activated, if the signal peptide sequence is disrupted the protein is trapped in the endoplasmic reticulum in a cell and consequently becomes non-functional (Vey *et al.*, 1994). The ChopChop software tool (Thyme *et al.*, 2016) was used to design optimal gRNAs to target exon 2 of *furina*. The gRNA sequences were selected based on their predicted efficiency, the number of mismatches required to target different sequences, and self-complementarity (Thyme *et al.*, 2016). As shown in Figure 3.7 A and B schematics, the first gRNA was designed 20 bp upstream of the first methionine and the second gRNA was designed within the first 40 bp of the signal peptide. The final size of the deletion was predicted to be approximately 50 bp. To generate stable mutant fish, we used germline specific Cas9:nanos mRNA and injected it together with the gRNAs into zebrafish embryos. Samples were grown to adulthood and then the F0 generation was screened with PCR and positive samples were sequenced to confirm the deletion.

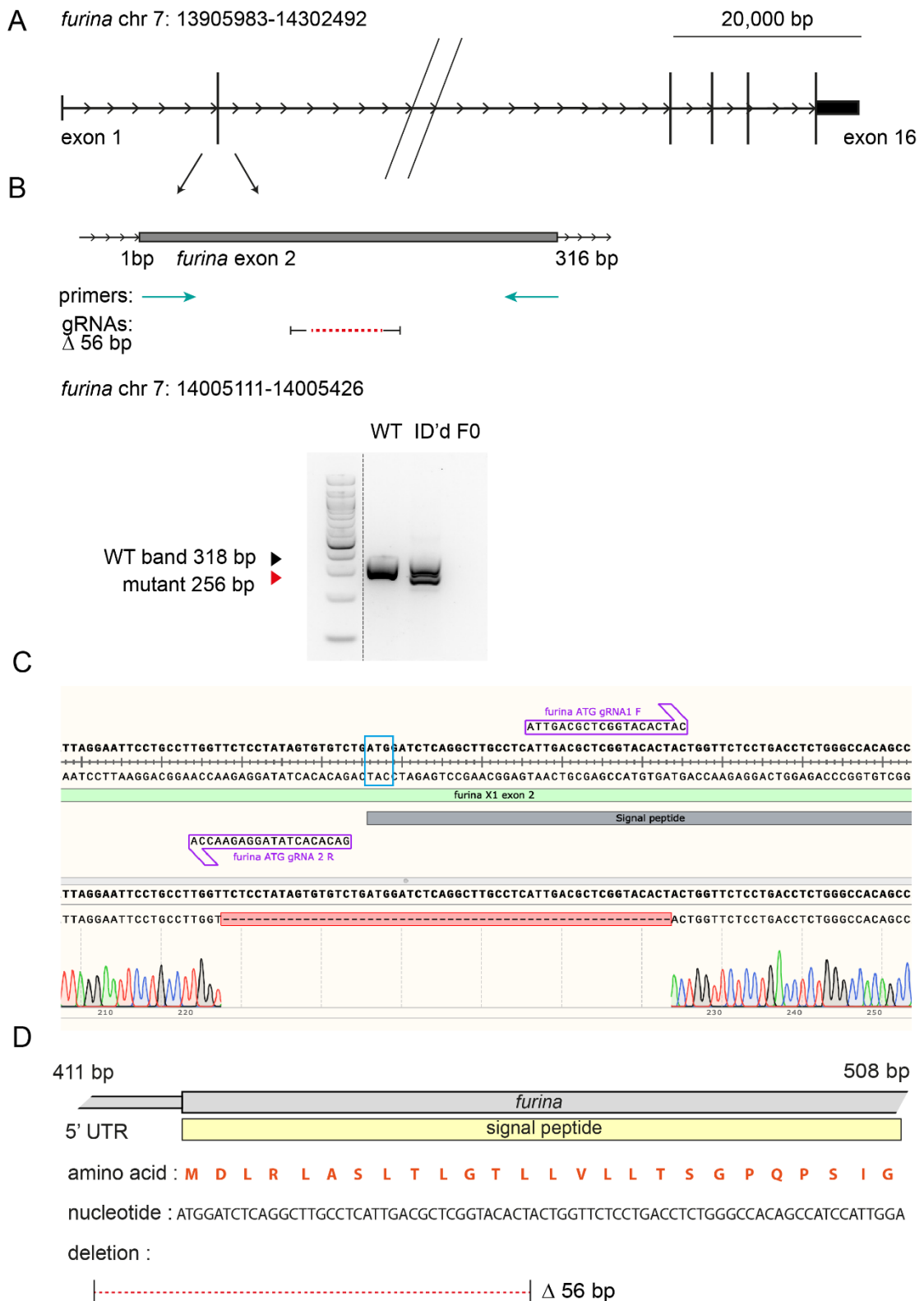


Figure 3.7 Generating *furina* protein knockout.

A) Schematic of *furina* locus *X1* on chromosome 7. In the top right corner scale of the locus for reference 20,000 bp.

B) Schematic of the *furina* exon 2, showing primers designed for locus amplification and below there is a red dotted line to highlight the region of deletion in relation to the rest of the exon. Under schematic there is a genotyping gel, that shows a wild type embryo control on the left and on the right side, there is a heterozygous embryo for the deletion. 100 bp ladder was used in this agarose gel.

C) Sequencing results excerpt from a mutant embryo positive for a $\Delta 56$ bp deletion aligned to the wild type sequence at the top. The gRNAs are shown in purple and a blue box highlights the start codon ATG of *furina*. The red line between the peaks indicates the absence of nucleotides.

D) Schematic of the *furina* transcript sequence, including 5'UTR, CDS and signal peptide, amino acid and corresponding nucleotide sequences. The red dotted line shows the region of $\Delta 56$ bp deletion and which amino acids are consequently removed.

Figure 3.7 B shows an example of the genotyping agarose gel result. On the left side, there is a wild type control amplification of the *furina* locus from genomic DNA. On the right side, however, there are two bands. The top band is a wild type and the lower band is a mutant band. Both PCR bands were purified and sequenced to confirm that deletion has occurred and to determine its length. The positive sequencing results for mutation are shown in Figure 3.7 C. These results also revealed that the mutagenesis started 4 to 7 bp downstream from the PAM sequence, which serves as a binding signal for Cas9 protein. Interestingly, I found that the deletion was 56 bp, as expected, starting 11 bp downstream from the start codon and continued for 45 bp within the CDS as illustrated in Figures 3.7 C and D. Next, in panel 3.7 D I aligned the sequence of the mutant embryo, positive for $\Delta 56$ bp deletion to a wild type protein sequence and compared them to analyse the effects of this deletion. I found that this mutation removed 13 amino acids, including a start codon. Additionally, from the last codon, which should synthesise leucine, it removed the first nucleotide, which effectively knocks the entire *furina* protein sequence out of frame, as shown in 3.7 D.

From this analysis, I concluded that the $\Delta 56$ mutation will generate null *furina* protein zebrafish embryos. This mutation was propagated by further outcrossing mutants with

a wild type fish. Additional outcrosses with wild type fish ensure that any off-target mutations that could arise from using genome editing techniques are not dominantly expressed and so will not interfere with the study. Finally, the heterozygous F2 generation of fish was incrossed to obtain homozygous mutants. In the literature, it has been reported that only 20% of homozygous *furina* mutant females survive to adulthood, therefore F2 generation of fish was incrossed multiple times to raise as many fish as possible and optimise the chance of retrieving homozygous females fish for $\Delta 56$ bp deletion (Tessadori *et al.*, 2015).

While waiting for the F2 generation incross to mature and be ready to be used for experiments, I started incrossing heterozygous fish from generation F2 to observe if there is an early phenotype that can be detected in zebrafish larvae. I obtained zygotic mutants from the $\Delta 56$ bp heterozygous incross and at the 5 dpf, I was able to distinguish homozygous mutants from heterozygous or wild type larvae, due to key phenotypic differences. Figure 3.8 A shows an image of the wild type larva at 5 dpf from a heterozygous $\Delta 56$ bp incross, with perfectly normal morphology. In panel 3.8 B, however, the homozygous larva has a slightly different jaw, and mild oedema of the heart and it also did not develop a swim bladder. This is consistent with previous findings of other *furina* mutants such as the *ace of hearts* and *pku338* (Tessadori *et al.*, 2015; Zhou *et al.*, 2021). I confirmed the genotype of the fish with PCR and was able to conclude that I successfully generated *furina* null protein mutants and observed a preliminary phenotype.

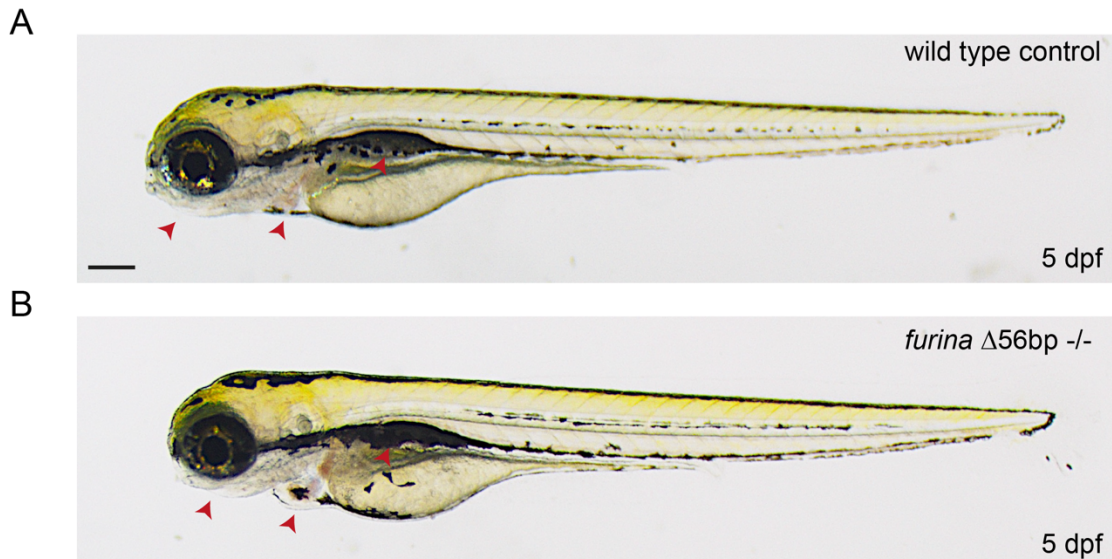


Figure 3.8 *Furina* Δ56 bp zygotic mutants show a range of defects at the 5 dpf.

A) Wild type larva at 5 dpf from the Δ56 bp heterozygous incross clutch of embryos. Key areas jaw, heart and swim bladder are highlighted with red arrowheads for comparison to mutant embryos. Scale Bar, 200 μm

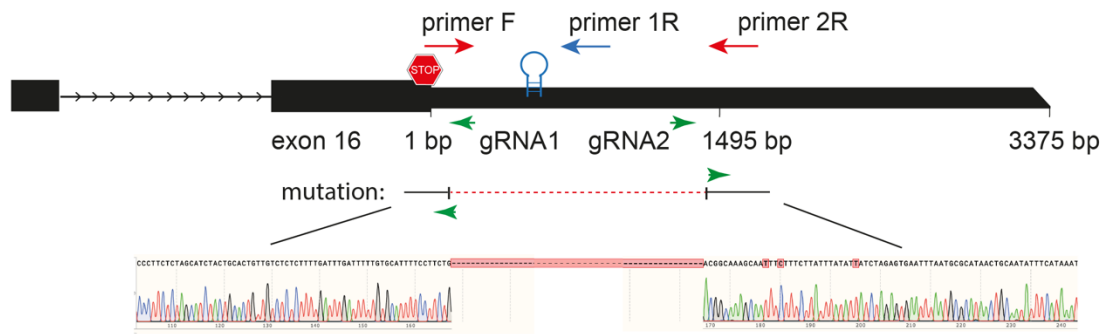
B) Homozygous Δ56 bp larva at 5 from heterozygous incross. Red arrowheads point to jaw defects, cardiac oedema and lack of swim bladder.

To uncover the role of the *furina XI* variant, a 3'UTR mutation was generated using CRISPR/Cas9. Variant *XI* has a long 3'UTR and two gRNAs were used to generate a deletion as shown in the schematic in Figure 3.8 A. The first gRNA is 59 bp and the second one is at 1377 bp downstream of the *furina XI* stop codon, together they remove 1.3 kb of the sequence of the 3UTR and also the YBE motif. Additionally, to ensure that the transcript is stable after generating deletion, the poly(A) signal at the end of the 3'UTR was left intact.

Figure 3.9 A and B show the strategy to genotype fish for a Δ3'UTR mutation. Three primers were used in a single PCR reaction, with the forward primer at the beginning of the 3'UTR, the first reverse primer (shown in blue) was designed to amplify the wild type band, and a second reverse primer amplifies the sequence after the second

gRNA. The wild type band was 404 bp and the mutant band indicating removal of a 1.3 kb of the 3'UTR was 180 bp. The amplified bands were sequenced and it was confirmed that the deletion was present in embryos, then the mutant sequence was aligned to the wild type sequence as shown in Figure 3.9 A.

A *furina* chr 7: 14192829-14207006



B

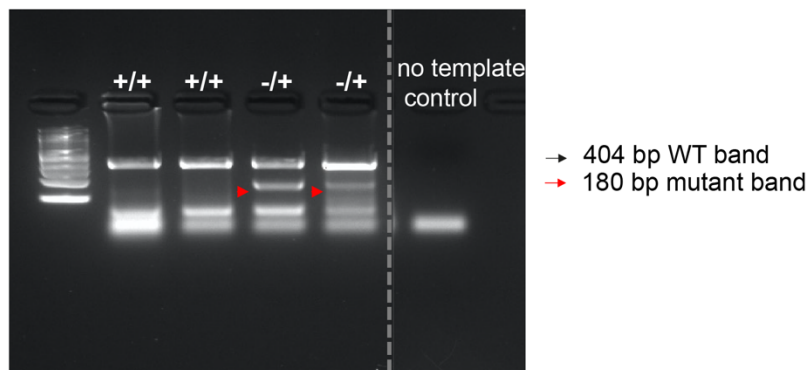


Figure 3.9 Generating *furina* XI Δ 3'UTR mutation in zebrafish.

A) Schematic of the *furina* transcript XI 3'UTR in chromosome 7, exon 16 has an end part of the CDS and the entire 3375 bp of the 3'UTR. The stop sign indicates a stop codon, the blue hairpin shows YBE motif gRNAs are in green, genotyping primers outside the gRNAs are red arrows, and the blue arrow is the internal primer amplifying wild type band. The red dotted line shows the part of the 3'UTR removed, below are the sequencing results from a mutant embryo aligned to wild type genome.

B) PCR result showing wild-type samples in lanes 1 and 2, lanes 3 and 4 show heterozygous fish. The fifth lane is a no template control. Wild type band is 404 bp and 180 bp is a mutant band.

Generating the *furina* Δ 3'UTR mutant locus was much more difficult than the *furina* protein knockout fish line. As was mentioned above, *XI* 3'UTR has many repeats of sequences and AT-rich residues. This made the gRNA design and genome editing with CRISPR very challenging and time consuming. Similarly, to when generating Δ 56 bp locus, identified variant *XI* Δ 3'UTR heterozygous fish were outcrossed twice in a wild-type background and then incrossed and grown to adulthood to generate homozygous fish. However, I was not able to retrieve homozygous fish.

3.3 DISCUSSION

In this chapter, I describe a novel *furina XI* isoform and analyse its expression at different developmental stages of the zebrafish embryos. I show that the sequence of the computationally predicted variant *XI* is expressed in zebrafish embryos. Extensive PCR amplifications and sequencing results confirm that the sequence prediction from the genomic databases such as UCSC and ensembl is correct. I find that variant *XI* and *furina* transcript 1 have the same expression patterns at the 4-cell stage, bud, 10 and 18 som, as shown in Figure 3.6. The real time PCR analysis in Figure 3.5 revealed that at the 10-som stage, there is significant upregulation of variant *XI* expression. In other developmental stages, however, there is no difference in expression levels in both transcripts. This particular result was interesting, because in zebrafish during somitogenesis Nodal related-3, Spaw is expressed and cleaved by FurinA protein. Spaw is expressed on the left side of the embryo and is important in the establishment of left-right asymmetry (Tessadori *et al.*, 2015). This suggests that FurinA upregulation occurs just prior to the expression of Spaw in lateral plate mesoderm. Therefore there is a possibility that *furina* variant *XI* might contribute to the organ positioning via interaction with Spaw. This hypothesis, however, requires additional studies and is explored further in the next chapters.

Owing to duplications in the genome, annotations of the zebrafish genome quite often have errors and are less reliable compared to human or mouse datasets. Therefore, it was necessary to carefully check the sequence of *furina* variant *XI*. Various PCR fragments were amplified, as shown in Figures 3.2, 3.3 and 3.4, and were then extracted, purified and sequenced. The sequencing results for these regions were identical to gene predictions in UCSC and ensembl browsers. Out of the prediction of 3870 bp of variant *XI* 3'UTR, 3579 bp were amplified with R8 reverse primer. Primer R9 which was shown in Figure 3.3 was located at the end of predicted variant *XI* 3'UTR and it did not amplify in any of the zebrafish cDNA libraries. One of the causes could be long stretch of guanine and thymine (GT) nucleotide repeats within the sequence that prevented efficient PCR amplification. Another likely reason might be that it is not found in variant *XI* 3'UTR. According to the ensembl database primer R9 is located outside predicted exon of variant *XI*. Therefore, I did not pursue this issue further. I obtained sufficient evidence that the *XI* variant is expressed in fish and was able to amplify almost the entire sequence including the YBE motif.

Interestingly when comparing the genomic databases I looked at the *Furin* 3'UTR in mammals and found that in mice *Furin* transcript 3'UTR is 1513 bp and in humans, it was approximately 1579 bp. There are also some isoforms of human and mouse *Furin* annotated, but these mostly have few nucleotide differences within the CDS and the 3'UTR sequence is the same in all of them. This suggests that the *furina* variant *XI* long 3'UTR is a zebrafish specific phenomenon and is not found in *Furin* orthologs in mammalian species (<https://www.ensembl.org/index.html>).

Another important part of this chapter is generating CRISPR-Cas *furina* protein and *XI* 3'UTR mutants. The rationale for making these two alleles was to be able to compare mutations affecting the non-coding regions and the CDS of *furina*. Generation of both deletions was confirmed by sequencing and F0 generation from $\Delta 56$ bp and $\Delta 3'$ UTR was outcrossed twice to wild type background fish to minimise non specific phenotype. There are currently a few *furina* knockout fish mutants that have been published and their function was described in scientific journals. There are

Sturgeon^{tg419}, *ace of hearts* and *pku338*. *Sturgeon*^{tg419} has been identified during a genetic screen and was mapped to the *furina* locus, it has a C to A nucleotide change, which results in a premature stop codon in a catalytic domain of *furina* protein (Walker *et al.*, 2006). *Ace of heart* causes a G to A nucleotide substitution that also changes tryptophan at 411 amino acid into a premature stop codon in a catalytic domain (Tessadori *et al.*, 2015). Finally, the recently published *pku338* mutant has a nucleotide change from 637 to 641, which causes FurinA to be out of frame after the propeptide domain (Zhou *et al.*, 2021). As shown in Figure 3.7 *furina* Δ 56 bp locus removes 11 nucleotides of the 5'UTR and 45 nucleotides of the CDS. This removes the first methionine start codon, 13 amino acids from the signal peptide and changes the open reading frame of the FurinA protein. The phenotypic effects of *furina* mutations *Sturgeon*^{tg419}, *ace of hearts* and *pku338* are fairly similar. Embryos exhibit open jaw defects, heart looping and trabeculation defects, cardiac oedema, fin ruffling and lack of swim bladder. Although the Δ 56 bp allele has not been studied in such depth, the preliminary data suggests that these mutants exhibit a similar phenotype, as the open jaw, cardiac oedema and lack of swim bladder have been observed in all zygotic homozygous mutants from heterozygous incrosses as shown in Figure 3.8.

Generating a *furina XI* Δ 3'UTR large deletion by CRISPR was challenging, due to the lack of appropriate target sites for the gRNAs. To date, there has not been a *furina* 3'UTR mutant generated in zebrafish. Multiple gRNAs were tested and finally, only two showed efficient cleavage. In Figure 3.9 there is a schematic of variant *XI* locus, gRNAs are marked with red arrows and when co-injected with Cas9 mRNA into zebrafish embryos they remove 1323 bp of the 3'UTR. This includes a YBE motif, which may have a regulatory function in the variant *XI*. The final half of the transcript 3'UTR with poly(A) signal at the end of the variant *XI* transcript has been left intact and is not affected by Δ 3'UTR deletion. There were concerns that the removal of the entire variant *XI* 3'UTR sequence may affect the stability of the transcript. I have not retrieved homozygous mutants yet and heterozygous in-crosses of the F2 generation of Δ 3'UTR fish have not revealed any obvious preliminary phenotypes.

When making CRISPR mutants it is worth noting that in fish there is also an ortholog to FurinA, called FurinB expressed. There have been numerous studies emerging about genetic compensation and how the loss of one gene can trigger increased expression of a gene with an overlapping function (El-Brolosy and Stainier, 2017). It was suggested in the literature that the FurinA ortholog called FurinB may have redundant functions and compensate in some cases when FurinA expression is absent. FurinA and FurinB share high protein sequence similarity and conservation of key domains such as the prodomain, a catalytic domain and the P domain. One of the factors in the variation of the jaw phenotype in *furina* mutant fish was the result of compensation by *furinb* (Walker *et al.*, 2006). However, the sequence of the *furinb* 3'UTR is only 166 bp and no additional isoforms have been described.

Previous reports in the literature have shown that endogenous *furina* mRNA is expressed ubiquitously in embryonic development with slight enrichment in somites (Walker *et al.*, 2006; Tessadori *et al.*, 2015). Analysis of the expression patterns of *furina* transcript 1 and variant *XI* in Figure 3.6 shows similar results, I consistently observed ubiquitous expression of endogenous transcripts at all stages. There was an exception at 10 and 18 som, however, because both transcripts showed slight enrichment in the hindbrain and eyes. It would have been interesting to explore this further, as this enrichment suggests that *furina* might be important in the genetic pathways involved in the development of these structures.

In conclusion in this chapter, I analysed a novel *furina* variant *XI* sequence and expression. I show the expression patterns between two transcripts are identical and I also generated two fish lines with mutations on different loci. One mutation causes knock out of FurinA protein and the second mutation deletes a large proportion of *furina* 3'UTR in variant *XI*. As shown in the early schematic in Figure 3.1, variant *XI* 3'UTR has a YBE motif, which has an AGCAC sequence and a 3 base stem loop. A similar RNA motif has been already annotated in the nodal pathway components in the Sampath laboratory in *sqt*, *lefty1* and *lefty2* and has been shown to be a target of RNA binding protein Ybx1. This mechanism has been shown to cause translational

repression and control the premature expression of Sqt, Lefty1 and Lefty2 proteins (Gore *et al.*, 2005; Kumari *et al.*, 2013; Zaucker *et al.*, 2017). In the next chapter, this RNA motif is characterised in *furina* variant *X1* and its potential function is explored.

CHAPTER 4
TRANSLATIONAL CONTROL BY YBX1
RNA BINDING PROTEIN

4.1 INTRODUCTION

RNA localisation is essential in living organisms for a cell to be able to carry out physiological functions. In the cytoplasm, RNA localisation establishes cell polarity and allows interactions with various proteins (Medioni, Mowry and Besse, 2012; Blower, 2013). In early *Drosophila* embryos, the localisation of *bicoid* and *oskar* mRNA establishes anterior-posterior axis formation. *Bicoid* mRNA localizes to the anterior of the oocyte using microtubule-dependent machinery. This requires the presence of the Exu protein that stimulates translation of the Bicoid protein gradient. As a result, the formation of the head and thorax occurs in fly embryos. However, *oskar* mRNA localizes to the posterior of the embryo, after which its translation is initiated and consequently the pole plasm forms, which is the *Drosophila* germ plasm equivalent (Chang *et al.*, 2011). This is an example of how mRNA localisation affects embryonic development and morphogenesis.

Additionally, RNA localisation allows translational repressors to modulate the expression of various proteins at the appropriate time points in development. In zebrafish, the maternally contributed Nodal signalling ligand *sqt* localises to dorsal progenitors at the 4-cell stage (Gore *et al.*, 2005). This process is important as the dorsoventral axis formation determines the basic body plan of an early embryo (Gore *et al.*, 2005). Injection of a fluorescently labelled *sqt* mRNA reporter at the 1-cell stage resulted in the RNA localisation towards the two blastomeres and at the 4-cell stage recapitulated endogenous localisation. Disruption of microtubules using inhibitors has prevented localisation and also resulted in an aberrant dorsal axis. This led to the conclusion that RNA localisation determined how the dorsal axis is formed in zebrafish embryos (Gore *et al.*, 2005; Gilligan *et al.*, 2011). Further experiments showed that the 3'UTR of *sqt* was required for the localisation to occur at the 4-cell stage. Analysis of the 3'UTR sequence via different reporter constructs has shown that there is an 'AGCAC' sequence motif followed by a stem and a loop that plays a key role in the asymmetric localisation of the *sqt* RNA. Deletions of the 3'UTR motif within the fluorescent mRNA reporter reduced the RNA localisation by 75% in the

embryos. The deletions of the AGCAC sequence or a stem separately caused a reduction of localisation by 40% and changing the sequence within the loop had no further effect on the RNA localisation (Gilligan *et al.*, 2011). This led to the conclusion that the sequence and the stem-loop structure were important for the mRNA's ability to localise.

Proteomic analysis has shown that a likely candidate for interaction with *sqt* 3'UTR is a ubiquitously expressed RNA-binding protein (RBP) Ybx1 (Kumari *et al.*, 2013). Ybx1 is a very well conserved nucleic acid-binding protein, and mammalian studies have demonstrated its importance in processes such as translation, mRNA packaging and regulation of mRNA stability. The Ybx1 family of proteins is named after its ability to bind a short sequence on a DNA strand: 'CTGATTGG', which is called a Y-box sequence (Lyabin, Eliseeva and Ovchinnikov, 2014; Prabhu *et al.*, 2015). Additionally, *in vitro* studies have shown that it can compete with proteins facilitating translation such as eIF4F complex and PABP for binding on the mRNA strand and consequently cause translational repression (Lyabin *et al.*, 2011).

In vivo binding assays confirmed that Ybx1 protein was binding to the *sqt* RNA motif. In the *ybx1* mutant embryos, endogenous *sqt* mRNA is not localised. Additionally, translation of Sqt protein occurs prematurely and is followed by its accumulation in the yolk. Consequently, embryonic specification occurs too quickly and there is a yolk syncytial layer expansion. Finally, severe gastrulation defects cause embryonic lethality (Kumari *et al.*, 2013; Sampath and Robertson, 2016). Interestingly, transcriptome analysis has shown that other Nodal pathway components harbour the 3'UTR RNA motif. Inhibitors *lefty1* and *lefty2*, also contain the 3'UTR motif and their fluorescent mRNA reporters localise to the blastomeres at the 4-cell stage. This shows a well conserved regulatory mechanism within the Nodal pathway in zebrafish (Zaucker *et al.*, 2017). Another interesting candidate identified in transcriptome analysis was a pro-protein convertase FurinA. As described in Chapter 3, zebrafish *furina* has two transcripts and one of them, the computationally predicted transcript

XI, has a YBE motif in the 3'UTR. In this chapter, the YBE motif in *furina* variant *XI* is analysed and the interaction of *furina* mRNA with the Ybx1 protein is studied.

The aims of this chapter are:

- To validate the 3'UTR element in variant *XI furina*
- To determine if there is an interaction between Ybx1 protein and *furina* mRNA
- To examine if Ybx1 translationally represses *furina*

4.2 RESULTS

The RNA secondary structure is important for interactions with RNA binding proteins (Gilligan *et al.*, 2011). As mentioned in Chapters 1 and 3, studies from the Sampath laboratory have shown that the YBE motif in the 3'UTR causes asymmetric RNA localisation at the 4-cell stage and Ybx1 RBP binds to the YBE motif (Gore *et al.*, 2005; Gilligan *et al.*, 2011; Kumari *et al.*, 2013) Wider transcriptome analysis has shown that many Nodal pathway components have the YBE motif in the 3'UTR. This could indicate that this regulatory mechanism has a broader relevance in the Nodal signalling pathway (Zaucker *et al.*, 2017). In Figures 4.1 A and B the identified mRNAs with the motif are illustrated. Within the Nodal signalling pathway, ligand *sqt*, the inhibitors *lefty1* and *lefty2*, the receptor *acvr2*, the intracellular transducer *smad2* and the pro-protein convertase *furina* all contain the motif in the 3'UTR. Nearly all of the identified YBE motifs contained AGCAC sequence followed by a three base stem and a loop, however, interestingly in *smad2* there is a four-base stem. Additionally, it is also worth noting that Nodal ligands: *spaw* and *cyclops*, receptor *acvr1*, EGF-CFC, *smad3* and *smad4* do not have the YBE motif in their 3'UTR.

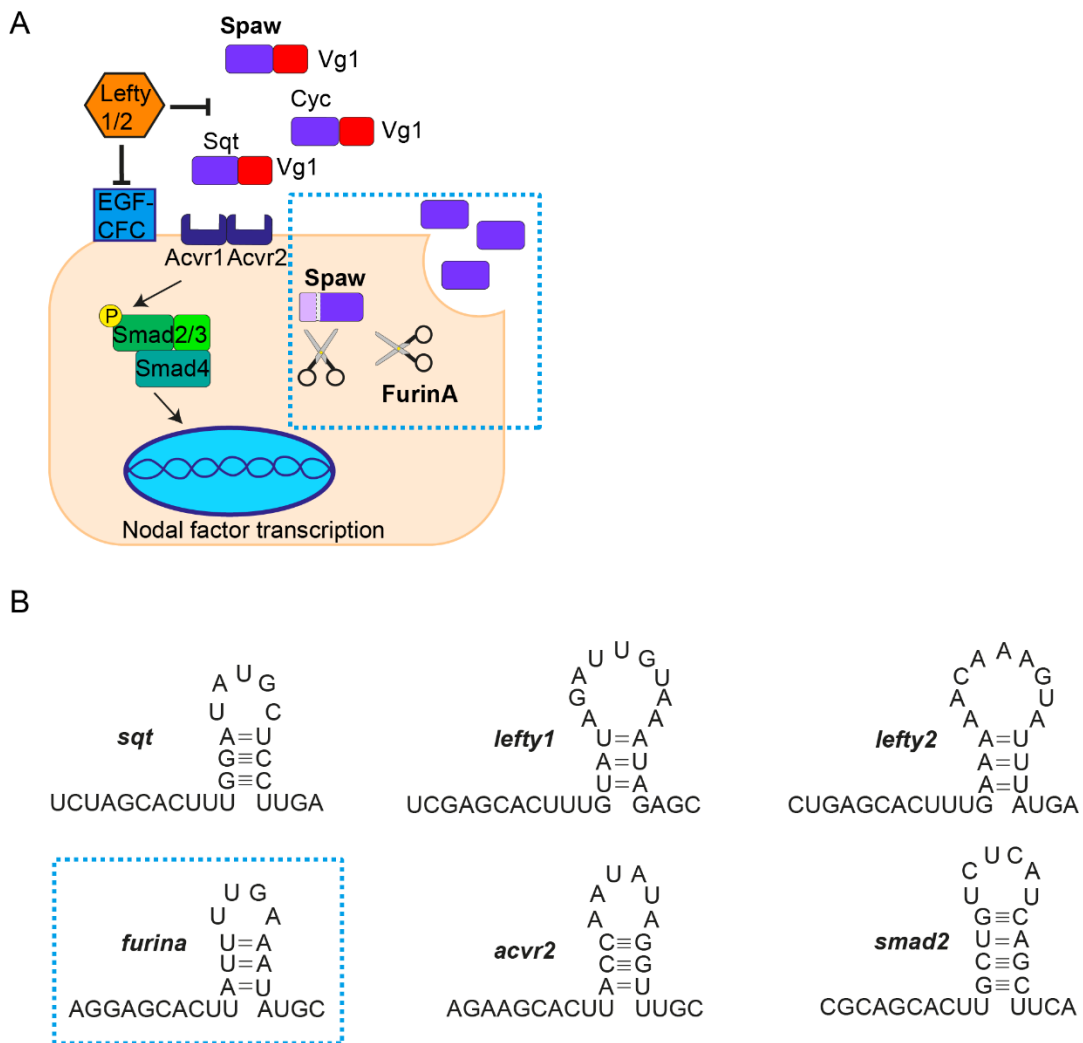


Figure 4.1 Nodal pathway components have the YBE motif.

A) Nodal pathway schematic showing zebrafish Nodal ligands: Sqt, Cyclops, Spaw forming heterodimers with Vg1. Lefty 1 and Lefty 2 inhibitors of the Nodal signalling. Acvr1 and Acvr2 receptors, Co-receptor EGF-CFC. Intracellular transducers Smad2/3 and proprotein convertase FurinA.

B) Nodal pathway transcripts were found to contain the YBE motifs in the 3'UTR. The blue box highlights *furina* transcript *XI*

In this study, I was interested in the YBE motif in the *furina* variant *XI* 3'UTR and therefore I decided to analyse the RNA element further. To determine if the YBE motif

in *furina* mRNA was functional, I utilized a previously developed localisation assay protocol. Fluorescent mRNA reporters with YBE motifs localise asymmetrically at the 4-cell stage in zebrafish embryos. To find out if *furina* was indeed localising, I co-injected *lefty1* and *furina XI* fluorescent mRNA reporters labelled with a different fluorophore. Fluorescent *lefty1* mRNA served as a positive control. In Figure 4.2 there is a schematic of the experiment where embryos were injected at the 1-cell stage and then examined for localisation at the 4-cell stage (Gore *et al.*, 2005; Gilligan *et al.*, 2011; Zaucker *et al.*, 2017). Consistent with previous studies, in Figure 4.2 I observed that at the 4-cell stage fluorescent mRNA reporters *lefty1* and *furina* were tightly localising to the blastomeres in the exact cells. This result was observed in all injected embryos (n=11). From the co-localisation assay I concluded that the YBE motif in *furina* mRNA is functional and likely to behave in the same way as Nodal ligand *sqt*, and inhibitors *lefty1* and *lefty2*.

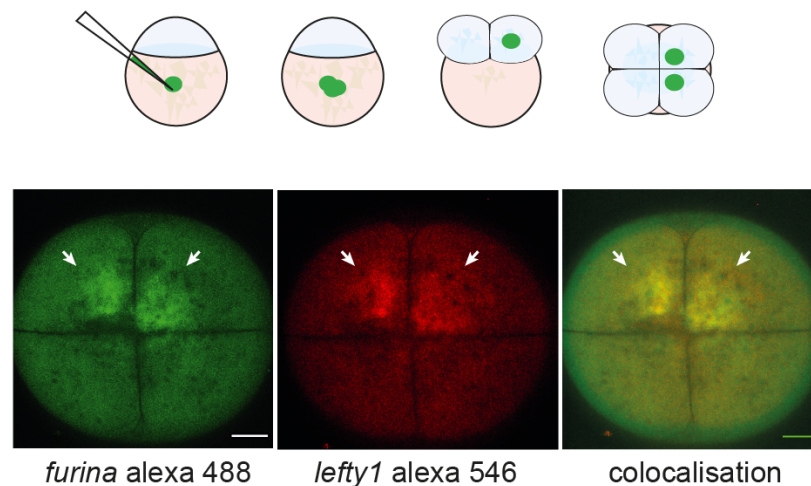


Figure 4.2 Fluorescent mRNA reporters for *furina* and *lefty1* mRNAs co-localise at the 4-cell stage in zebrafish.

Schematic of the localisation experiment at the top panel showing mRNA reporter injected in the yolk at the 1-cell stage and then asymmetrically localising at the 4-cell stage. Below are confocal images showing fluorescent localisation of *furina* mRNA reporter labelled with Alexa 488, *lefty1* mRNA reporter with Alexa 546 separately and then merge image of co-localisation. The scale bar corresponds to 50 μm . Arrows point to fluorescently labelled mRNA.

To verify that the 3'UTR motif in *furina* is required for RNA localisation, various constructs with deletions of the YBE motif were generated. The first construct was *furina* Δ YBE, which consisted of complete deletion of the motif. Next, the *furina* stem break resulted in breaking the bonding within the stem, disrupting the entire hairpin structure of the element. Finally, the *furina* stem restore construct, which has the sequence within the stem swapped but does not affect the bonding. *Sqt* mRNA served as a positive control construct and *lacZ*- β globin was a negative control. All constructs were synthesized as mRNA reporters labelled with Alexa 488 or 546 fluorophore, injected into 1-cell stage embryos, and their localisation was examined at the 4-cell stage. As illustrated in Figure 4.3, I observed three distinct categories of mRNA localisation. Localised asymmetric, which was shown in Figure 4.2. Diffuse asymmetric embryos have fluorescence asymmetrically distributed across 1 or 2 cells. The final category is diffuse and it consists of embryos with evenly distributed fluorescence in all 4 cells.

All of the injected embryos were given a category and were included in the graph in Figure 4.3. As expected the positive control, *sqt* fluorescent mRNA reporter was localised in 95% of the embryos, which is indicated with green colour for the localisation category. *LacZ* does not have a 3'UTR motif and in approximately 95% of the embryos was diffuse everywhere, as shown in red. Interestingly, the third result in Figure 4.3 is the *furina* variant *XI* mRNA reporter and it localised in 75% of the embryos, whereas 20% of the embryos were diffuse asymmetric and 5% diffuse. The deletion of the YBE motif in variant *XI* resulted in disruption of the RNA localisation, resulting in 55% of embryos showing diffuse localisation and 35% being diffuse asymmetric. The breaking of the stem in the YBE motif of the *furina XI* variant mRNA reporter had a similar effect on the localisation, as it was reduced in embryos by 35% when compared to wild type mRNA. In addition, 50% of embryos were diffuse asymmetric and 15% were diffuse. Restoration of the bonding of the stem slightly increased the localisation, as was observed in 55% of embryos. In the remaining embryos, about 25% were diffuse asymmetric and 20% were diffuse.

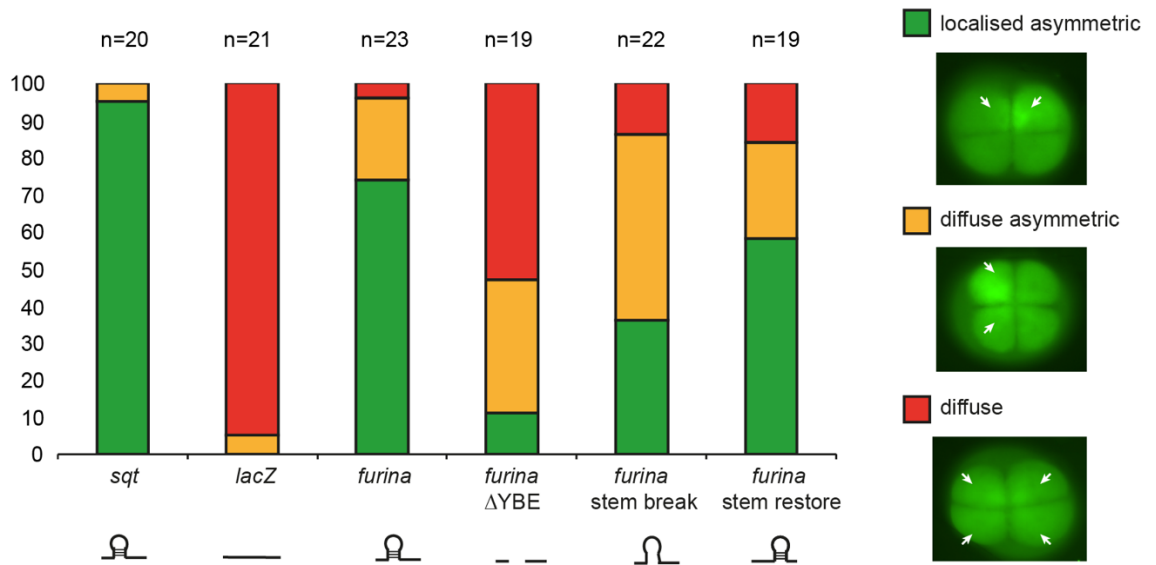


Figure 4.3 Disruptions of the YBE motif affect localisation at the 4-cell stage embryos.

On the right categories of the mRNA localisation used in the assay with corresponding microscopy images: localised asymmetric is shown in green, diffuse asymmetric is shown in yellow and diffuse is in red. Arrows point to fluorescently labelled mRNA. The left panel showed the proportion of localisation categories per given fluorescent mRNA reporters *sqt*, *lacZ*, *furina*, *furina* ΔYBE, *furina* stem break and *furina* stem restore. Below the graph are schematics showing predictions of how each mutation affects the hairpin structure of the 3'UTR motif. Arrows point to fluorescently labelled mRNA.

From the localisation assay, I learned that the 3'UTR motif is important for the mRNA localisation at the 4-cell stage in zebrafish embryos. I was also able to conclude that the behaviour of *furina* variant *X1* fluorescent reporter is similar to what was observed with *sqt*, *lefty1* and *lefty2*. Disruption of the 3'UTR element resulted in a reduction of localisation and most of the embryos having fluorescent mRNA diffuse across all cells in the blastoderm. However, when the stem loop structure was restored in the *furina* mRNA reporter, the proportion of localised embryos also increased. This shows that

the hairpin structure has a key role in directing the RNA to the correct place in the cell.

Previously published studies have shown that mRNA localisation was important for interaction with the Ybx1 RBP (Kumari *et al.*, 2013; Zaucker *et al.*, 2017). Ybx1 is a global translational repressor but also interacts with specific sequences of mRNAs (Sun *et al.*, 2018). *In vitro* binding assays have shown that Ybx1 binds directly to the 3'UTR YBE motif in *sqt*, *lefty1* and *lefty2* (Zaucker, Kumari and Sampath, 2019). I was interested to find out if Ybx1 binds to *furina* mRNA *in vivo*. The RT-PCR and qPCR analysis described in Chapter 3 have shown that the expression of the *furina XI* variant was most prominent during somitogenesis. I decided to use similar developmental stages as in Figure 3.2 because that was when variant *XI* is expressed at the highest levels, and it is more likely to be in a complex with Ybx1. To determine if there is *furina* interaction with Ybx1, I collected 50% epiboly, 10 som and 18 som embryonic lysates and did RNA immunoprecipitation (RNA IP). In Figure 4.4 A, I show how the experiment was performed. Following elution of the Ybx1 protein bound with mRNAs, the sample was split in half for qPCR and western blot analysis. I was able to pull down Ybx1 protein efficiently at 50% epiboly and 10 som as shown in Figure 4.4 B western blot gel. At 18 som, however, the amount of protein found was much lower when compared to other embryonic stages.

As shown in the schematic in Figure 4.4 A, the extracted RNA from the RNA IP samples was used to prepare cDNA libraries and ultimately perform qPCR analysis. Previous studies have shown that Ybx1 pulls down *lefty1* mRNA, therefore it served as a positive control in the qPCR analysis (Zaucker *et al.*, 2017). The analysis of the qPCR results revealed that *lefty1*, shown in blue in Figure 4.4 C, was largely enriched at 50% epiboly and to a lesser extent at the 10-som stage. Both amplifications for *furina* coding region (CDS) shown in orange on a graph and *furina* 3'UTR *XI* shown in grey were detected at comparable levels and were enriched at both 50%-epiboly and 10-som stages. Ribosomal 5S amplification shown in yellow served as a negative control to estimate the specificity of the experiment. The negative control was detected

at much lower levels when compared to other samples. At 18 som no enrichment of any samples was detected, which was expected given the little amount of Ybx1 protein being pulled down in the first place.

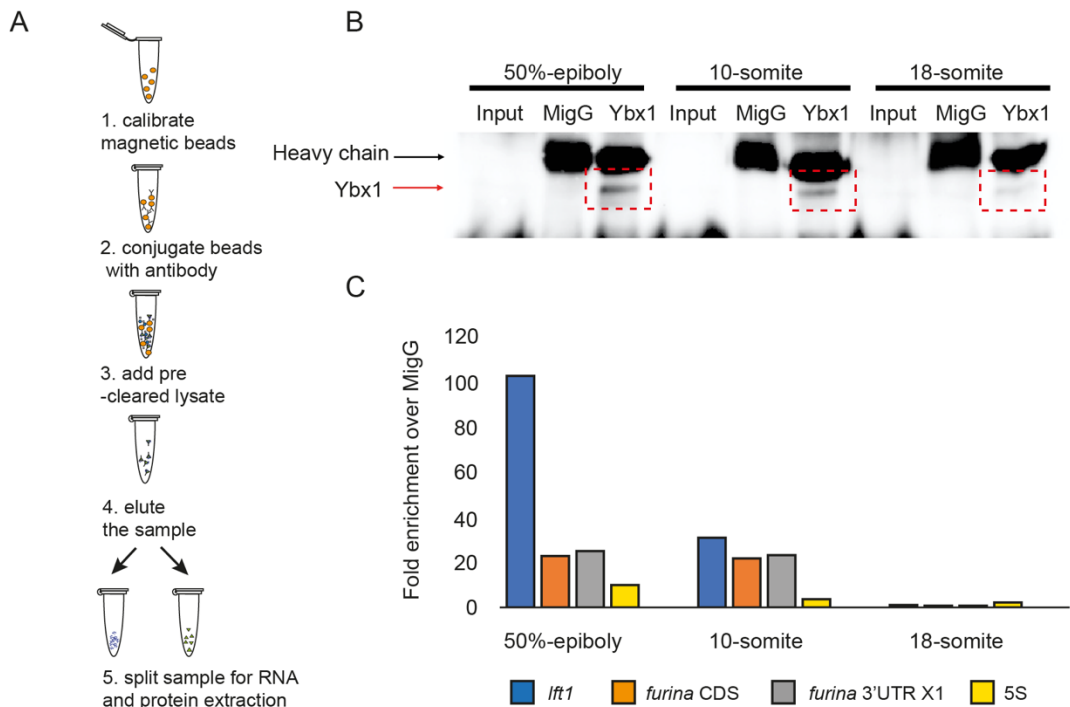


Figure 4.4 Furina mRNA is enriched in Ybx1 pull down in zebrafish.

- Schematic of how the antibody was conjugated to the beads and RNA immunoprecipitation was performed.
- Next western blot from embryonic lysates from 50% epiboly, 10 som, and 18 som showing a Ybx1 band was pulled down (red box). Mouse IgG (MIgG) served as a control per each lane for non-specific interactions, and no Ybx1 band was detected.
- qPCR amplifications for *lefty1* positive control, *furina* CDS, *furina XI* 3'UTR and 5S negative control detected in the RNA IP. Enrichment was calculated from CT values against input and normalised to MIgG controls in accordance with published protocols (Marmisolle, García and Reyes, 2018).

Taken together, the results of the Ybx1 pull down shown from embryonic lysates led to the conclusion that *furina* is enriched and Ybx1 forms complexes with *furina* in

vivo. This was a very promising finding because if Ybx1 protein is being pulled down together with *furina* mRNA this also suggests that it is likely to be involved in the regulation of *furina*.

To be able to study how Ybx1 interacts with *furina*, a previously generated *ybx1^{sa42}* mutant fish line was used. The *ybx1^{sa42}* allele contains a missense mutation in exon 4 of a cold-shock domain (CSD) (Kumari *et al.*, 2013). In Figure 4.5 A the schematic shows the mutation that changes nucleotide guanine (G) to thymine (T). This results in amino acid valine changing into phenylalanine. Ybx1 contains a very well conserved CSD, which is shown in blue in Figure 4.5 B. CSD was first identified in *E. coli* and it retains an ability to be expressed even at low temperatures. Additionally, studies in bacteria showed that when organisms are exposed to cold temperatures the proteins with the CSD increase in expression by 2 to 10-fold, thus protecting cellular integrity (Prabhu *et al.*, 2015). In zebrafish the CSD has been shown to play a critical role in facilitating the binding of Ybx1 protein to the YBE motif, however, the *ybx1^{sa42}* mutation diminishes this function. Additionally *in vitro* assays have shown that the RNP, single-stranded DNA binding domain and dimerization domain are also required for Ybx1 binding to the 3'UTR motif. In contrast mutations to the nuclear localisation signal (NLS), the actin binding domain and the first half of the C terminus are dispensable for RNA binding (Kumari *et al.*, 2013).

Mutations of the Ybx1 protein have also been shown to cause embryonic lethality in zebrafish. Maternal *ybx1* mutant embryos fail to initiate gastrulation movements, and so arrest at epiboly and die. Zygotic *ybx1* mutants, however, do not show severe developmental defects (Kumari *et al.*, 2013; Sun *et al.*, 2018). The schematic in Figure 4.5 B shows that *ybx1^{sa42}* is a temperature sensitive allele. At 28 °C homozygous maternal *ybx1^{sa42}* mutant embryos are viable and indistinguishable from wild types, at 22 °C, however they show gastrulation arrest and enlarged yolk syncytial layer. This phenotype is comparable to other *ybx1* mutant alleles but less severe. Additionally, *ybx1^{sa42}* mutation at 22 °C was rescued by maternal expression of Ybx1 GFP transgene (Kumari *et al.*, 2013).

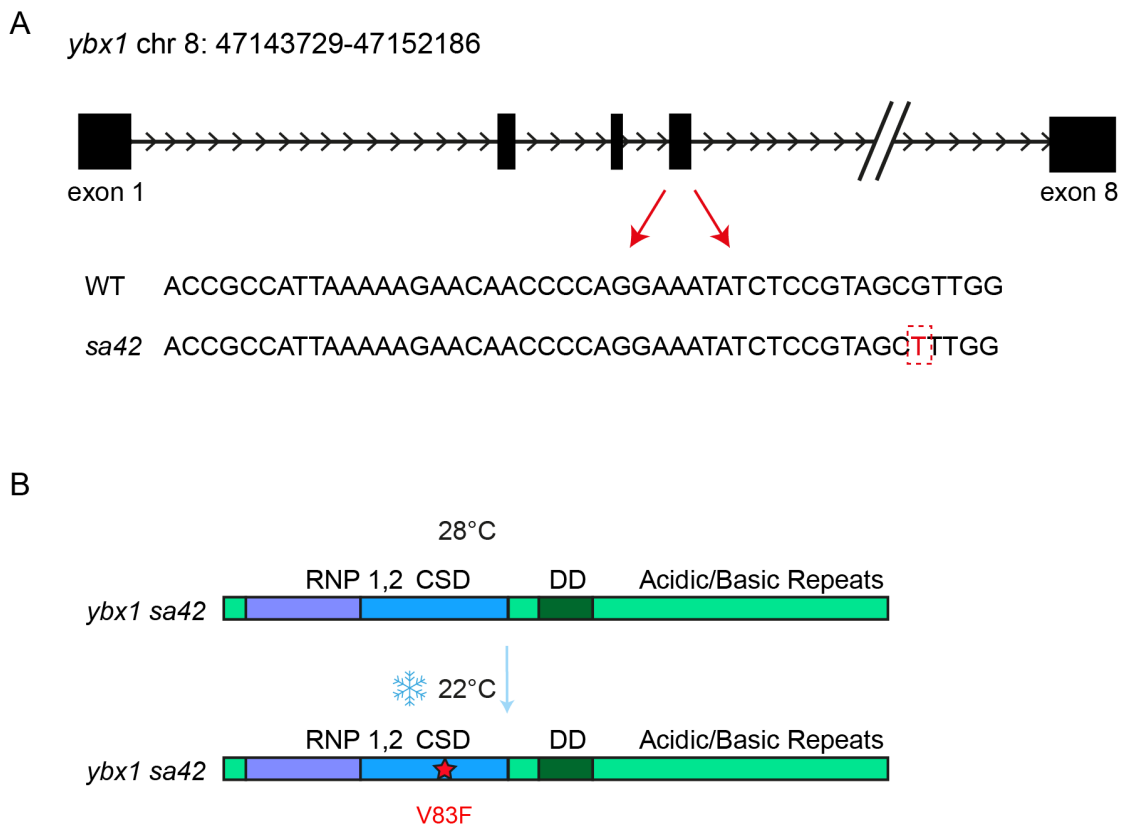


Figure 4.5 *Ybx1^{sa42}* temperature sensitive allele.

A) Schematic of the *ybx1* locus in zebrafish, the *ybx1^{sa42}* mutation is located on exon 4 red arrows pointing to the first 47 bp sequence of exon 4 show the G to T nucleotide change.

B) Schematic of the Ybx1 protein domains purple is single-stranded DNA binding domain (ssDBD), RNA binding domain 1,2 (RNP 1,2) is partially overlapping ssDBD and the cold shock domain (CSD) shown in blue. In dark green, there is a dimerization domain (DD) and light green acidic/basic repeats. Upon temperature shift, the *ybx1^{sa42}* mutation in the CSD gets triggered, as indicated by a red star.

Ybx1 acts as a translational repressor of many mRNAs. I was specifically interested in the translational control of Nodal pathway via a YBE motif. In *ybx1* mutant zebrafish embryos, translation of many mRNA reporters is premature and elevated. Translational control by Ybx1 is therefore essential for the correct development of zebrafish (Kumari *et al.*, 2013; Sampath and Robertson, 2016; Zaucker *et al.*, 2017;

Sun *et al.*, 2018). The next step was to determine if Ybx1 translationally represses *furina* mRNA in embryos.

FurinA is a subtilisin-like proprotein convertase (SPCs), which has a well conserved catalytic domain and a P domain (Beck *et al.*, 2002; Thomas, 2002). I considered using commercially available antibodies, but most of them were specific to the mammalian epitope. The alignment of zebrafish FurinA protein sequence to mammalian Furin sequences, given in Figure 4.6, shows that they are not well conserved, except for the catalytic domain labelled in green and the P domain in blue. However, both domains are shared with other SPCs family member proteins as well as *furina* ortholog *furinb* (Walker *et al.*, 2006). This raised concerns about the specificity of the antibody and the validity of the experiment since I would not be able to distinguish which protein is being detected. To avoid all these issues I decided to generate a *furina* sfGFP mRNA reporter. The sfGFP sequence was inserted in-frame between the amino acid residues serine 592 and cysteine 593, as illustrated in the red box in Figure 4.7 A. In mice, this region has been previously reported as an appropriate site for the insertion of a fusion tag as it does not interfere with protein function and enzyme cleaving properties (Mesnard *et al.*, 2011).

zebrafish	MDLRLAS---LTLGTLVLLTSGPQPSIGQKVTNTWAVHIEGGEEADRIARKHSFVN	56
human	MELRPWLLWVVAATGTLVL-L---AADAQGQKVFNTWAVRI PGGPAVANSVARKHGFLN	56
mouse	MELRSLWLVVAAAGAVL-L---AADAQGQKIFTNTWAVHIPGGPAVADRVAQKHGFHN	56
	: * : *::: * : *:::*****:* * * : *:::***	
zebrafish	HGNVFGDYHFRHRTVVKRSLSEHRGTHIRLHTEPQVMWAEQQVVKRRKRDVYYEPTDP	116
human	LGQIFGDYHFWHRGVTKRSLSPHRPHRSRLQREPOVQWLEQQVAKRRTKRDVYQEP TDP	116
mouse	LGQIFGDYHFWHRAVTKRSLSPHRPHRSRLQREPOVQWLEQQVAKRRAKRDVYQEP TDP	116
	*:***** ** *.***** ** * ** : **** * ****.*** * **** *****	
zebrafish	KFAQQWYLYNQDHLDLNVKNAWKQVGTGQGVVVSILDDGIEKNHPDLVQNYDPDASYDVN	176
human	KFPQQWYLSGVTQRDLNVKAAWAQGTGHGIVVSILDDGIEKNHPDLAGNYDPGASFVNV	176
mouse	KFPQQWYLSGVTQRDLNVKEAWAQGTGHGIVVSILDDGIEKNHPDLAGNYDPGASFVNV	176
	** ***** . : ***** ** * ** *:::*****. *****.***	
zebrafish	DGDPDPQPRYTQLNDRHGTRCAGEVAAVANDNICGVGVAYNARI GGVRMLDGEVTDVVE	236
human	DQDPDPQPRYTQMNDNRHGTRCAGEVAAVANNNGVCGVGVAYNARI GGVRMLDGEVTD AVE	236
mouse	DQDPDPQPRYTQMNDNRHGTRCAGEVAAVANNNGVCGVGVAYNARI GGVRMLDGEVTD AVE	236
	* *****:*****:*****:*. :*****:*****.*****.***	
zebrafish	AQSLSLNPQHIDIYSASWGPEDDGKTVDPKAKLAKEAFQGVIEGRGGRGSI FVWASGNG	296
human	ARSLGLNPNHIIHYSASWGPEDDGKTVDPKARLAEAEFFRGVSGRGGLSIFVWASGNG	296
mouse	ARSLGLNPNHIIHYSASWGPEDDGKTVDPKARLAEAEFFRGVSGRGGLSIFVWASGNG	296
	: *.***:*.*****:*****:***:*** ** * :**** *****	
zebrafish	GRMKDSCNCDGYTNSIYTLSSISSTQNGNVPWYSEACSSTLASTYSSGGVNEKQIVTDL	356
human	GREHDSNCDGYTNSIYTLSSISSTQFGNVPWYSEACSSTLATYSSGNQNEKQIVTDL	356
mouse	GREHDSNCDGYTNSIYTLSSISSTQFGNVPWYSEACSSTLATYSSGNQNEKQIVTDL	356
	** :*****:*****:*** *****:*****.*****	
zebrafish	RQKCTDSHTGTSASAPLAAGIIALALEANKNLTWRDMQHLVVRTSNPAHLTNDW KINGV	416
human	RQKCTESHTGTSASAPLAAGIIALTLEANKNLTWRDMQHLVVQTSKPAHLNANDWATNGV	416
mouse	RQKCTESHTGTSASAPLAAGIIALTLEANKNLTWRDMQHLVVQTSKPAHLNADDWATNGV	416
	*****:*****:*****:***:***.***:*** ** *	
zebrafish	GRRVSHSYGYGLLDAGAI VALAKNWTNVGPQHKCVLSLVSEPRNIGSYLVINKTVDACTG	476
human	GRKVSHSYGYGLLDAGAMVALAQNWTTVAPQRKCI IDILTEPKDIGRLEVRKVTACL G	476
mouse	GRKVSHSYGYGLLDAGAMVALAQNWTTVAPQRKCI VEILVEPKDIGRLEVRKAVTACL G	476
	** :*****:*****:***:***.***:***:***:***:***.*** ** *	
zebrafish	MANFVSSLEHVQAQLTLYSNRRGNLAIYLI SPQGRSTRLLPPRPHDYSSEG FNDWAFMTT	536
human	EPNHI TRLEHAQARLTLYSNRRGDLAIHLVSPMGTRSTLLAARPHDYSADGFNDWAFMTT	536
mouse	EPNHI TRLEHVQARLTLYSNRRGDLAIHLI SPMGTRSTLLAARPHDYSADGFNDWAFMTT	536
	*. : * ** .***:*****:*****:***:*** ***** *****:*****	
zebrafish	HSWDEDPRGEWVLEIKNVAGTSDYGTLTQFTLVLYGTASSLSRSTAGSSQTADSSCKTY	596
human	HSWDEDPSGEWVLEI ENTSEANNYGTLTKFTLVLYGTAPEGLP-----VPESSGCKTL	590
mouse	HSWDEDPAGEWVLEI ENTSEANNYGTLTKFTLVLYGTAPEGLS-----TPESSGCKTL	590
	***** ** *.***:*. :.*****:***** ***** . * .***	
zebrafish	DLNQICTECNPGFYLYQKGCVRDCPAGFTEGSRPTI--LNNELSSVLHPACLPC HSVCLT	654
human	TSSQACVVCEEGFSLHQKSCVQHCPPGFAPQVLDTHYSTENDVETIRASVCAPCHASCAT	650
mouse	TSSQACVVCEEGYSLHQKSCVQHCPPGFIPQVLDTHYSTENDVEIIRASVCTPCHASCAT	650
	* * . * : * :*.***:*** ** * :***. : * .***: * *	
zebrafish	CSGTGPQDCLSCPPHSHLGPLTGTCLHQNQIQRES PDGRLFQAQ---GDSLSFVHQ PALS	711
human	CQGPALTDCLSCPSHASLDPVEQTCRSRQSQSSRESPPQQPPRLPPEVEAGQRLRAGLLP	710
mouse	CQGPAPTDCCLSCPSHASLDPVEQTCRSRQSQSSRESRPQQPPALRPEVEMEPRLQAGL-A	709
	. . ***** * : *.** : * :*. * .*** : : : : *	
zebrafish	SSLPAIVAVLSCAFI VATFVGVFGLLQLRTLQKQHLGQEEP GSGLLVWGLNRTEVAY	771
human	SHLPEVVAGLSCAFI VLVFVTVFLVQLRSGFSFR-----GKVTMDRGLISY	759
mouse	SHLPEVLAGLSCLI I VLFIVFLFHRCSGFSFR-----GKVTMDRGLISY	758
	* ** :* ** * :** * ** .*: : . : : : : * : : * : **	
zebrafish	KGIPSVWREDEEESENEFGIHNERTAFIKTQSAL	806
human	KGLPPEAWQEECPDSEDEGRGERTAFIKDQSAL	794
mouse	KGLPPEAWQEECPDSEDEGRGERTAFIKDQSAL	793
	:* :* ** * :* ** * :*** ** *	

Figure 4.6 Conservation of FurinA protein sequence compared to mammalian FURIN sequences.

Clustal Omega protein sequence alignment (Madeira *et al.*, 2019), * (asterisk) underneath amino acid indicates fully conserved residue in three species. : (colon) shows conservation between residues with strongly similar properties, . (period) indicates conservation between residues with weakly similar properties. The region marked in the green box is a catalytic domain and the blue box shows a P domain. The red box shows the region where the sfGFP fusion tag was inserted.

To examine if Ybx1 was translationally repressing *furina*, a mRNA reporter was generated and injected into maternal (M) *ybx1* mutant embryos. In Figure 4.7 A, there is a schematic of the *furina* sfGFP mRNA reporter that was used in this experiment. Additionally, in Figure 4.7 B I show a schematic describing how the experiment was performed and when *ybx1*^{sa42} mutation was induced. Interestingly, in the western blot in Figure 4.7 B, at the 512-cell stage there is a strong FurinA GFP protein band in the *Mybx1* at 22 °C samples, but not in the control *Mybx1* at 28 °C. Overall, in the *Mybx1* at 28 °C samples, FurinA sfGFP protein was either not detected or detected at very small amounts. In the *Mybx1* embryos temperature shifted to 22° C, there were consistently higher amounts of protein present. The graph in Figure 4.7 C there is a quantification of the FurinA sfGFP band normalised to Actin from each biological replicate of the experiment. From this quantification of the band intensities, I confirmed that expression of FurinA sfGFP was higher in the *Mybx1* at 22°C embryos. Taken together this indicates that in the *ybx1* mutant embryos there is a premature translation of FurinA protein and Ybx1 is required for translational control and repression of *furina* mRNA.

Previous studies have shown that FurinA cleaves Spaw at the prodomain and facilitates its maturation and diffusion to extracellular space in the embryo (Tessadori *et al.*, 2015). I previously concluded from figure 4.7 C that FurinA protein is upregulated in *ybx1* mutant embryos, and this led to the hypothesis that maturation of Spaw should also be increased. In Figure 4.7 A there is a schematic of a Spaw GFP

reporter, which was injected into the *Mybx1* mutant embryos in this experiment. Temperature shifts of *ybx1^{sa42}* embryos were performed in the same way as illustrated in Figure 4.7 B. The western blot analysis revealed that Spaw mature domain appeared to be elevated in *Mybx1* at 22 °C when compared to the control *Mybx1* samples at 28 °C. However, the Spaw pro-domain was also increased in the *Mybx1* at 22 °C. It was therefore not clear if the Spaw maturation was increased or if the overall level of protein was higher in the mutant *Mybx1* at 22 °C sample. In Figure 4.7 C on the right side, there is quantification of the band intensities in all biological replicates was performed and revealed a significant increase in Spaw mature domain. But it was not clear whether this increase was due to overall higher amount of Spaw protein or the Ybx1 translational control.

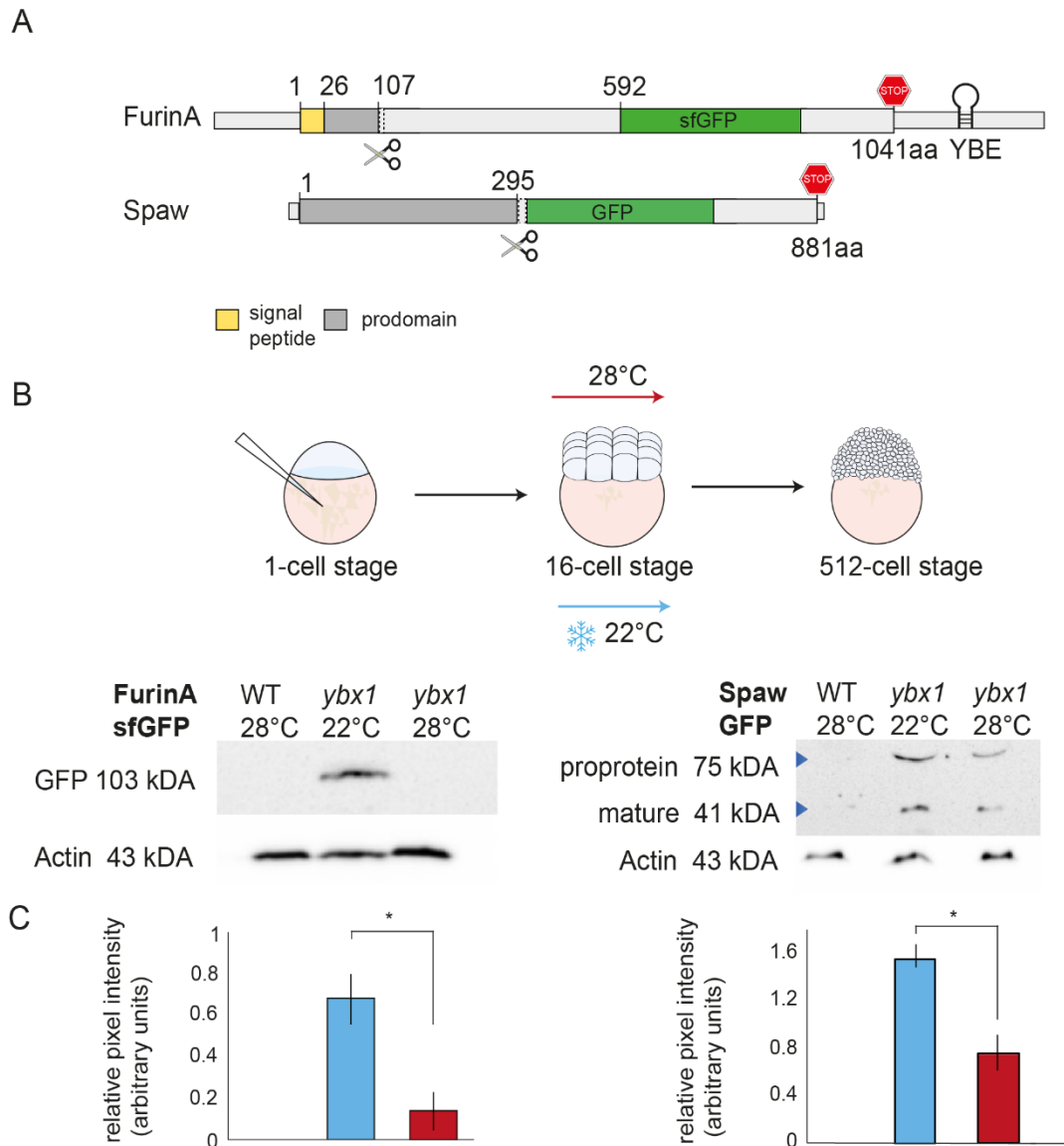


Figure 4.7 FurinA translation and Spaw maturation are elevated in *ybx1* mutant embryos.

A) Schematic of *furina* sfGFP tag fusion reporter and *spaw* GFP reporter used for injections. The signal peptide in the yellow box, prodomain is indicated in dark grey. YBE motif is shown in the FurinA 3'UTR.

B) Schematic of how temperature shift was performed in *Mybx1^{sa42}* mutant embryos. RNA was injected at the 1-cell stage, samples were incubated at 28 °C until the 16-cell stage and then *ybx1^{sa42}* mutation was activated at 22 °C. Control embryos were kept at 28 °C at all times. At the 512-cell stage, all samples were collected and

extracted for western blot analysis. The lower left panel shows FurinA sfGFP western blot after injection with the reporter mRNA, from the left side, lane one is uninjected wild-type control, lane two is *Mybx1* at 22 °C and the lane three is *Mybx1* control at 28 °C. Actin loading control gel is aligned to GFP gel per each lane, to ensure there are comparable amounts of protein lysates. The right panel shows Spaw GFP western blot from embryonic lysates after injection with the mRNA reporter. Starting from the left side lane one is uninjected wild-type control, lane two is *Mybx1* at 22 °C and lane three is *Mybx1* control at 28 °C. Spaw proprotein band is 75 kDA and mature domain band is 41 kDA. Below the GFP gel, there is corresponding Actin for each sample.

C) The graphs showing the relative intensity of the protein band normalised to Actin loading control of FurinA GFP and proportion of Spaw GFP cleaved normalised to the Actin loading control, *p* values $* < 0.05$.

Previous experiments have suggested that Spaw maturation might be increased in the *ybx1^{sa42}* mutants. However, I decided to examine if only the maturation of Spaw was elevated, rather than overall protein levels. Figure 4.8 A illustrates that embryos were injected with *spaw* GFP reporter and then imaged at different time points such as 1K-cell stage, sphere and epiboly. As an additional control, the *mCherry* reporter was injected together with *spaw* GFP mRNA to verify that the result was not due to an injection artefact. As shown in a schematic in Figure 4.8 A, this time following injection of *spaw* GFP *mCherry* mRNA mix, at the 16-cell stage both maternal-zygotic (MZ) *ybx1* mutant embryos and wild-type controls were temperature shifted to 22 °C until 512-cell stage. This step ensured that the temperature shifting of embryos to 22 °C does not affect the expression levels of GFP. Next, samples were imaged at 1K-cell stage (3hpf), sphere (4hpf) and 30% epiboly (4.7hpf) to examine fluorescence levels.

In Figure 4.8 B, confocal imaging of wild-type embryos at the 1K stage showed that there is a GFP signal detected and some secretion to extracellular space, but most of the Spaw GFP remains intracellular. At the sphere stage, the GFP signal is increased further and there is also a slight increase in Spaw GFP maturation. Finally, at a 30%

epiboly, the GFP signal is the strongest and is diffused across the entire blastoderm. However, in *MZybx1* mutant embryos, shown in a lower panel in Figure 4.8 B, at the 1K-cell stage the fluorescence signal is quite weak, but there is a substantial GFP expression at the extracellular space detected. Imaging at the sphere stage revealed a strong Spaw GFP signal that is almost entirely accumulated in extracellular space and the same is true at 30% epiboly. In a majority of *MZybx1* mutant embryos, there was a clear upregulation of Spaw GFP maturation, whereas in wild-type embryos Spaw GFP was more diffuse across the entire blastoderm, with little detectable secretion. The expression levels of *mCherry* reporter injection control were comparable between wild types and *MZybx1* mutants, suggesting equal amounts of mRNAs being injected. Additionally, the uninjected wild-type control did not show any fluorescence.

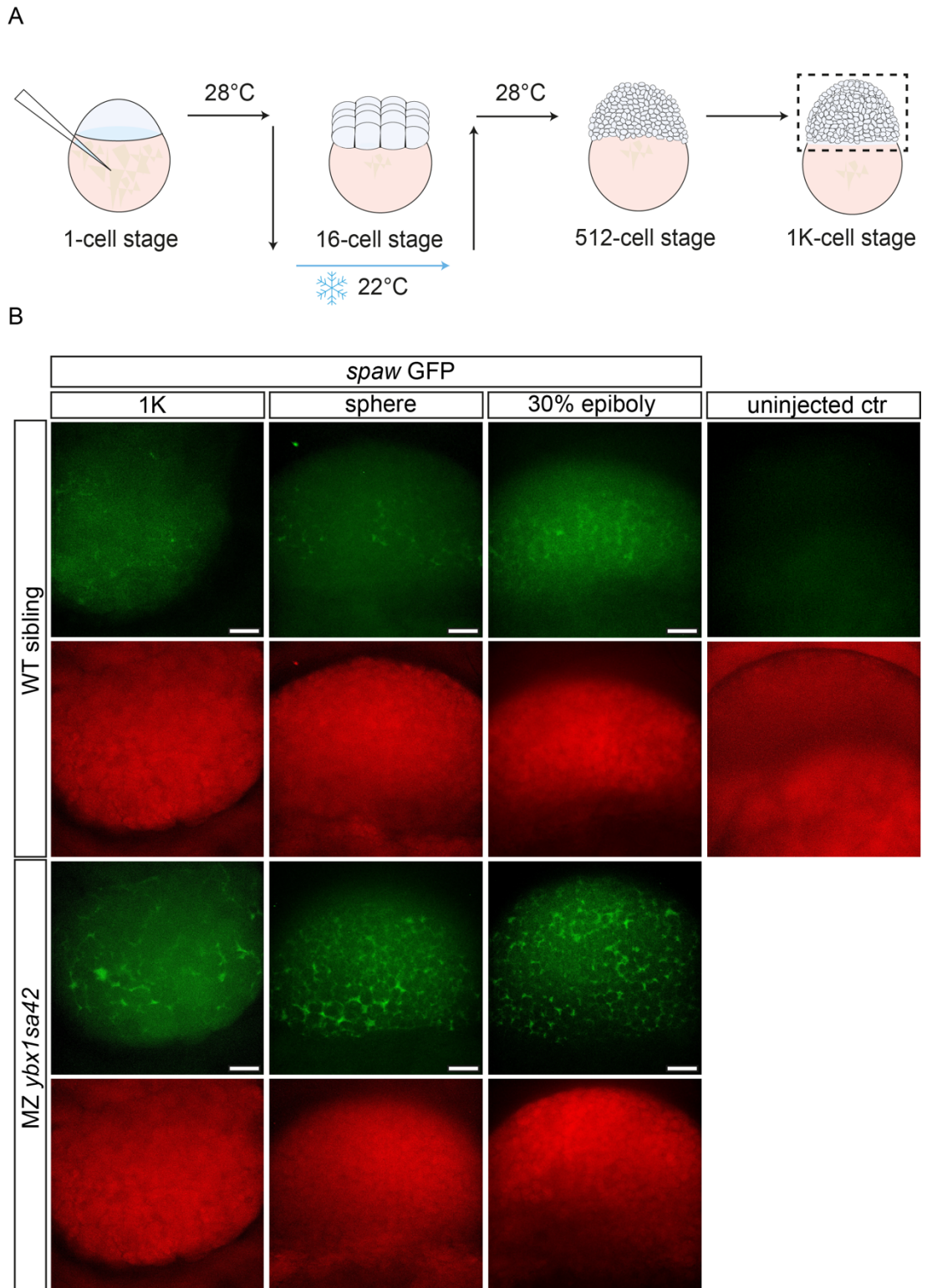


Figure 4.8 Spaw secretion to extracellular space is increased in *ybx1* mutants.

A) Schematic of how temperature shift was performed during the experiment, embryos were injected in a yolk at the 1-cell stage and then both MZ*ybx1* embryos

and wild-type controls were temperature shifted at 16-cell stage to 22 °C until the 512-cell stage. At the 1K cell stage embryos were imaged with a confocal microscope from the vegetal view focusing on blastoderm as shown in the black box.

B) Confocal images of the translation assay, in top panel images of wild-type embryos injected with *spaw* GFP and *mCherry* globin reporters at 1K stage, sphere and 30% epiboly. Below are corresponding samples showing uniform mCherry expression. Next are images of MZ*ybx1* mutant embryos at 1K stage, sphere and 30% epiboly injected with *spaw* GFP and *mCherry* globin reporters. The top panel shows the GFP channel and the bottom channel shows the mCherry channel. On the far right side uninjected control. The scale bar is 50 µm.

To quantitate the results from this experiment, the relative fluorescence levels of the Spaw GFP and the ubiquitous mCherry were measured. Each embryo used in the experiment has been imaged under the same conditions and separately analysed to ensure they were comparable. In Figure 4.9 the GFP signal in the blastoderm was normalised to the mCherry injection control and statistically analysed at each developmental stage of the zebrafish embryo. The results showed that at the 1K-cell stage, sphere and 30% epiboly the overall GFP signal in the blastoderm remains at approximately similar levels in both wild-type and *ybx1* mutant embryos. As the cells in the embryos divide and progress to the next developmental stage, the fluorescence slightly decreases in both wild-type and mutant embryos but continues to be comparable. The number of embryos per stage in each group differs, as embryos that moved to the next stage faster or became abnormal during the experiment were excluded from the analysis.

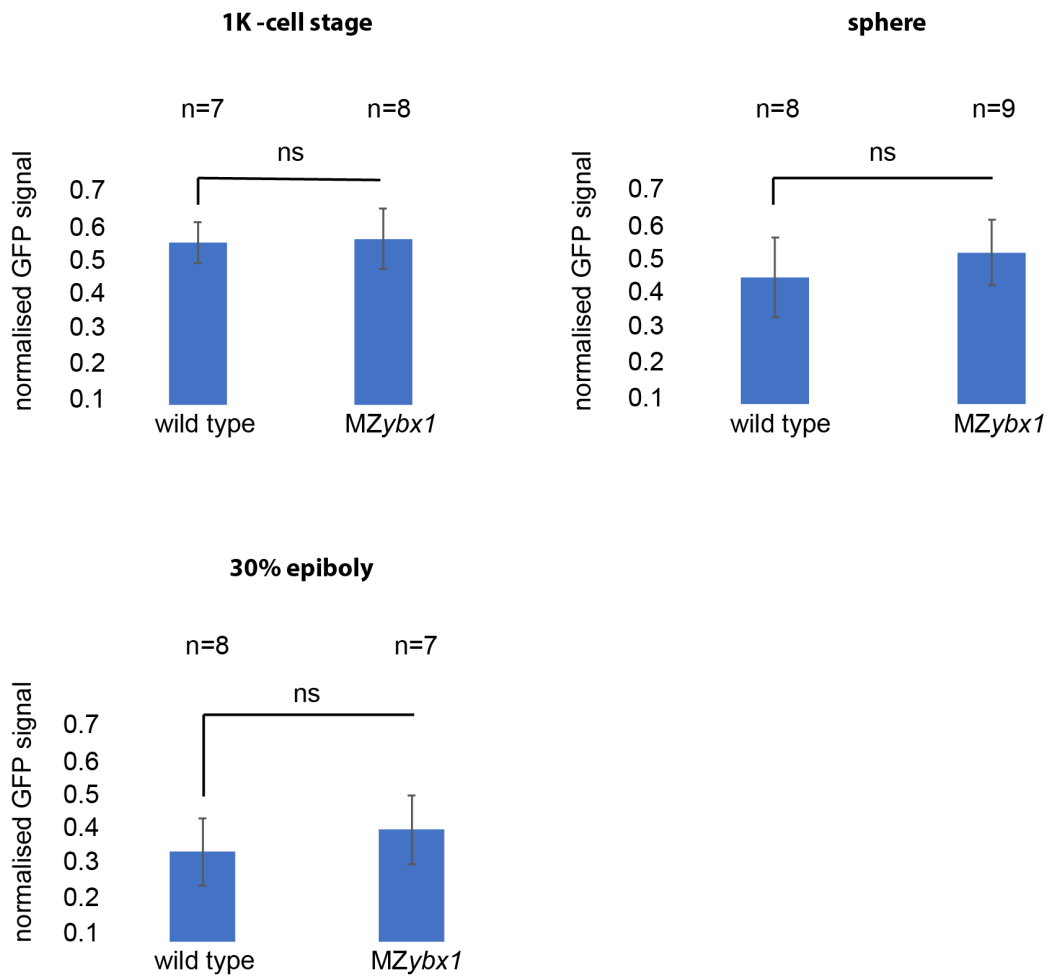


Figure 4.9 Relative fluorescence levels are very similar between wild-type and MZybx1 mutant embryos.

Spaw GFP fluorescence levels in the blastoderm normalised to mCherry globin control at 1K stage, sphere and 30% epiboly in all injected embryos, ns $p > 0.05$.

The results of Figure 4.8 indicated that cleaving of Spaw protein is increased in *ybx1* mutant embryos, as there is a significant increase in the accumulation of the GFP reporter in the extracellular space. In the wild type at the same developmental stages, there is a mixture of intracellular and extracellular expression as shown in Figure 4.8 B. In Figure 4.9 quantification of Spaw GFP fluorescence levels normalised to mCherry in wild-type and mutant embryos confirmed that the overall fluorescence

levels are similar between the two groups of embryos, and it is only the distribution that is affected.

4.3 DISCUSSION

In this chapter, the 3'UTR motif of *furina* containing the AGCAC sequence motif and a hairpin was examined. I also describe the interaction between *furina* variant *XI* and the Ybx1 RBP. In Figure 4.3 I show that fluorescent mRNA *furina XI* reporter localises at the 4-cell stage similarly to other identified Nodal pathway components, which contain the YBE motif. I also show that disruptions to the *furina XI* YBE motif reduce the RNA localisation. However, changing the sequence within the stem, to restore the bonding within the hairpin recovers the RNA reporter localisation. In Figure 4.4 it is shown that Ybx1 is in a complex with *furina XI* mRNA. Results from Figures 4.7 and 4.8 confirm that Ybx1 is translationally repressing *furina* and Spaw maturation is upregulated in the *ybx1^{sa42}* mutant embryos.

The 3'UTR YBE motif causes RNA localisation at the 4-cell stage. Initially the proposed role of the YBE was to facilitate translational repression of maternally contributed mRNAs (Kumari *et al.*, 2013). The inhibitors *lefty1* and *lefty2* mRNAs are not maternally contributed and are not endogenously localised during cleavage stages in zebrafish embryos. However, the *in vitro* binding assays have shown that Ybx1 specifically binds to YBE and in *ybx1* mutant there is premature translation detected at 1K and sphere stages (Zaucker *et al.*, 2017; Zaucker, Kumari and Sampath, 2019). These results and the transcriptome analysis suggest that the role of the YBE motif is much broader and is relevant to both maternal and zygotic transcripts. Similarly, with *furina* variant *XI*, I was able to detect reporter fluorescent mRNA localisation at the 4-cell stage even though RNA-IP variant *XI* is being pulled down with Ybx1 protein at 50% epi and 10-som stages.

Interestingly, in Figure 4.1 I observed that the left-right asymmetry determinant Nodal ligand *spaw* does not have the RNA element. The pro-protein convertase FurinA that cleaves Spaw, however, does contain a YBE motif in the 3'UTR. This led to the possibility that Spaw protein expression could be mediated via the translational regulation of FurinA through the RNA element. The translation assay results in Figure 4.8 support this hypothesis, as there is an increase in processing of Spaw detected.

RNA immunoprecipitation revealed that at 50%-epiboly and 10-som stages there are Ybx1 protein and *furina* mRNA complexes present, as shown in Figure 4.4. This indicates that Ybx1 is binding to *furina* and is likely to regulate it. Surprisingly, at 18 som I was not able to pull down Ybx1 protein. This was confusing because Ybx1 should be present within the embryo at high levels throughout the embryonic development according to the expression atlas database (White *et al.*, 2017). There is no obvious reason why the pull down of Ybx1 protein would be less efficient at the 18-som stage. Additionally, to be able to identify the mRNAs that were complexed with the Ybx1, two sets of primers for *furina* were designed. This is the same set used as in the qPCR analysis in Chapter 3 Figure 3.5. The first set is within the CDS of *furina* and the second set of primers targets the variant *XI* 3'UTR. I did not observe any differences in the amount of enrichment between the two sets of primers. In the RNA immunoprecipitation samples, entire mRNA sequences will be crosslinked and pulled down together with the Ybx1 protein. Also in *furina* variant *XI*, CDS is identical to the *furina* transcript 1. Since the 3'UTR primer set targets exclusively variant *XI* and enrichment from both primer sets are comparable, I, therefore, concluded that most likely only variant *XI* mRNA is present in the Ybx1 pull down.

To analyse the interaction between Ybx1 and *furina XI*, a *ybx1^{sa42}* mutant fish line that was previously generated in our laboratory was used. Deletion of Ybx1 in the embryos causes embryonic lethality around the gastrulation stages. In addition to the described phenotype, homozygous *ybx1^{sa42}* embryos also show expansion of the yolk syncytial layer, which is required for embryonic cell fate specification and morphogenesis of early cell layers (Carvalho and Heisenberg, 2010). Ybx1 is

ubiquitously expressed and has interactions with a range of mRNA and DNA targets. The *ybx1^{sa42}* mutant allele is only activated upon temperature shifting of the embryos to 22 °C, and when the temperature is raised to 28 °C the embryos resemble wild type sibling embryos and do not exhibit morphological defects. This allows the activation of mutations and the blocking of pathways at specific timepoints in embryonic development. Previous studies in the Sampath laboratory have shown that the CSD in the Ybx1 protein has an important function in recognising and binding the YBE motif in the 3'UTR of the mRNAs. The *ybx1^{sa42}* mutation, however, reduces this ability to bind by the YBE motif (Kumari *et al.*, 2013).

Ybx1 has been shown to act as a translational repressor of the Nodal components containing YBE motif such as *sqt*, *lefty1* and *lefty2* (Kumari *et al.*, 2013; Zaucker *et al.*, 2017). Consistently with previous findings, in Figure 4.7 it was observed that Ybx1 acts as a translational repressor of FurinA protein and in absence of Ybx1, FurinA expression is elevated and occurs prematurely. I demonstrated that as a result of an increase in FurinA levels, its downstream target Spaw has increased processing and secretion to extracellular space in *ybx1* mutant embryos. This has been shown by *spaw* GFP mRNA reporter injection into embryos and analysis of proprotein and mature protein levels by western blot and confocal imaging, as shown in Figure 4.8. Ybx1 has been described as a global translational repressor that binds to many target mRNAs with very little specificity (Dong *et al.*, 2009). To ensure that the system is not saturated the dosage of injection was kept low, below 50 pico grams (pg), because when higher amounts of mRNA reporters are injected, I noticed that there is an increase in the variation of the results.

To conclude, in this chapter I validated the *furina* 3'UTR motif and established the interaction of Ybx1 with *furina* mRNA through the RNA IP. Using *ybx1* mutant embryos I also showed that Ybx1 translationally represses *furina*. I was next interested to see if *ybx1* mutant embryos share any of the phenotypes that were previously published on *furina* and *spaw* zebrafish mutants. FurinA has been implicated in heart morphogenesis and visceral organ positioning in zebrafish embryos. Overexpression

of *FurinA* leads to left-right asymmetry and heart looping defects (Tessadori *et al.*, 2015). In the next chapter, I will explore if there is a link between such phenotypes in *MZybx1* mutant embryos.

CHAPTER 5
ANALYSIS OF THE LEFT RIGHT
ASYMMETRY AND CARDIAC
DEVELOPMENT IN *YBX1* MUTANT
EMBRYOS

5.1 INTRODUCTION

Zebrafish heart development is a complex process that is initiated by the formation of a linear tube, which is followed by a gradual progression to a mature organ. A number of different processes in the embryo must be completed for a heart to develop normally. These include asymmetric positioning of the heart along the left-right (L/R) axis, cardiac growth, and cardiac valve morphogenesis (Noël *et al.*, 2013). In zebrafish embryos, the protein FurinA has been described to have a role in the establishment of L/R asymmetry and heart development. This pro-protein convertase cleaves the Nodal-related Southpaw (Spaw) protein intracellularly at the cleavage site Arg-His-Lys-Arg in zebrafish embryos, thus allowing its secretion in a diffusible mature form in the left lateral plate mesoderm (LPM) (Tessadori *et al.*, 2015). In addition to the cleavage of Spaw protein, other intrinsic mechanisms facilitate its leftward expression in the LPM. Monocilia within the Kupffer's vesicle starts anticlockwise rotation and the fluid flow. This causes enrichment of Ca^{2+} from the left-right organizer to the cells in the left LPM, simultaneously directing the expression of *spaw* to the left side. Left-sided *spaw* expression extends from the posterior to the anterior LPM. These two mechanisms are essential in the establishment of the future L/R visceral organ positioning in early zebrafish embryos (Francescato *et al.*, 2010).

FurinA protein has an important regulatory role in zebrafish heart development. During the first 4 days of a zebrafish larva's life, the process of heart morphogenesis occurs rapidly. During gastrulation, at the 5 hpf atrial and ventricular precursors localize to the marginal zone of the blastula. By 12-somite (som) stage they localise to the anterior lateral plate mesoderm (ALPM), cardiogenic differentiation is initiated, and ventricular precursors differentiate into myocytes. They form bilateral cardiac primordia giving rise to two distinct cardiac progenitor pools at the ALPM (Brown *et al.*, 2016; Dong, Qian and Liu, 2021). Sarcomere myosin genes are found at the 14 som in the ALPM. At the 17 som atrial precursors differentiate into myocytes and endocardial cells migrate towards midline. Between the 21- and 25-som stages,

ventrally positioned endocardial progenitor cells fuse with atrial and ventricular myocytes to create the cardiac disk, which then rotates and extends into a tube that gives rise to the early beating organ. At 48 hpf the zebrafish heart is looped, with two distinct chambers, and migrates to the pericardial cavity (Bakkers, 2011). At these timepoints, tissue convergence occurs, and cells rapidly change shape. Cardiomyocytes within the ventricle and atrium gain greater cell volume and a squamous shape, however, the atrioventricular canal (AV) cells become more compact and cuboidal in shape. Within the AV canal, an epithelial to mesenchymal transition occurs to form the endocardial cushions, which begin differentiating into functional heart valves (Bakkers, 2011; Vignes *et al.*, 2022). Interestingly, recent studies have shown that FurinA is expressed at the AV canal at 3 dpf in zebrafish embryos, suggesting it might have additional roles in heart development (Zhou *et al.*, 2021).

Studies in mice showed that *Furin* knock out results in abnormal heart development. Defects of the outflow tract were found including heart tube fusion and ventral closure. In addition, these mice also display aberrant heart looping, and therefore *Furin* mutant mouse embryos die between stages E10.5-E11.5 (Dupays *et al.*, 2019). In zebrafish, maternal-zygotic (MZ) *furina* mutant embryos also show impaired heart development. They manifest cardiac dextral looping and trabeculation defects. Whole mount *in situ* hybridization (WISH) has shown that in these embryos there is the complete absence of *spaw* mRNA expression and its downstream target *pitx2* at the LPM, which ultimately leads to visceral organ positioning defects. Finally, *furina* mutants do not develop a swim bladder and consequently, 80% of them do not survive beyond larval stages (Tessadori *et al.*, 2015; Zhou *et al.*, 2021).

In the previous chapter, we demonstrated that FurinA GFP reporter is upregulated in the *ybx1* mutant embryos and that Spaw maturation is also increased. We concluded that Ybx1 translationally represses FurinA, and in its absence, FurinA expression is elevated and occurs prematurely. In this chapter, we examine if *ybx1* mutant embryos exhibit organ positioning and heart morphogenesis defects.

Aims

- To investigate if *ybx1* mutant embryos have left-right asymmetry defects
- To determine if *ybx1* mutants have defective cardiac development

5.2 RESULTS

In all vertebrate species, there is a left-sided expression of Nodal in the LPM, which is associated with correct left-right axis formation and normal visceral organ positioning (Varlet and Robertson, 1997). Similar to other vertebrate species, in zebrafish expression of the Nodal homolog *spaw* is asymmetric on the left side of the LPM during somitogenesis, and disruptions to this process are associated with the left-right asymmetry defects (Long, Ahmad and Rebagliati, 2003). To be able to study the left-right asymmetry defects in *ybx1* mutant embryos, we utilised the previously described temperature sensitive *ybx1^{sa42}* mutant allele (Kumari *et al.*, 2013). Since I already established that FurinA translation is elevated and Spaw protein maturation is increased, the next step was to analyse the endogenous *spaw* expression range in *ybx1* mutant embryos.

The MZ*ybx1* mutant embryos and wild type controls were temperature shifted to 22 °C at 75% epiboly until the 18-som stage, as shown in Figure 5.1 A. During these stages, *furina* variant *XI* is expressed at its highest levels according to the qPCR data from Figure 3.5 in Chapter 3. To avoid interference from other factors that could affect the result of the experiment, the temperature shift was done after mid-gastrulation and the expression of *spaw* was examined in both mutants and wild-type embryos at 18 som by WISH. Figure 5.1, in wild type control embryos, 95% of *spaw* expression is left-sided and 5% of embryos have bilateral expression. Interestingly, in mutant *ybx1* embryos, 35% have bilateral *spaw* expression. These results show that many *ybx1*

mutant embryos have abnormal *spaw* expression and they are likely to exhibit left-right asymmetry defects.

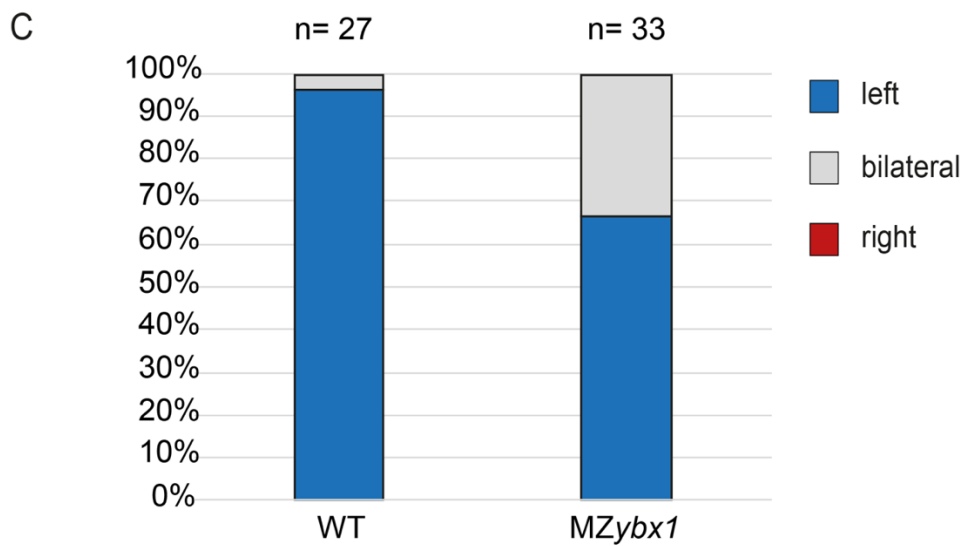
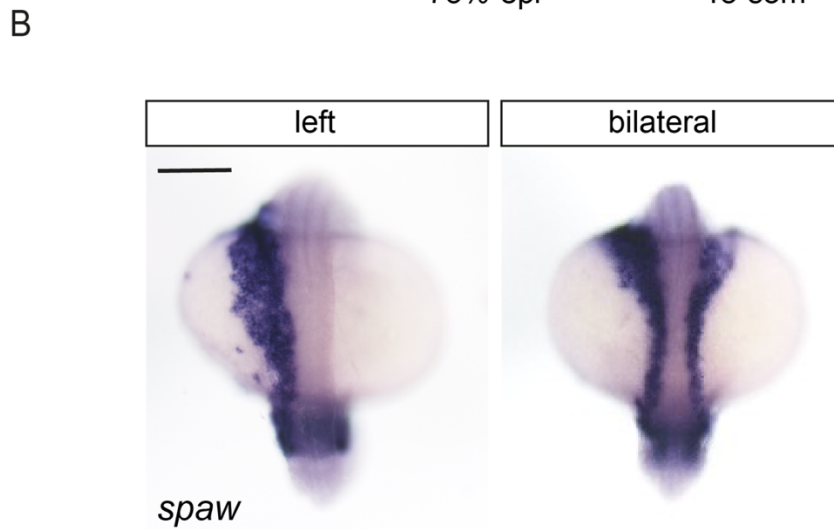
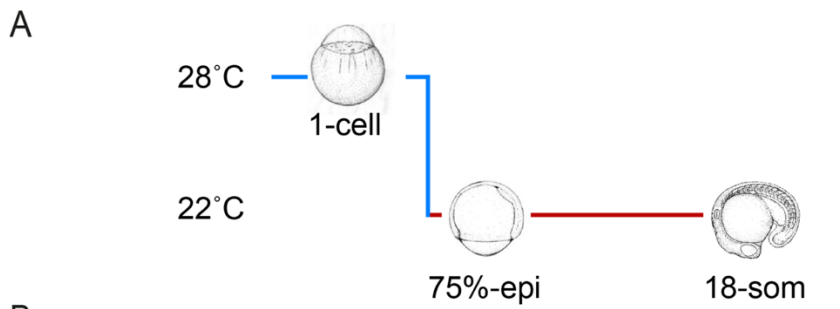


Figure 5.1 Mutant *ybx1* embryos have abnormal left-right expression.

- A) Schematic of the temperature shift of both MZ*ybx1* mutant and control samples. Embryos were temperature shifted to 22 °C at 75% epiboly until 18 som.
- B) WISH with *spaw* probe at 18-som stage. Images from top left: example of left-sided *spaw* expression, on the right example of bilateral *spaw* expression. The scale bar is 100 µm.
- C) Quantification of *spaw* expression patterns in wild type (WT) embryo controls and MZ*ybx1* mutants from one biological replicate.

Previous studies have shown that although *spaw* is not necessary for correct heart looping to occur, abnormal *spaw* expression causes some dextral looping defects and randomisation of intestinal organs in embryos (Long, Ahmad and Rebagliati, 2003; Noël *et al.*, 2013). Zebrafish *furina* mutants also display abnormal heart looping (Tessadori *et al.*, 2015; Zhou *et al.*, 2021). In Chapter 4, I show that Ybx1 interacts with *furina* mRNA and now in Figure 5.1 B that *ybx1* mutants exhibit aberrant *spaw* expression. Next, I wanted to determine if these *ybx1* mutant embryos have abnormal heart looping. To test this hypothesis double immunofluorescence staining was performed, using antibodies labelling the ventricle and the atrium. The temperature sensitive *ybx1*^{sa42} allele was shifted to 22 °C from 75% epiboly until the 21-som stage to disable the Ybx1 function. Next, the embryos were grown until 55 hpf at 28 °C, as illustrated in Figure 5.2A. Staining of samples was performed at 55 hpf to ensure that the looping of heart chambers is complete. Wild type embryos were temperature-shifted at the same timepoints, simultaneously with MZ*ybx1* mutants, to control for random phenotypic effects that could have occurred due to temperature shift. MZ*ybx1* embryos grown exclusively at 28 °C served as additional controls.

Analysis of the immunostaining in Figure 5.2 B was divided into three categories. 1) D loop, which indicates normal heart looping, shown in blue; 2) The no loop category is shown, in grey 3) and the complete inversion of the heart chambers, shown in red. The analysis showed that 92% of WT embryos, which were temperature shifted to 22 °C had the normal D loop. Consistently, 90 % of MZ*ybx1* control embryos kept at 28

°C (without activating the mutation) had a D loop. The *MZybx1* mutant embryos that were temperature shifted to 22 °C, however, exhibited approximately a 15% increase in abnormal heart looping. In total, 75% of embryos exhibited a normal D loop, 18% showed a lack of looping between ventricle and atrium and 7% showed complete inversion of the heart. From these results, I concluded that a significant proportion of *MZybx1* mutant embryos showed abnormal looping of the heart and are also likely to have other visceral organ positioning defects.

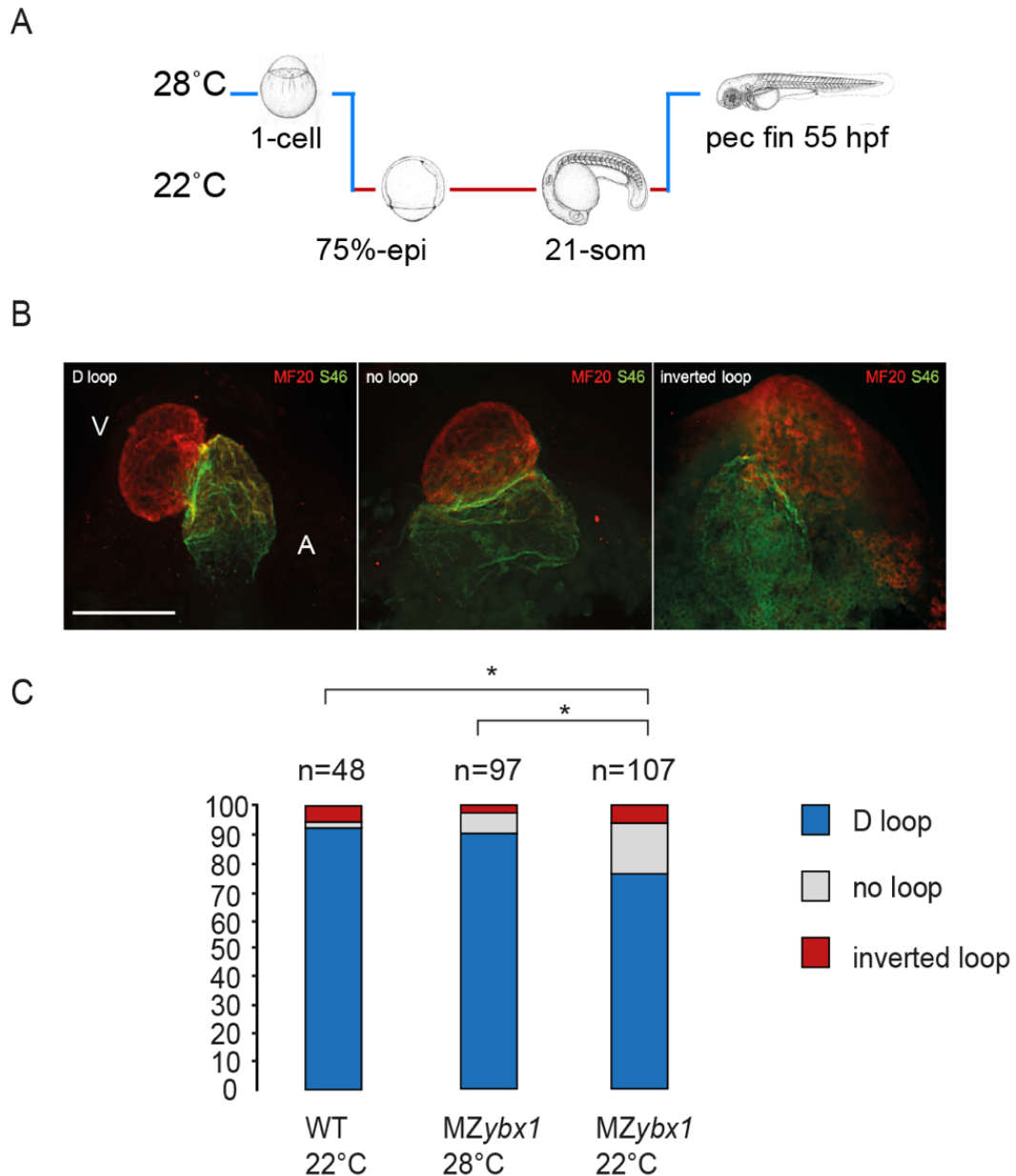


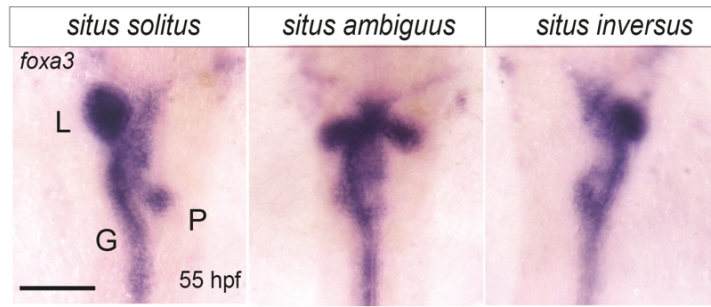
Figure 5.2 *Ybx1* mutant embryos exhibit heart looping defects.

- A) Schematic of the temperature shift of MZ*ybx1* mutants and controls. Embryos were collected and grown until 75% epiboly stage at 28 °C, then WT and approximately half of the MZ*ybx1* temperature shifted to 22 °C until 21-som stage. After the 21-som stage, MZ*ybx1* and WT were grown at 28 °C until the pec-fin stage (55 hpf). As an additional control, half of the MZ*ybx1* embryos were grown at 28 °C from the 1-cell stage until pec-fin.
- B) Double immunofluorescence of zebrafish hearts with MF20 antibody- Myosin heavy chain sarcomere (shown in red) staining the ventricle and S46 antibody Myosin heavy chain, cardiac muscle alpha isoform (shown in green) staining the atrium. Images represent three heart looping categories. D loop, which is a normal looping of the heart. Abnormal no loop, and inverted loop categories.
- C) Quantification of each category found in three samples: temperature shifted to 22 °C WT embryos, MZ*ybx1* grown at 28 °C, and temperature shifted to 22 °C MZ*ybx1*. Statistical analysis of three biological replicates using Student's T-test, * $p < 0.05$.

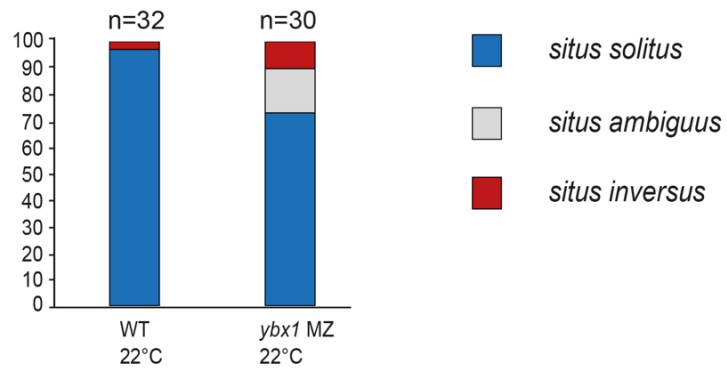
Next, I wanted to determine if visceral organ positioning is affected in the *ybx1* mutants using WISH on the *ybx1* mutant embryos and wild type controls. Afterwards, I analysed the positioning of the liver, pancreas, and gut at 55 hpf and the liver at 5 dpf. To trigger *ybx1* mutation the temperature shifts were performed at the same developmental stages as described in Figure 5.2 A. In Figures 5.3 A and B samples with normal organ positioning or *situs solitus* are shown in blue on a graph. Embryos with organ abnormalities such as duplications or placed in mirror images from their normal position were shown in grey colour as *situs ambiguus*. Finally, embryos with complete inversion of the organs are referred to as *situs inversus*. Results from Figure 5.3 A have shown that in the *ybx1* mutant sample 10 % of embryos had a complete inversion of the organs and 16% had organ arrangement abnormalities, including duplications of either both liver and pancreas or just single organs and general mispositioning. Additionally, 74% of *ybx1* mutant embryos displayed normal organ morphogenesis. In wild type embryo control clutch, however, 87% of samples exhibited *situs solitus*.

Staining of the liver at the 5 dpf in Figure 5.3 C and D has revealed a similar pattern in the results, where we observed 95% of wild type embryos with liver on the left side and 3% with organ inversion. In *MZybx1* mutants, however, 81% of embryos had their liver on the left side, 14% of embryos showed liver duplication and arrangement on both the left and right axis, and finally, 5% had their liver on the right side only. Taken together, the results from both Figures 5.2 and 5.3 indicate that *ybx1* mutant embryos exhibit abnormal left right axis formation. There is an increase in randomisation of visceral organ arrangement, duplication and mispositioning of the liver, pancreas and gut, and heart looping defects when compared to wild type controls. This is a consistent phenotype associated with an increase in bilateral *spaw* expression, as previously described in left-right patterning studies (Varlet and Robertson, 1997; Long, Ahmad and Rebagliati, 2003).

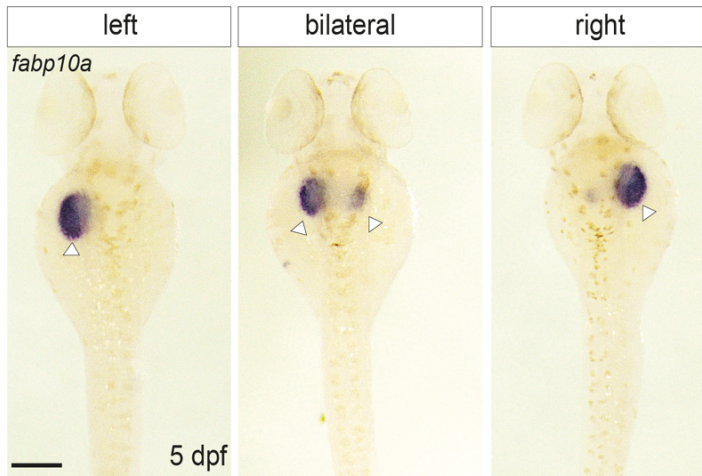
A



B



C



D

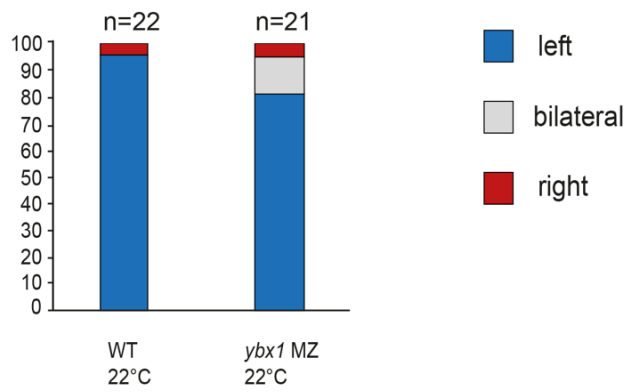


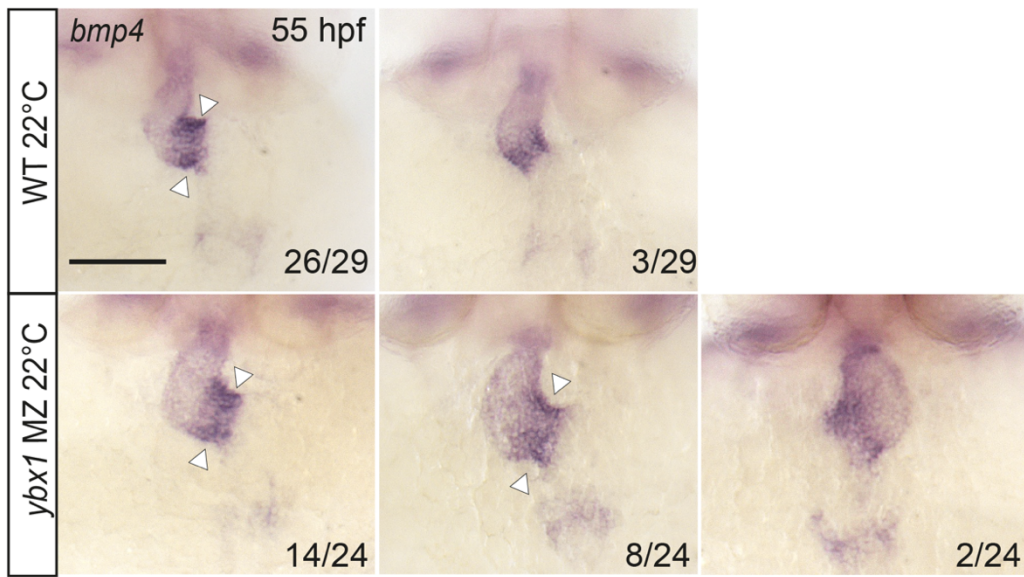
Figure 5.3 *Ybx1* mutant embryos show organ positioning defects.

- A) WISH with *Foxa3* probe labelling visceral organs at 55 hpf. L points to the liver, G is the gut and P is the pancreas. Three images represent categories shown from the left are *situs solitus* – normal organ positioning, *situs ambiguous* – abnormal organ arrangement and *situs inversus* showing complete organ mirroring. The scale bar is 100 μ m.
- B) Quantification of the proportion of such defects in WT temperature shifted to 22 °C control embryos and MZ*ybx1* mutants from one biological replicate.
- C) WISH with *fatty acid binding protein 10, fabp10a* probe at 5 dpf. White arrowheads point to the liver. From left, normal positioning of the liver, abnormal middle positioning of liver and inverted liver on the right side. The scale bar is 200 μ m.
- D) Proportion of WT and MZ*ybx1* mutant embryos with the given categories from one biological replicate.

FurinA has been shown to have a crucial role in heart development and a range of studies have demonstrated its importance in dextral looping of the heart in zebrafish (Tessadori *et al.*, 2015; Zhou *et al.*, 2021). Studies in mice have shown that deletion of *Furin* causes defects in the outflow tract of the heart. Furin protein has a number of targets, and one of them is BMP4, which has a critical role in the septation of the AV canal and also outflow tract morphogenesis (Dupays *et al.*, 2019). To explore whether this is also true in zebrafish, I decided to analyse the heart morphogenesis in more detail and performed additional WISH staining on *ybx1* zebrafish mutant embryos. The expression of *BMP4* and *notch1b* probes was analysed at 55 hpf in embryos. *Ybx1* function was disabled as described in Figure 5.2 A for both the *ybx1* mutants and the wild type controls. In Figure 5.4 A, I observed that the expression patterns for *BMP4* were comparable between the wild type and *ybx1* mutant embryos. The probe was expressed in the AV canal in both clutches of embryos. In the wild type sample, two embryos showed a weaker looping of the heart, as shown in the top panel on the right side. In the MZ*ybx1* mutant sample, shown in the bottom panel of Figure 5.4 A, there were two embryos with complete inversion of the heart. Staining with *notch1b*, as shown in Figure 5.4 B, has revealed some differential expression between the mutant and wild type samples. Staining was mostly contained to the AV canal in the wild type

control embryos and *MZybx1* mutants. However, in the middle bottom image it can be observed that in the *MZybx1* mutant clutch, 4 embryos have slightly expanded *notch1b* staining around the AV canal. Furthermore, there were 7 embryos in the *MZybx1* sample with either no loop or inverted looping of the heart. Interestingly in both the *BMP4* and *notch1b* staining shown in Figures 5.4 A and B we observed that overall, the hearts of *MZybx1* mutant embryos appeared larger than in the control embryos. It was not clear if this was a phenotype, because the differences observed could have been a result of embryos being fixed at different phases of their heartbeat.

A



B

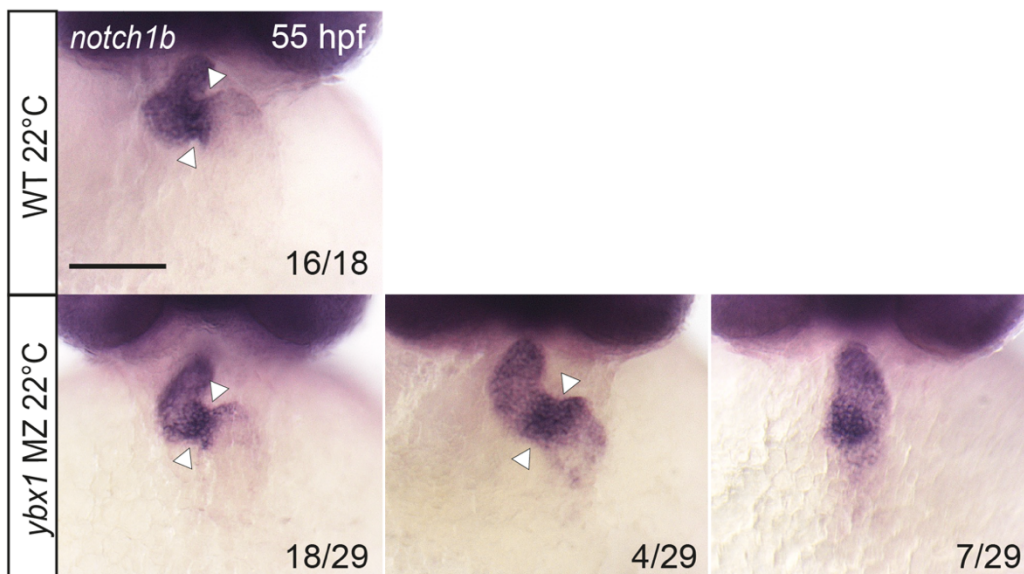


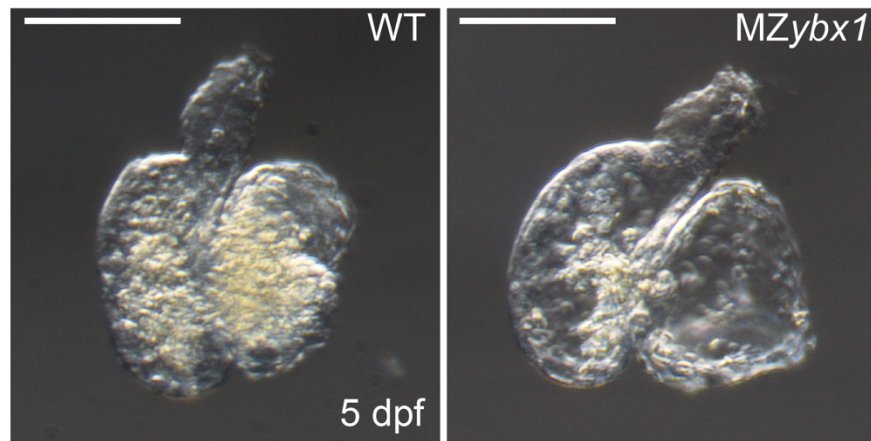
Figure 5.4 The expression of the heart markers BMP4 and *notch1b* is normal in *ybx1* mutant embryos.

A) WISH with *BMP4* probe at 55 hpf. White arrows point to the AV canal in both wild type and mutant embryos. Top panel examples of staining in wildtype embryos, bottom panel examples of results from MZ*ybx1*. Scale bar is 100 μ m.

B) WISH with *notch1b* probe at 55 hpf. White arrows point to the AV canal. The scale bar is 100 μ m.

Previous WISH experiments have suggested that the heart in *ybx1* mutant embryos may be larger when compared to the wild type controls. To test this hypothesis, I expanded the sample size for the analysis. Wild type (WT), paternal (P), maternal (M), and maternal-zygotic (MZ) *ybx1* mutant embryos were collected simultaneously, grown until 75% epiboly at 28 °C and then temperature shifted to 22 °C until 21 som, as shown in Figure 5.2 A. Following this, embryos were grown at 28° C until day 5 of embryogenesis. Previously in Figure 5.4, the heartbeat of embryos being at different phases prior to fixation caused problems when analysing the phenotype, therefore this time to ensure larvae hearts were at the same phase prior to fixation, embryos were treated with tricaine. This treatment caused relaxation of the heart chambers in larvae prior to fixation. Hearts were then manually extracted, imaged and finally, the total area of the heart was analysed. Examples of images of the hearts that were extracted are shown in Figure 5.5 A. The quantification of the total area of the heart shown in Figure 5.5 B revealed that the MZ*ybx1* mutant hearts had a significantly larger area when compared to wild type controls. Furthermore, the area of the hearts in P*ybx1*, M*ybx1* and MZ*ybx1* mutant embryos was comparable. Overall, there appeared to be a small increase in the size of the hearts in mutant embryos when compared to wild types, however, this difference was subtle and unlikely to cause serious heart defects.

A



B

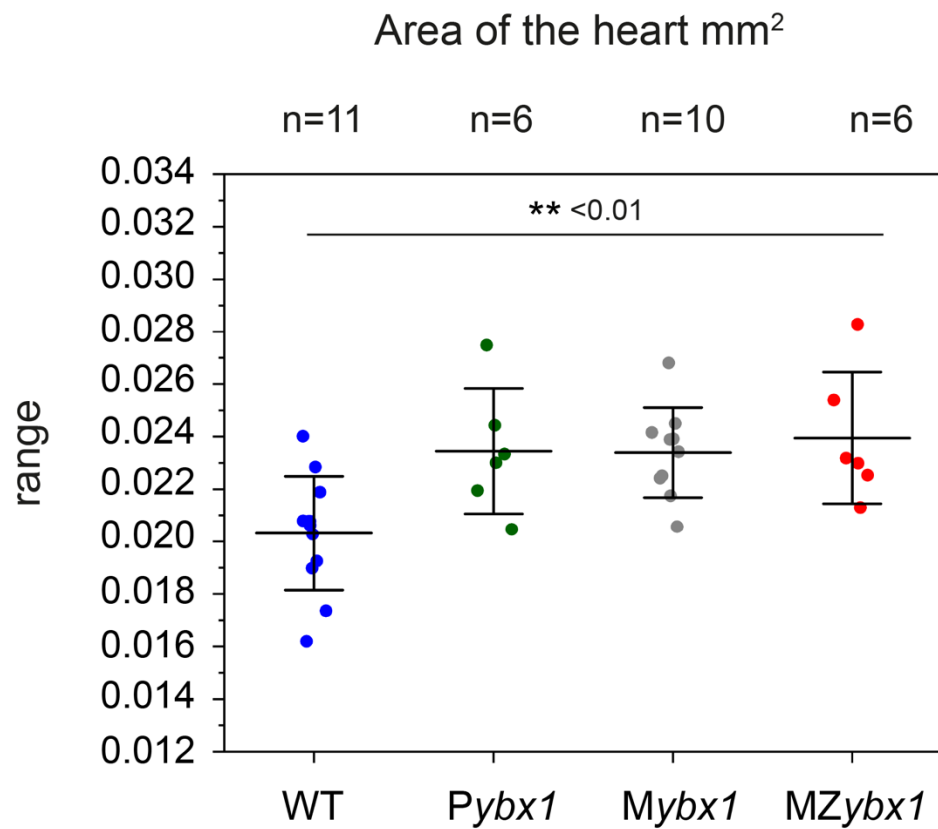


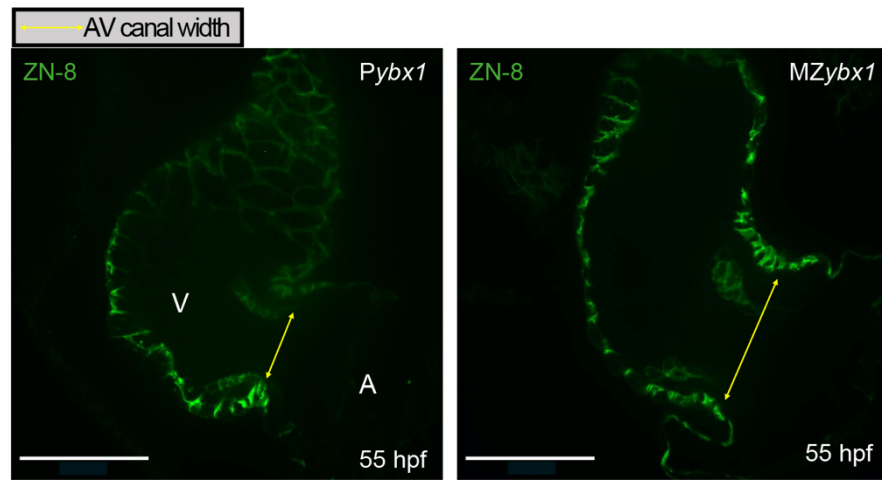
Figure 5.5 The total area of the heart is bigger in *MZybx1* mutant embryos at the 5 dpf.

A) Images of the heart extracted from embryos at 5 dpf. The left side shows an example of the wild type heart and on the right side example of a *ybx1* mutant. The scale bar is 100 μ m.

B) Quantification of the total area of the heart in mm² (from left) in wild type, *Pybx1*, *Mybx1* and *MZybx1* mutant embryos. Statistical analysis was performed using single factor ANOVA, ** $p < 0.01$.

The AV canal in zebrafish larvae undergoes extensive remodelling between day 2 and day 5 post fertilization to differentiate into functional heart valves, which have a critical role in preventing retrograde blood flow (Gunawan *et al.*, 2019). In Figures 5.4 A and B, we observed that the heart morphology appears to differ in mutant embryos, even though the expression pattern of AV canal markers is comparable to wild types. To explore this idea further we performed immunostaining and analysed the width of the AV canal in *ybx1* mutant embryos. Similarly, to previous experiments *ybx1^{sa42}* mutation was triggered according to the schematic in Figures 5.2A. Additionally, prior to fixation, embryos were treated with tricaine to ensure that all hearts are fixed in the diastole phase. Next embryos were stained with ZN-8 antibody and imaged. Figure 5.6 A shows examples of images of the immunostaining of *Pybx1* and *MZybx1* mutants. In Figure 5.6 B there is a quantification showing a graph with AV canal width in μm of individual embryos from different sample clutches, which revealed that the AV canal width in the *ybx1* mutant embryos was larger than in wild type control group. The *MZybx1* mutants had the largest AV canal width shown in red colour, then *Mybx1* and *Pybx1* mutant embryos and finally WT controls. We observed that in the wild type controls the measurements represented in blue on the left side of the graph were rather grouped together, whereas in all the *ybx1* mutant groups we observed more of a spread of data. Furthermore, results in Figure 5.6 B from the *Pybx1* (green) and *Mybx1* (black) mutant embryos were comparable. This result was very exciting because it could mean that *Ybx1* has a role in heart morphogenesis. The AV canal is a key structure in the heart, and abnormalities in its width could mean that the valve leaflet differentiation or function is impaired. To be able to further understand the consequences of the increased AV canal width, I decided to study zebrafish larvae's heartbeat at the 5 dpf, when all the dynamic developmental processes begin to slow down and the key morphological events are completed.

A



B

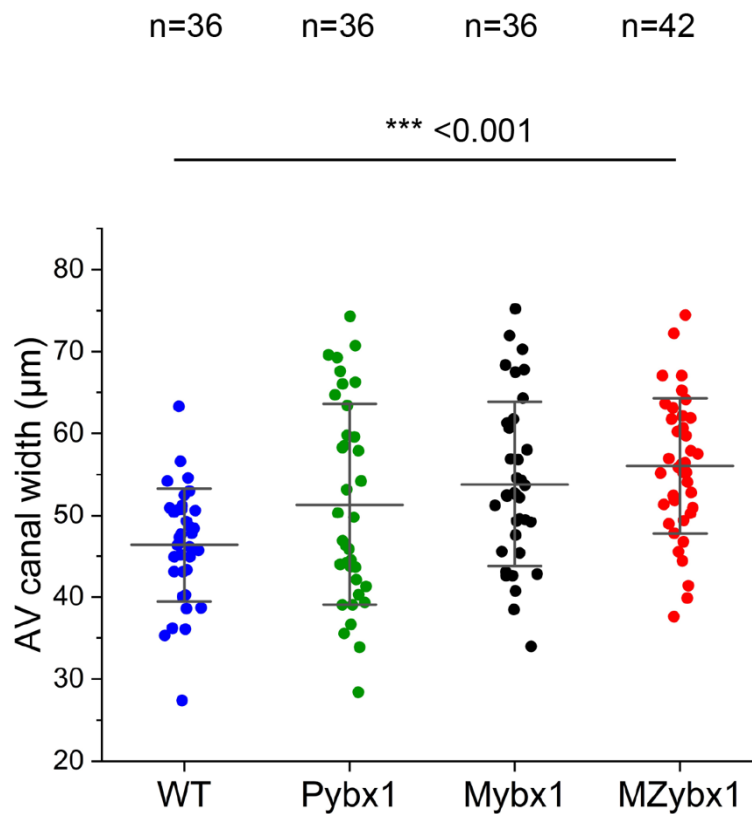


Figure 5.6 The atrioventricular canal is enlarged in *MZYbx1* mutant embryos.

A) Confocal image of immunofluorescence with ZN-8 antibody, the yellow line represents the width of the AV canal. V shows ventricle and A shows atrium.

B) Quantification of the width of the AV canal from three independent biological replicates from WT embryos, *Pybx1*, *Mybx1* and *MZybx1* mutant embryos. Statistical analysis performed using single factor ANOVA, * $p < 0.05$, ** $p < 0.005$, *** $p < 0.001$. The scale bar is 50 μm .

To analyse the function of the zebrafish heart in both *ybx1* mutant embryos and wild type control, DIC microscopy was used to image blood flow at the 5 dpf. Both wild type and mutant embryos were temperature shifted as shown in the schematic in Figure 5.2 A and then raised at 28 °C until 5 dpf. In Figure 5.7 A the black box highlights the area of the main heart valves where the imaging was focussed. Yellow arrows in the schematic and Figures 5.7 A and B show the direction of the red blood cells. Interestingly, extensive imaging of the *MZybx1* mutant and wild type hearts showed that a proportion of the mutant embryos has a retrograde blood flow at 5 dpf. To be able to analyse the blood flow patterns in these mutants I used particle image velocimetry (PIV) for tracking the movements of the red blood cells in the heart. In Figure 5.7 A mutant and wild type hearts are compared at different time points of the heartbeat: during relaxation of the chambers, atrial contraction, and ventricular contraction. At the diastole phase, in wild type hearts, there is not much movement of the red blood cells. A similar pattern is observed in the *ybx1* mutant hearts at this point. During the contraction of the atrium, in wild type and mutant embryos, the cells are moving to the ventricle, although some of the cells in the *ybx1* mutants show slightly altered directionality. In wild type sample, once the heart valves, shown in a white dotted line, are shut during the ventricular contraction, the red blood cells forcefully exit the ventricle and there is not much movement detected in the atrium. In mutants, at this stage, the cells are moving back and squeezing through the heart valves back from the ventricle to the atrium. It is very clear that there is reverse blood flow in the mutant embryos. In Figure 5.7 B, there is the quantification of the proportion of embryos showing reverse backflow. In the wildtype clutch of embryos, there was one example of reverse blood flow found out of 11 samples imaged. In *MZybx1* mutant embryos, however, I observed that 6 out of 12 embryos showed retrograde blood flow at 5 dpf.

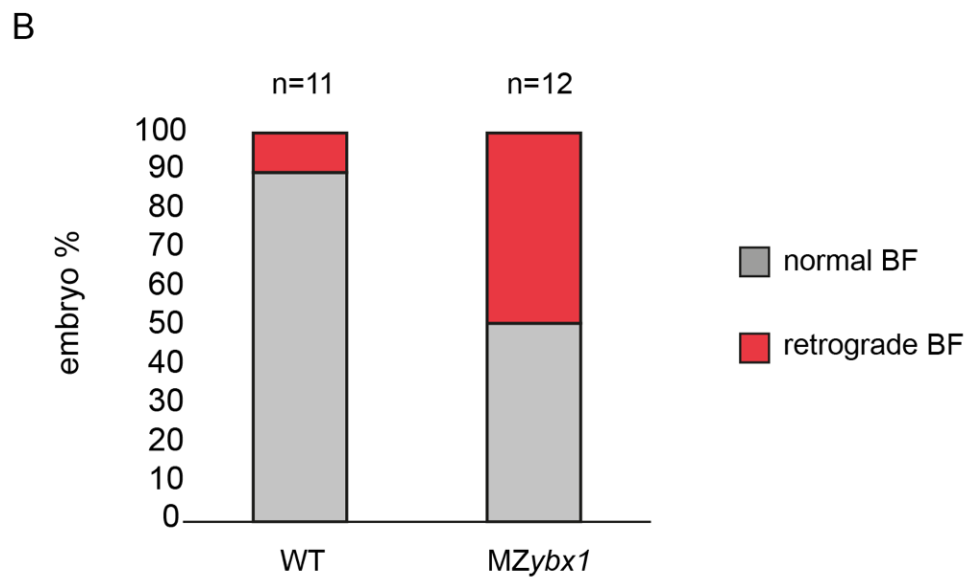
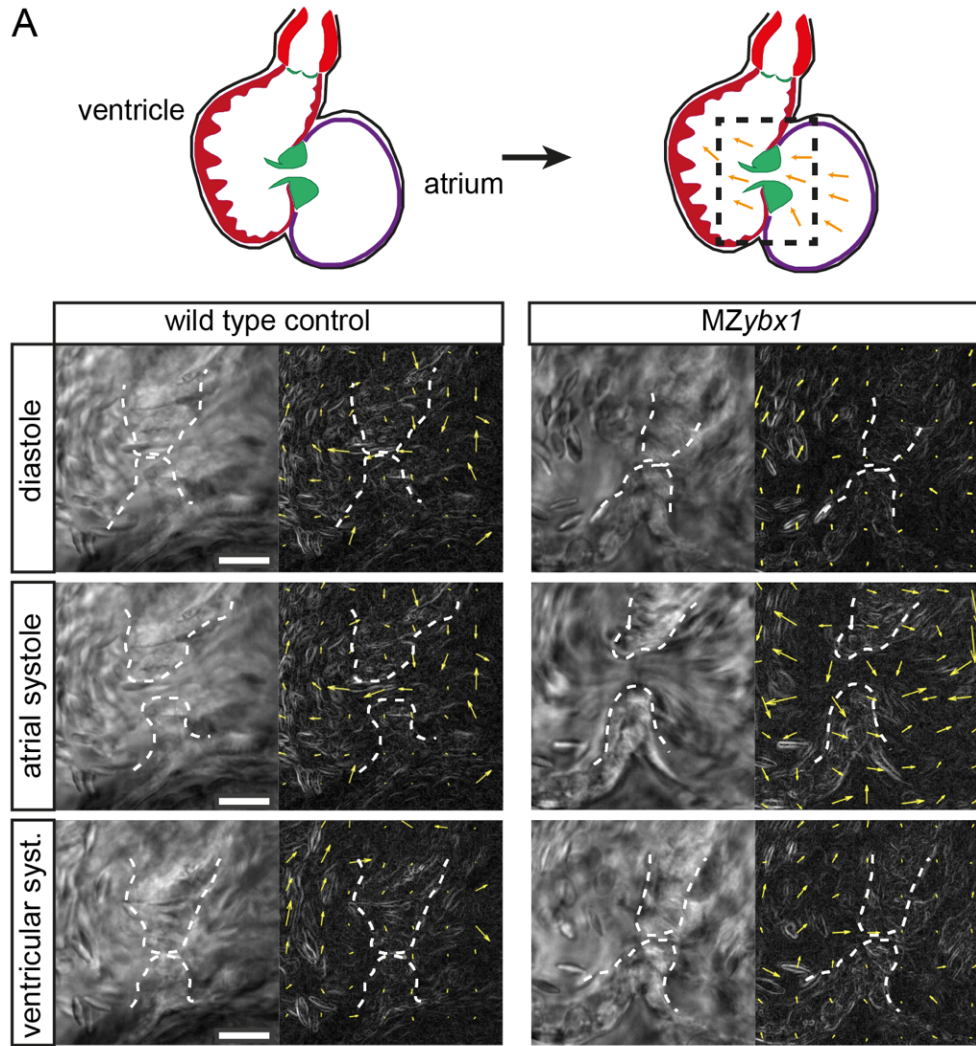


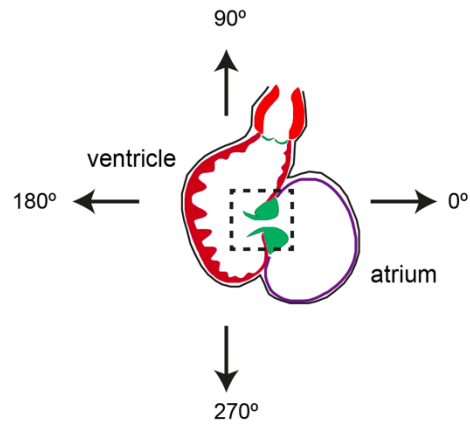
Figure 5.7 Proportion of the MZybx1 mutant embryos has retrograde blood flow.

- A) Basic schematic of the zebrafish heart at the 5 dpf. A black box with a dotted line shows the area that was imaged, and yellow arrows mark the movement of the red blood cells. Below are DIC images from the 30 s movies of the zebrafish heartbeat, next to the DIC image, there is an image of PIV analysis for the corresponding frame from the movie, yellow arrows show the movement of red blood cells. On left, there is a representation of the wild type, diastole, atrial systole, and ventricular systole. Mutant MZybx1 is on the right side. White dotted lines show the position of the heart valves at a given timepoint. The scale bar is 20 μm
- B) Graph showing the proportion of embryos with normal blood flow (BF) or retrograde blood flow (BF) in wild type embryos imaged and MZybx1 mutant embryos at 5 dpf from two biological replicates.

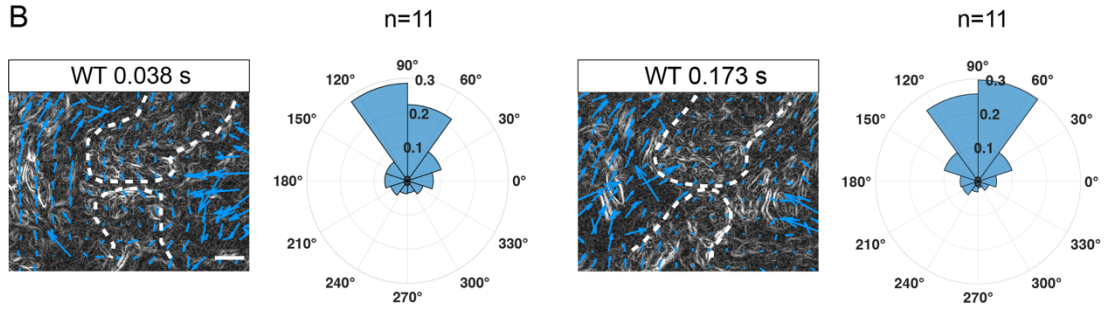
Next, I wanted to examine the blood flow in wild type and *ybx1* mutant embryos in more detail. From the movies in Figure 5.7 B, I observed that backflow mostly happened during the ventricular contraction in MZybx1 mutants, therefore I focussed on this phase of the heartbeat. Blood flow patterns of embryos imaged in Figure 5.7 B were studied using PIV. For each embryo, red blood cells were tracked and then the vectors generated from each movement were analysed for directionality. To avoid generating vectors due to heart muscle movements, the region of the heart valve was masked out and excluded from the analysis. In the schematic in Figure 5.8 A, the black square represents the area of the heart that was analysed and tracked for direction. In zebrafish, contraction of the heart is a very dynamic process, and the ventricular systole lasts only 0.192 s in total. Vectors were analysed at the beginning of ventricular systole at 0.038 s and towards the end at 0.173 s. In Figure 5.8 B, in wild type embryos (n=11), the direction of movement of red blood cells remains consistent throughout ventricular contraction and the cells are moving forcefully at 60° and 120° out of the ventricle. In all the *ybx1* mutant embryos (n=12), shown in Figure 5.8 C, the average movement of the red blood cells is comparable to wild type embryos at 0.038 s of ventricular contraction. At the 0.173 s however, in a proportion of the embryos, there is a change in the direction of the red blood cells and some increase in movements in

backward directions. Next in Figure 5.8 D, only *ybx1* mutant embryos with retrograde blood flow (n=6/12) were analysed for blood flow direction and by the end of ventricular contraction at 0.173 s, all the blood cells were going back to the atrium. In summary, when tracking the direction of the movement of blood in the wild type, I observed consistent movement out of the ventricle, but in *MZybx1* mutant embryos, there was more variation in the directionality of blood flow. In *ybx1* embryos with retrograde blood flow, backflow is clearly detected at 0.173 s, showing a heart defect at the 5 dpf.

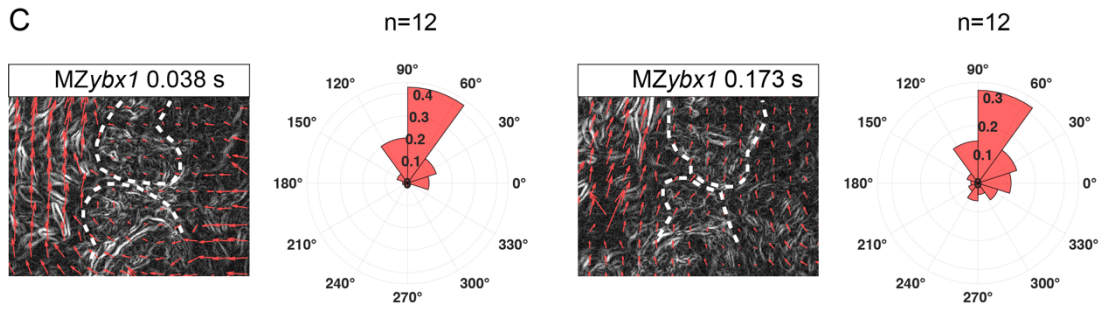
A



B



C



D

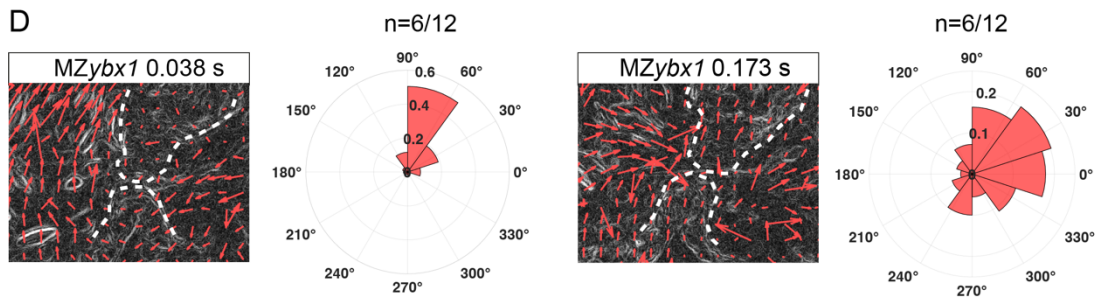


Figure 5.8 Analysis of the direction of the blood flow in MZybx1 mutant embryos at 5 dpf.

- A) Schematic of zebrafish heart at 5 dpf, the angle showed on a schematic corresponds to diagrams for quantification. The dotted line shows the area that was imaged.
- B) Representative example of wild type embryo using an image from PIV application at 0.038s and 0.173 s. Vectors generated from red blood cells are shown as blue arrows. Next to images corresponding quantification for 0.5s and 0.173 s timepoints showing the direction of the blood flow for all imaged wild type samples (n=11). The scale bar is 20 μm .
- C) A PIV image of an example of an analysed MZybx1 embryo at 0.038s and 0.173 s with vectors shown as red arrows. The corresponding quantification showing the direction of blood flow of all imaged MZybx1 embryos (n=12) at 0.038s and 0.173s. The scale bar is 20 μm .
- D) A PIV image showing the direction of blood flow only in MZybx1 embryos with retrograde blood flow at 0.038s and 0.173. Vectors are shown as red arrows. Next to the images is the analysis of the direction of blood flow in all MZybx1 embryos with retrograde blood flow (n=6/12) at 0.038s and 0.173s. The scale bar is 20 μm .

5.3 DISCUSSION

In this chapter, the left-right asymmetry and heart morphogenesis phenotype in *ybx1* mutant embryos was analysed in-depth. In Chapter 4, I described the translational repression of *furina* mRNA by Ybx1. The reporter assay has shown that there is a premature expression of FurinA protein in *ybx1* mutant embryos. Since FurinA is a protein that is important for the establishment of left-right asymmetry and heart morphogenesis, I focus on these two processes in *ybx1* mutant embryos in this chapter. In Figure 5.1 I show that a proportion of MZybx1 mutant embryos have an abnormal expression of *spaw*. Analysis of the organ development also shows that *ybx1* mutant

embryos have heart looping and organ positioning defects, as demonstrated in Figures 5.2 and 5.3. Interestingly, I also find that MZ*ybx1* mutant embryos have heart morphogenesis defects. For my experiments, I decided to activate the *ybx1^{sa42}* allele at 75% epiboly until the 21-som stage, because this is when *furina* variant *XI* mRNA is most expressed, according to the qPCR datasets shown in Figure 3.5 A. RNA immunoprecipitation has also shown that at these stages Ybx1 protein interacts with *furina XI* mRNA. Additionally, at these developmental stages, cardiogenic differentiation takes place, and the development of specialized ventricular and atrial myocyte cells occurs in the ALPM. These cells slowly progress towards more lateral regions of the ALPM, whilst endocardial cells form in the midline, fusing the cell groups together and forming a cardiac disc at the 25-som stage (Bakkers, 2011).

An exciting aspect of this study was studying the role of RNA binding protein Ybx1 in left-right asymmetry establishment. Embryos with *ybx1^{sa42}* mutation show bilateral *spaw* expression. At 55 hpf a proportion of embryos show defective heart looping and duplication or inversion of visceral organs, such as the liver and pancreas. These defects are clearly indicative of left-right asymmetry problems and demonstrate that Ybx1 protein has a role in organ positioning. To date, there are not many studies showing the involvement of RNA binding protein in left-right asymmetry establishment in zebrafish. There is one study describing the translational repression of *Bicc1* on *dand5* 5'UTR mRNA having a role in the establishment of laterality (Maerker *et al.*, 2021). The phenotype observed in *ybx1* mutant embryos is likely due to a lack of translational control of *furina* mRNA and is consistent with overexpression of FurinA protein. When there is an excess of FurinA protein, cleavage of Spaw is upregulated and the midline of an embryo is saturated with Spaw, which causes bilateral expression and consequently left-right asymmetry defects (Tessadori *et al.*, 2015).

Analysis of the atrioventricular canal markers in the *ybx1* mutant embryos revealed that although expression patterns of the *BMP4* and *notch1b* probes in Figure 5.4 were comparable in mutant and wild type embryos, there is an expansion in the AV canal

region. Overall, hearts also appeared bigger. Additionally, the looping in mutant hearts appeared weaker than in wild types. Recent studies show that FurinA protein is expressed in the AV canal and it cleaves Notch1B, and this mechanism has been shown to affect heart looping and trabeculation (Zhou *et al.*, 2021). Therefore, if the FurinA protein is upregulated in *ybx1* mutant fish, it could result in abnormal AV canal formation and aberrant looping. Although I observed these phenotypes, I was not certain that they were not just a consequence of the embryos being fixed at different phases of the heartbeat. The heart expands when it is relaxed and shrinks during contraction and the observed variation could arise from such differences. Treating embryos with an anaesthetic prior to fixing improved the reliability of this experiment, because all the hearts were stopped at the same phase in the heartbeat. Next, the area of the hearts was measured, as shown in Figure 5.5, and the results were compared between wild type and mutant embryos.

In Figure 5.5 I showed that the area of a heart in the *ybx1* mutant embryos group is significantly larger than in wild type control embryos. The sample size of this experiment, however, was very small and working with extracted hearts was difficult. In the literature, cardiomegaly is defined as a condition when the heart is enlarged. In zebrafish larvae, for a condition to be described as an enlargement of the heart the observed differences in the total area are normally much larger when compared to the controls (Gu *et al.*, 2017). In adult zebrafish, some studies report an increase of up to 4 times in the size of the heart and larger cardiomyocytes at the 5 dpf. These defects can be accompanied by cardiac oedema and reduced heart rate. Consequently, the strain on the heart is so large that it leads to cardiac failure and sudden death (Sun *et al.*, 2009; Shi *et al.*, 2021). As I did not observe these associated phenotypes and the differences in the surface area of zebrafish hearts were subtle, I decided to move on to analyse the AV canal.

The AV canal staining was performed in embryos at 55 hpf and using the same fixing method as for the area of the heart analysis to ensure the hearts of the embryos are in the same phase. In Figure 5.6 I observe that *ybx1* mutant embryos have significantly

enlarged AV canal. This was a very interesting finding because it meant that the heart morphogenesis was affected by activating the *ybx1* mutation. I found that in the wild type control the AV canal width measurements were comparable and close together, but in mutant embryos, there is more of a range and spread of measurements. Although this result was very exciting it was unclear if this phenotype affects heart function in any way. As the AV canal differentiates into heart valves, one possibility could be that valve morphogenesis might be disrupted in *ybx1* mutant embryos. At 55 hpf endocardial cushions can be observed and these structures at 5 dpf become functional heart valves (Gunawan *et al.*, 2019). From extensive imaging of the embryos stained with the ZN-8 antibody, shown in Figure 5.6, I was able to detect endocardial cushions consistently in all samples and they were comparable in appearance. This suggested that the heart valve morphogenesis was initiated as normal in both wild type and *ybx1* mutant embryos, but it was still unclear if the heart valves formed were defective. Although analysis of the heart morphogenesis is useful with staining on a fixed sample, it might not be as informative as using live embryos. Many details regarding organ function might be missed, when relying solely on immunostainings and WISH results. To address this issue, I started standard DIC live imaging on the zebrafish hearts to determine if the function of the heart is affected by having a larger AV canal.

Analysis of *ybx1* mutant hearts with live microscopy at 5 dpf has revealed key aspects of the effect of the mutation on the heart's function. I observed a proportion of the mutant embryos with retrograde blood flow. During ventricular systole, in wild type control embryos, all red blood cells leave the ventricle, in 6 out of 12 mutant embryos, however, there is clear backflow and cells are squeezing back through the heart valves to the atrium. Interestingly, I noticed there are different extents of backflow. In one mutant embryo, only a few red blood cells are going back and in five others a larger number of cells are going back.

Previous studies have suggested that prior to valve formation, initial reverse blood flow in zebrafish is important for the correct morphogenesis of the AV canal in the developing heart. *Klf2a* has been identified as a heart valve precursor and upon its

deletion, the AV canal loses its shape and heart valves that are formed are not functional. Additionally, in *klf2a* morphants there is a decrease in the AV marker *notch1b* at 36 hpf and at 46 hpf its expression is completely absent (Vermot *et al.*, 2009). In our *ybx1* mutants, however, the heart valves form normally. This variation in results in Figure 5.7 B could be due to differences in the width of the atrioventricular canal, which was observed in Figure 5.6. From the movies I did not observe any morphological defects of the heart valves, however, there is a possibility that leaky valves arise from the two valve flaps being too far from each other or being misaligned and consequently, are not able to shut properly.

A key issue to consider when analysing retrograde blood flow in *ybx1* mutant embryos is the severity of phenotype. Heart imaging was done at the 5 dpf and afterwards, embryos were culled. It is well known that zebrafish have regenerative properties, especially when it comes to cardiac development. For example, zebrafish heart valves can regenerate a few days after ablation (Bensimon-Brito *et al.*, 2020). It would be useful to study what happens to larvae with retrograde blood flow later in development and if they are viable with such a phenotype. There is a possibility that due to the backflow of blood, as the fish grows it does not obtain enough oxygen. Its blood pressure would then increase and eventually lead to such a strain on the heart that the fish is not able to survive. Another possibility could be that *ybx1* mutation causes developmental delay and later the heart fully recovers. These are important issues to consider, but due to the time limit on my project, I was not able to completely analyse the *ybx1* heart phenotype and answer these questions. However, these studies show an interesting insight into heart AV canal morphogenesis in zebrafish. A human cardiovascular disorder called mitral valve regurgitation is characterised by a leaky valve, which causes a backflow of blood. The extent of the symptoms varies, with some patients being asymptomatic and others experiencing dizziness, breathlessness, and irregular heartbeat (Adams, Rosenhek and Falk, 2010). Zebrafish embryos present a good research model to study this condition on a molecular level.

CHAPTER 6
CONCLUSIONS AND FUTURE
DIRECTIONS

In this work, I focussed on the regulatory mechanisms controlling the Nodal pathway. I describe a novel transcript *XI* of a proprotein convertase *FurinaA* and compare it to the annotated transcript 1. Interestingly, variant *XI* also has the 3'UTR RNA motif that is found in other nodal pathway components. This indicates that it is likely to interact with the RNA binding protein Ybx1. I confirmed the interaction between Ybx1 and *furina* mRNA, showing that they form complexes *in vivo* and that *furina* is translationally repressed by Ybx1. Finally, I study the phenotype of *ybx1* mutant embryos and show that they exhibit left-right asymmetry defects such as abnormal heart looping and randomisation of the visceral organ positioning. Additionally, I found that *ybx1* mutant embryos have a larger atrioventricular canal when compared to mutants and a proportion of the mutant embryos have retrograde blood flow as a result. In this important work, I demonstrated a novel mechanism of translation control by Ybx1 that has a key function in heart morphogenesis in zebrafish embryos.

In Chapter 3 I compare *furina* transcript 1 and transcript *XI* and analyse their expression levels and patterns at different stages of the zebrafish development. I found that variant *XI* is expressed at the highest levels during early somitogenesis and that similarly to transcript 1, it is ubiquitous in zebrafish embryos. During my studies the focus of the project was *furina* variant *XI*, taking this project forward I believe extensive analysis of embryonic samples from different developmental stages and even adult zebrafish tissues would help to clarify the differences between two transcripts and their potential roles. It would be useful to study the expression levels of transcript 1 and variant *XI* further and look in more detail at later embryonic stages through qPCR and WISH experiments. My analysis focused on embryonic stages up to 18 som, which is approximately 16 hpf. It would have been interesting to study datasets from other stages such as larvae and adult fish tissues to determine expression levels of variant *XI* in more detail. Furthermore, extensive sequencing of zebrafish embryos through experiments like RNA-seq would help to address in more detail the differences between both transcripts. It is not known why *furina* in zebrafish requires two transcripts and why variant *XI* needs a 3.5 kb 3'UTR sequence. My initial WISH analysis has shown that there is enrichment of variant *XI* in the eyes, hindbrain, and

somites, therefore it is very likely that *furina* is also involved in other developmental processes than left-right asymmetry establishment and heart development.

In Chapter 3 I also introduced two novel alleles, *furina* Δ 56 bp, which removed part of the 5'UTR and the signal peptide disrupting the protein function and the second allele *furina XI* Δ 3'UTR. This mutation caused a deletion of 1500 bp fragment out of the 3375 bp variant *XI* 3'UTR sequence including the YBE motif. Poly(A) tail was left intact to ensure stability of the *XI* transcript. The comparison of both alleles to determine the role of *furina* variant *XI* was very challenging. In both mutant zebrafish lines, I have not been able to retrieve homozygous fish. In the first instance of the *furina* Δ 56 bp, this was due to the fact that maternal-zygotic *furina* mutants do not inflate a swim bladder and die at the day 5 of development. The survival of homozygous female fish is approximately 20% (Walker *et al.*, 2006; Tessadori *et al.*, 2015). Similarly, in the *furina* Δ 3'UTR trying to expand the fish line through homozygous incrosses was very difficult as approximately 14 days post fertilization the survival of fish dropped, and many did not survive to adulthood. I have been able to recover only wild type or heterozygous fish from heterozygous crosses. Furthermore, heterozygous incrosses up to 5 days post fertilization looked indistinguishable from wild type fish. One of the possible explanations for this could be that *furina* variant *XI* has a critical role later in juvenile fish development, which I did not observe earlier, as my research focussed on the initial 5 days of development. On the other hand, due to Covid-19 pandemic there were many disruptions with growing new fish lines and screening them. The access to the facility and laboratory occupancy were limited to help ensure staff safety, and this meant that routine fish care and feedings were reduced, which affected the survival of new fish lines. As a result, I was not able to determine with certainty why I was not able to recover maternal-zygotic *furina XI* Δ 3'UTR fish and analyse the phenotype of these embryos.

Analysis of the phenotype of *furina* variant *XI* is a key experiment that would shed some light on the novel variant *XI* function. The essential experiment to complete this work would be to study the establishment of the left-right asymmetry, atrioventricular

canal development and heart morphogenesis in these mutant fish. Extensive analysis with heart WISH markers as performed in Chapter 5 and live imaging would confirm the hypothesis of importance of *furina* in left-right asymmetry and heart development.

One of the key aspects of this work is the interaction between Ybx1 protein with *furina* mRNA. Using RNA immunoprecipitation and microinjections I demonstrated that Ybx1 binds to the *furina* mRNA and causes translational repression. Consistently I also found that maturation of FurinA downstream target Spaw is upregulated in the *ybx1* mutant embryos. From the results in Chapter 4, it is clear that *furina* and Ybx1 interact in zebrafish embryos, however, I have not shown that Ybx1 binds directly to the 3'UTR motif. In previous work from the Sampath laboratory, *in vitro* binding assays with different deletion constructs were performed to demonstrate the direct binding of Ybx1 with the YBE motif in *sqt*, *lefty1* and *lefty2* mRNAs (Kumari *et al.*, 2013; Zaucker *et al.*, 2017). For additional analysis of the Ybx1 *furina* variant *XI* interaction, it would be useful to directly show the binding and determine how deletions of the YBE motif affect binding to *furina XI* mRNA *in vitro*.

One of the most exciting parts of this thesis is the analysis of the left-right asymmetry phenotype and cardiac morphogenesis. In Chapter 4 using the GFP fusion reporter assay I observed premature expression and upregulation of FurinA. Additionally, I also observed upregulation of Spaw maturation, and this led to the hypothesis that if the expression of Spaw in *ybx1* mutants is aberrant, they might exhibit heart looping and visceral organ positioning defects. Using immunofluorescence and WISH staining I confirm that *ybx1* mutant embryos exhibit left-right asymmetry defects in Chapter 5. Interestingly, the bilateral or inverted *spaw* is observed in 30% of mutant embryos, heart looping and inversion of visceral organs in 25% of maternal zygotic *ybx1*^{sa42} embryos. These numbers suggest that the phenotype is not as severe as expected. Upregulation in FurinA protein via lack of Ybx1 translational control are considered the reason for the left-right asymmetry defects. However, Ybx1 also translationally regulates other Nodal pathway components such as ligand *sqt*, *lefty1* and *lefty2* inhibitors (Gore *et al.*, 2005; Kumari *et al.*, 2013; Zaucker *et al.*, 2017). Furthermore,

computational analysis also predicted that it is likely to regulate *acvr2a* receptor and *smad2* intracellular transducer, but this has not been experimentally verified. Lefty1 is expressed at the midline of the embryos when the *ybx*^{sa42} mutation was triggered from 60% epiboly to 21-somite stage. Lefty1 also has a role of inhibiting Spaw and preventing it from crossing the midline. It is possible that upregulation of Lefty1 in the *ybx1* mutants also restricts the additional mature Spaw that is cleaved by increased levels of FurinA protein. This offers an explanation of why only a proportion of *ybx1*^{sa42} mutants has left-right asymmetry defects. To examine this hypothesis further using transgenic *lefty1* GFP fish line with *ybx1* mutants to determine if the endogenous Lefty1 GFP is upregulated with western blot analysis and to examine the expression levels during somitogenesis at the midline of an embryo. Additionally, during the somitogenesis *lefty2* is expressed in the second and first heart field and although *lefty2* mutations do not affect the left-sided expression of *spaw*, they do affect heart looping in the embryos (Baker, Holtzman and Burdine, 2008; Montague, Gagnon and Schier, 2018). The overexpression of Lefty2 might also be a contributing factor in the heart looping phenotype and heart morphogenesis in *ybx1* mutant embryos.

During the analysis of this data, I also observed that the atrioventricular canal of *ybx1* mutant embryos is enlarged, and some embryos show retrograde blood flow. This was particularly interesting because in zebrafish there are reports of *furina* expression in the atrioventricular canal and some mice studies have shown that *Furin* knock down results in valve defects (WooJin *et al.*, 2012; Zhou *et al.*, 2021). Taken together, these results suggest that the Ybx1 and *furina* interaction may play a role in valve morphogenesis. The origin the AV canal and heart morphogenesis phenotype might be an effect of increased Spaw maturation. Studies have shown that during late somitogenesis Spaw activates BMP4 close to the heart field in the left LPM (Chocron *et al.*, 2007). In *ybx1* mutant embryos due to increased and premature Spaw processing, there could be also increased BMP4. The key roles of BMP4 are heart septation and endocardial cushion formation in the AV canal, therefore disruption to these processes could affect the heart morphogenesis and explain *ybx1* mutant phenotype (McCulley *et al.*, 2008).

Recent studies have uncovered that FurinA is required to cleave Notch1B and both colocalise in the AV canal at the day 4 of development (Zhou *et al.*, 2021). Notch pathway has been described as an important interactor in the AV canal development, and both gain and loss of Notch function studies resulted in the AV canal defects in mice (Niessen and Karsan, 2008). Similarly as in zebrafish, aberrant Notch1B expression causes heart defects (Samsa *et al.*, 2015). Upregulation of FurinA in *ybx1* mutant embryos would also increase the cleavage of Notch1B, which consequently could cause AV canal defects.

Ybx1 is a global translational repressor and although the observed left-right and cardiac morphogenesis phenotypes are interesting, there is always a possibility that upregulation of other genetic pathway may affect the embryonic development (Sun *et al.*, 2018). Analysis of the *furina* Δ ATG and *furina* Δ 3'UTR mutants is one of the possible methods to ensure the specificity of the phenotypes. Experiments should be performed to determine if *furina* Δ 3UTR homozygous mutants exhibit similar left-right asymmetry defects and AV canal enlargement and retrograde blood flow.

One of the challenging aspects of using zebrafish as a model organism is the unavailability of commercial antibodies for some less conserved proteins. The easiest way to measure the endogenous protein levels would be to perform a western blot analysis. This would help to quickly determine if other Nodal proteins, such as Lefty1 and Lefty2, are also upregulated. Another possible method would be generating a transgenic line or a knock in with a desired tag and to cross it with *ybx1* mutants. There have been many useful studies showing the use of CRISPR genome editing to insert various tags such as: polyhistidine or GFP in the zebrafish genome (Tessadori *et al.*, 2018). Although this would help to study expression patterns and protein levels of various Nodal proteins live, it would be very time consuming to generate. It would take at least 6 months to retrieve positive fish with an insertion. To be able to understand the mechanism of translational control by *Ybx1* better, it would be useful to carry out ribosomal profiling. This is a deep sequencing method that identifies ribosome-protected mRNAs. This provides a genome-wide overview of actively

translated ribosome-mRNA complexes (Brar and Weissman, 2015). This method would provide a detailed information on how mutation of Ybx1 impacts translation of different targets and Nodal pathway components.

In the literature, there are already proposed mechanisms that are important for heart function by non-coding RNA molecules such as microRNAs (miRNAs). Abnormal expression of miRNAs is associated with defects in cardiac cell differentiation and cardiac dysfunction. In zebrafish, key cardiac development genes such as *tbx2*, *notch1* and *cspg2* are regulated by miRNAs (Kalayinia *et al.*, 2021). Studies in mice have shown that increased levels of miR-25 have led to depressed cardiac function, but inhibition of miR-25 reversed the phenotype and increased survival in a mouse heart failure model (Wahlquist *et al.*, 2014). In humans and mice, miR-133 and miR-1 are abundant in heart tissue and have important roles in myoblast proliferation and differentiation. Interestingly studies in mice found that overexpression of miR-133 or miR-1 suppressed cardiac hypertrophy, which is the thickening of the heart muscle. When miR-133 or miR-1 levels were reduced, however, cardiac hypertrophy was induced (Carè *et al.*, 2007; Romaine *et al.*, 2015). This leads to the conclusion that non-coding molecules are indispensable in cardiac morphogenesis.

To conclude, the CRISPR Cas-9 *furina* mutants $\Delta 56\text{bp}$ and *XI* $\Delta 3'$ UTR would be useful to explore the function of *furina* in the context of heart development. Especially for analysis of the atrioventricular canal, heart valve morphogenesis, and blood flow at 5 dpf. Such an analysis together with in depth sequencing methods would confirm if the phenotypes observed in *ybx1* mutant embryos are a result of an abnormal expression of FurinA and shed more detail on the nature of this interaction. Little is known about the function of the non-coding region in heart development. Therefore, a detailed analysis of the *furina XI* $\Delta 3'$ UTR mutant fish line might provide some exciting insight into the biomolecular mechanism of cardiac morphogenesis and would be a good continuation of the work presented in this thesis.

CHAPTER 7

REFERENCES

- Adams, D. H., Rosenhek, R. and Falk, V. (2010) 'Degenerative mitral valve regurgitation: best practice revolution', *European Heart Journal*, 31(16), pp. 1958–1966. doi: 10.1093/eurheartj/ehq222.
- Bae, B. and Miura, P. (2021) 'CRISPR-Mediated Knockout of Long 3' UTR mRNA Isoforms in mESC-Derived Neurons', *Frontiers in Genetics*, 12. doi: 10.3389/fgene.2021.789434.
- Baker, K., Holtzman, N. G. and Burdine, R. D. (2008) 'Direct and indirect roles for Nodal signaling in two axis conversions during asymmetric morphogenesis of the zebrafish heart', *Proceedings of the National Academy of Sciences*. Proceedings of the National Academy of Sciences, 105(37), pp. 13924–13929. doi: 10.1073/pnas.0802159105.
- Bakkers, J. (2011) 'Zebrafish as a model to study cardiac development and human cardiac disease.', *Cardiovascular research*, 91(2), pp. 279–288. doi: 10.1093/cvr/cvr098.
- Beck, S. *et al.* (2002) 'Extraembryonic proteases regulate Nodal signalling during gastrulation.', *Nature cell biology*. England, 4(12), pp. 981–985. doi: 10.1038/ncb890.
- Bensimon-Brito, A. *et al.* (2020) 'TGF- β 2; Signaling Promotes Tissue Formation during Cardiac Valve Regeneration in Adult Zebrafish', *Developmental Cell*. Elsevier, 52(1), pp. 9-20.e7. doi: 10.1016/j.devcel.2019.10.027.
- Bentley, D. L. (2014) 'Coupling mRNA processing with transcription in time and space', *Nature Reviews Genetics*, 15(3), pp. 163–175. doi: 10.1038/nrg3662.
- Bestle, D. *et al.* (2020) 'TMPRSS2 and furin are both essential for proteolytic activation and spread of SARS-CoV-2 in human airway epithelial cells and provide promising drug targets', *bioRxiv*. Cold Spring Harbor Laboratory. doi: 10.1101/2020.04.15.042085.
- Blower, M. D. (2013) 'Molecular insights into intracellular RNA localization', *International review of cell and molecular biology*, 302, pp. 1–39. doi: 10.1016/B978-0-12-407699-0.00001-7.
- Blum, M. and Ott, T. (2018) 'Animal left-right asymmetry', *Current Biology*. Elsevier, 28(7), pp. R301–R304. doi: 10.1016/j.cub.2018.02.073.
- Brar, G. A. and Weissman, J. S. (2015) 'Ribosome profiling reveals the what, when, where and how of protein synthesis', *Nature Reviews Molecular Cell Biology*. Nature Publishing Group, a division of Macmillan Publishers Limited. All Rights Reserved., 16, p. 651. Available at: <https://doi.org/10.1038/nrm4069>.
- Brown, D. R. *et al.* (2016) 'Advances in the Study of Heart Development and Disease Using Zebrafish', *Journal of Cardiovascular Development and Disease* . 3(2):13. doi: 10.3390/jcdd3020013.
- Brown, J. L. *et al.* (2008) 'Transcriptional profiling of endogenous germ layer precursor cells identifies *dusp4* as an essential gene in zebrafish endoderm specification', *Proceedings of the National Academy of Sciences*, 105(34), pp.

12337–12342. doi: 10.1073/pnas.0805589105.

Carè, A. *et al.* (2007) ‘MicroRNA-133 controls cardiac hypertrophy’, *Nature Medicine*, 13(5), pp. 613–618. doi: 10.1038/nm1582.

Carvalho, L. and Heisenberg, C.-P. (2010) ‘The yolk syncytial layer in early zebrafish development’, *Trends in Cell Biology*, 20(10), pp. 586–592. doi: <https://doi.org/10.1016/j.tcb.2010.06.009>.

Chang, C.-W. *et al.* (2011) ‘Anterior-posterior axis specification in *Drosophila* oocytes: identification of novel bicoid and oskar mRNA localization factors’, *Genetics*. Genetics Society of America, 188(4), pp. 883–896. doi: 10.1534/genetics.111.129312.

Chen, C. and Shen, M. M. (2004) ‘Two Modes by which Lefty Proteins Inhibit Nodal Signaling’, *Current Biology*, 14(7), pp. 618–624. doi: <https://doi.org/10.1016/j.cub.2004.02.042>.

Chocron, S. *et al.* (2007) ‘Zebrafish Bmp4 regulates left–right asymmetry at two distinct developmental time points’, *Developmental Biology*, 305(2), pp. 577–588. doi: <https://doi.org/10.1016/j.ydbio.2007.03.001>.

Choi, Y. J., Yoon, J.-H. and Chang, J. H. (2016) ‘Crystal Structure of the N-Terminal RNA Recognition Motif of mRNA Decay Regulator AUF1’, *BioMed research international*. 2016/06/29. Hindawi Publishing Corporation, 2016, p. 3286191. doi: 10.1155/2016/3286191.

Constam, D. B. (2009) ‘Riding Shotgun: A Dual Role for the Epidermal Growth Factor-Cripto/FRL-1/Cryptic Protein Cripto in Nodal Trafficking’, *Traffic*, 10(7), pp. 783–791. doi: <https://doi.org/10.1111/j.1600-0854.2009.00874.x>.

Constam, D. B. and Robertson, E. J. (2000) ‘SPC4/PACE4 regulates a TGFbeta signaling network during axis formation.’, *Genes & development*. United States, 14(9), pp. 1146–1155.

Cui, C., Little, C. D. and Rongish, B. J. (2009) ‘Rotation of organizer tissue contributes to left-right asymmetry.’, *Anatomical record (Hoboken, N.J. : 2007)*. United States, 292(4), pp. 557–561. doi: 10.1002/ar.20872.

Cui, Y. *et al.* (1998) ‘BMP-4 is proteolytically activated by furin and/or PC6 during vertebrate embryonic development’, *The EMBO journal*, 17(16), pp. 4735–4743. doi: 10.1093/emboj/17.16.4735.

Dasgupta, A. and Amack, J. D. (2016) ‘Cilia in vertebrate left-right patterning’, *Philosophical transactions of the Royal Society of London. Series B, Biological sciences*. The Royal Society, 371(1710), p. 20150410. doi: 10.1098/rstb.2015.0410.

Davis, B. M. *et al.* (1997) ‘Expansion of a CUG trinucleotide repeat in the 3’ untranslated region of myotonic dystrophy protein kinase transcripts results in nuclear retention of transcripts.’, *Proceedings of the National Academy of Sciences of the United States of America*, 94(14), pp. 7388–7393. doi: 10.1073/pnas.94.14.7388.

Deng, H., Xia, H. and Deng, S. (2014) ‘Genetic basis of human left–right asymmetry disorders’, *Expert Reviews in Molecular Medicine*. 2015/01/27. Cambridge University Press, 16, p. e19. doi: DOI: 10.1017/erm.2014.22.

Dong, J. *et al.* (2009) ‘RNA-binding specificity of Y-box protein 1’, *RNA biology*. 2009/01/19, 6(1), pp. 59–64. doi: 10.4161/rna.6.1.7458.

Dong, Y., Qian, L. and Liu, J. (2021) ‘Molecular and cellular basis of embryonic cardiac chamber maturation’, *Seminars in Cell & Developmental Biology*, 118, pp. 144–149. doi: <https://doi.org/10.1016/j.semcdb.2021.04.022>.

Dougan, S. T. *et al.* (2003) ‘The role of the zebrafish nodal-related genes *squint* and *cyclops* in patterning of mesendoderm’, *Development*. The Company of Biologists Ltd, 130(9), pp. 1837–1851. doi: 10.1242/dev.00400.

Drummond, D. L. *et al.* (2013) ‘The role of *Zic* transcription factors in regulating hindbrain retinoic acid signaling’, *BMC Developmental Biology*, 13(1), p. 31. doi: 10.1186/1471-213X-13-31.

Dupays, L. *et al.* (2019) ‘Furin, a transcriptional target of *NKX2-5*, has an essential role in heart development and function’, *PLOS ONE*. Public Library of Science, 14(3), pp. 1–21. doi: 10.1371/journal.pone.0212992.

El-Brolosy, M. A. and Stainier, D. Y. R. (2017) ‘Genetic compensation: A phenomenon in search of mechanisms’, *PLOS Genetics*. Public Library of Science, 13(7), p. e1006780. Available at: <https://doi.org/10.1371/journal.pgen.1006780>.

Feldman, B. *et al.* (1998) ‘Zebrafish organizer development and germ-layer formation require nodal-related signals’, *Nature*, 395(6698), pp. 181–185. doi: 10.1038/26013.

Field, S. *et al.* (2011) ‘*Pkd11l1* establishes left-right asymmetry and physically interacts with *Pkd2*’, *Development*, 138(6), pp. 1131–1142. doi: 10.1242/dev.058149.

Francescato, L. *et al.* (2010) ‘The activation of membrane targeted CaMK-II in the zebrafish Kupffer’s vesicle is required for left-right asymmetry’, *Development*. The Company of Biologists Ltd, 137(16), pp. 2753–2762. doi: 10.1242/dev.049627.

Furtado, M. B. *et al.* (2008) ‘BMP/SMAD1 signaling sets a threshold for the left/right pathway in lateral plate mesoderm and limits availability of SMAD4.’, *Genes & development*. United States, 22(21), pp. 3037–3049. doi: 10.1101/gad.1682108.

Galloway, A. and Cowling, V. H. (2019) ‘mRNA cap regulation in mammalian cell function and fate’, *Biochimica et Biophysica Acta (BBA) - Gene Regulatory Mechanisms*, 1862(3), pp. 270–279. doi: <https://doi.org/10.1016/j.bbagr.2018.09.011>.

Gilligan, P. C. *et al.* (2011) ‘Conservation defines functional motifs in the *squint/nodal-related 1* RNA dorsal localization element’, *Nucleic acids research*. 2010/12/10. Oxford University Press, 39(8), pp. 3340–3349. doi:

10.1093/nar/gkq1185.

Gore, A. V *et al.* (2005) 'The zebrafish dorsal axis is apparent at the four-cell stage', *Nature*. Nature Publishing Group, 438, p. 1030. Available at: <https://doi.org/10.1038/nature04184>.

Gritsman, K. *et al.* (1999) 'The EGF-CFC protein one-eyed pinhead is essential for nodal signaling.', *Cell*. United States, 97(1), pp. 121–132. doi: 10.1016/s0092-8674(00)80720-5.

Gros, J. *et al.* (2009) 'Cell movements at Hensen's node establish left/right asymmetric gene expression in the chick.', *Science (New York, N.Y.)*. United States, 324(5929), pp. 941–944. doi: 10.1126/science.1172478.

Gu, G. *et al.* (2017) 'Zebrafish Larvae Model of Dilated Cardiomyopathy Induced by Terfenadine', *Korean circulation journal*. 2017/09/20. The Korean Society of Cardiology, 47(6), pp. 960–969. doi: 10.4070/kcj.2017.0080.

Gunawan, F. *et al.* (2019) 'Focal adhesions are essential to drive zebrafish heart valve morphogenesis', *The Journal of Cell Biology*. Rockefeller University Press. doi: 10.1083/jcb.201807175.

Hill, C. S. (2018) 'Spatial and temporal control of NODAL signaling', *Current Opinion in Cell Biology*, 51, pp. 50–57. doi: <https://doi.org/10.1016/j.ceb.2017.10.005>.

Howe, K. *et al.* (2013) 'The zebrafish reference genome sequence and its relationship to the human genome.', *Nature*, 496(7446), pp. 498–503. doi: 10.1038/nature12111.

Izidoro, M. A. *et al.* (2009) 'A study of human furin specificity using synthetic peptides derived from natural substrates, and effects of potassium ions.', *Archives of biochemistry and biophysics*, 487(2), pp. 105–114. doi: 10.1016/j.abb.2009.05.013.

J., G. A. *et al.* (2006) 'Zebrafish MiR-430 Promotes Deadenylation and Clearance of Maternal mRNAs', *Science*. American Association for the Advancement of Science, 312(5770), pp. 75–79. doi: 10.1126/science.1122689.

Ji, Y., Buel, S. M. and Amack, J. D. (2016) 'Mutations in zebrafish *pitx2* model congenital malformations in Axenfeld-Rieger syndrome but do not disrupt left-right placement of visceral organs', *Developmental biology*. 2016/06/11, 416(1), pp. 69–81. doi: 10.1016/j.ydbio.2016.06.010.

Jukam, D., Shariati, S. A. M. and Skotheim, J. M. (2017) 'Zygotic Genome Activation in Vertebrates', *Developmental cell*, 42(4), pp. 316–332. doi: 10.1016/j.devcel.2017.07.026.

Kalayinia, S. *et al.* (2021) 'MicroRNAs: roles in cardiovascular development and disease', *Cardiovascular Pathology*, 50, p. 107296. doi: <https://doi.org/10.1016/j.carpath.2020.107296>.

Kane, D. A. and Kimmel, C. B. (1993) 'The zebrafish midblastula transition.', *Development (Cambridge, England)*. England, 119(2), pp. 447–456. doi:

10.1242/dev.119.2.447.

Kiecker, C., Bates, T. and Bell, E. (2016) 'Molecular specification of germ layers in vertebrate embryos.', *Cellular and molecular life sciences : CMLS*, 73(5), pp. 923–947. doi: 10.1007/s00018-015-2092-y.

Kimmel, C. B. *et al.* (1995) 'Stages of embryonic development of the zebrafish.', *Developmental dynamics : an official publication of the American Association of Anatomists*. United States, 203(3), pp. 253–310. doi: 10.1002/aja.1002030302.

Kishigami, S. *et al.* (2004) 'BMP signaling through ACVRI is required for left–right patterning in the early mouse embryo', *Developmental Biology*, 276(1), pp. 185–193. doi: <https://doi.org/10.1016/j.ydbio.2004.08.042>.

Kishimoto, Y. *et al.* (1997) 'The molecular nature of zebrafish swirl: BMP2 function is essential during early dorsoventral patterning', *Development*, 124(22), pp. 4457–4466. doi: 10.1242/dev.124.22.4457.

Kloesel, B., DiNardo, J. A. and Body, S. C. (2016) 'Cardiac Embryology and Molecular Mechanisms of Congenital Heart Disease: A Primer for Anesthesiologists.', *Anesthesia and analgesia*, 123(3), pp. 551–569. doi: 10.1213/ANE.0000000000001451.

Kumari, P. *et al.* (2013) 'An essential role for maternal control of Nodal signaling', *eLife*. Edited by R. Lehmann. eLife Sciences Publications, Ltd, 2, p. e00683. doi: 10.7554/eLife.00683.

Kumari, P. *et al.* (2018) 'Evolutionary plasticity of the NHL domain underlies distinct solutions to RNA recognition.', *Nature communications*. England, 9(1), p. 1549. doi: 10.1038/s41467-018-03920-7.

Laue, K. *et al.* (2019) 'The maternal to zygotic transition regulates genome-wide heterochromatin establishment in the zebrafish embryo', *Nature Communications*, 10(1), p. 1551. doi: 10.1038/s41467-019-09582-3.

Lee, M. T., Bonneau, A. R. and Giraldez, A. J. (2014) 'Zygotic genome activation during the maternal-to-zygotic transition', *Annual review of cell and developmental biology*. 2014/08/11, 30, pp. 581–613. doi: 10.1146/annurev-cellbio-100913-013027.

Lenhart, K. F. *et al.* (2011) 'Two additional midline barriers function with midline lefty1 expression to maintain asymmetric Nodal signaling during left-right axis specification in zebrafish', *Development*, 138(20), pp. 4405–4410. doi: 10.1242/dev.071092.

Li, J.-Y. *et al.* (2021) 'BNC1 Promotes Spermatogenesis by Regulating Transcription of Ybx2 and Papolb via Direct Binding to Their Promotor Elements', *Reproductive Sciences*, 28(3), pp. 785–793. doi: 10.1007/s43032-020-00342-z.

Li, Y. *et al.* (2012) 'Dynamic landscape of tandem 3' UTRs during zebrafish development', *Genome research*. 2012/09/05. Cold Spring Harbor Laboratory Press, 22(10), pp. 1899–1906. doi: 10.1101/gr.128488.111.

Li, Y. E. *et al.* (2017) 'Identification of high-confidence RNA regulatory elements

by combinatorial classification of RNA–protein binding sites’, *Genome Biology*, 18(1), p. 169. doi: 10.1186/s13059-017-1298-8.

Lin, C. R. *et al.* (1999) ‘Pitx2 regulates lung asymmetry, cardiac positioning and pituitary and tooth morphogenesis.’, *Nature*. England, 401(6750), pp. 279–282. doi: 10.1038/45803.

Logan, M. *et al.* (1998) ‘The Transcription Factor Pitx2 Mediates Situs-Specific Morphogenesis in Response to Left-Right Asymmetric Signals’, *Cell*, 94(3), pp. 307–317. doi: [https://doi.org/10.1016/S0092-8674\(00\)81474-9](https://doi.org/10.1016/S0092-8674(00)81474-9).

Long, S., Ahmad, N. and Rebagliati, M. (2003) ‘The zebrafish nodal-related gene southpaw is required for visceral and diencephalic left-right asymmetry’, *Development*. The Company of Biologists Ltd, 130(11), pp. 2303–2316. doi: 10.1242/dev.00436.

Lopez de Silanes, I. *et al.* (2004) ‘Identification of a target RNA motif for RNA-binding protein HuR.’, *Proceedings of the National Academy of Sciences of the United States of America*. United States, 101(9), pp. 2987–2992. doi: 10.1073/pnas.0306453101.

Lu, Z. H., Books, J. T. and Ley, T. J. (2005) ‘YB-1 Is Important for Late-Stage Embryonic Development, Optimal Cellular Stress Responses, and the Prevention of Premature Senescence’, *Molecular and Cellular Biology*. American Society for Microbiology Journals, 25(11), pp. 4625–4637. doi: 10.1128/MCB.25.11.4625-4637.2005.

Lyabin, D. N. *et al.* (2011) ‘Interplay between Y-box-binding protein 1 (YB-1) and poly(A) binding protein (PABP) in specific regulation of YB-1 mRNA translation’, *RNA biology*. 2011/09/01. Landes Bioscience, 8(5), pp. 883–892. doi: 10.4161/rna.8.5.16022.

Lyabin, D. N., Eliseeva, I. A. and Ovchinnikov, L. P. (2014) ‘YB-1 protein: functions and regulation’, *Wiley Interdisciplinary Reviews: RNA*, 5(1), pp. 95–110. doi: 10.1002/wrna.1200.

Madeira, F. *et al.* (2019) ‘The EMBL-EBI search and sequence analysis tools APIs in 2019’, *Nucleic acids research*. European Molecular Biology Laboratory, European Bioinformatics Institute (EMBL-EBI), Wellcome Trust Genome Campus, Hinxton, Cambridge CB10 1SD, UK., 47(W1), pp. W636–W641. doi: 10.1093/nar/gkz268.

Maerker, M. *et al.* (2021) ‘Bicc1 and Dicer regulate left-right patterning through post-transcriptional control of the Nodal inhibitor Dand5’, *Nature Communications*, 12(1), p. 5482. doi: 10.1038/s41467-021-25464-z.

Marmisolle, F. E., García, M. L. and Reyes, C. A. (2018) ‘RNA-binding protein immunoprecipitation as a tool to investigate plant miRNA processing interference by regulatory proteins of diverse origin’, *Plant Methods*, 14(1), p. 9. doi: 10.1186/s13007-018-0276-9.

Matsui, T. *et al.* (2011) ‘Canopy1, a positive feedback regulator of FGF signaling,

- controls progenitor cell clustering during Kupffer's vesicle organogenesis', *Proceedings of the National Academy of Sciences*. National Academy of Sciences, 108(24), pp. 9881–9886. doi: 10.1073/pnas.1017248108.
- Matsui, T. and Bessho, Y. (2012) 'Left-right asymmetry in zebrafish', *Cellular and Molecular Life Sciences*, 69(18), pp. 3069–3077. doi: 10.1007/s00018-012-0985-6.
- McCulley, D. J. *et al.* (2008) 'BMP4 is required in the anterior heart field and its derivatives for endocardial cushion remodeling, outflow tract septation, and semilunar valve development.', *Developmental dynamics : an official publication of the American Association of Anatomists*. United States, 237(11), pp. 3200–3209. doi: 10.1002/dvdy.21743.
- McKee, A. E. and Silver, P. A. (2007) 'Systems perspectives on mRNA processing', *Cell Research*, 17(7), pp. 581–590. doi: 10.1038/cr.2007.54.
- Medioni, C., Mowry, K. and Besse, F. (2012) 'Principles and roles of mRNA localization in animal development', *Development (Cambridge, England)*. Company of Biologists, 139(18), pp. 3263–3276. doi: 10.1242/dev.078626.
- Meno, C. *et al.* (1998) 'lefty-1 is required for left-right determination as a regulator of lefty-2 and nodal.', *Cell*. United States, 94(3), pp. 287–297.
- Mesnard, D. *et al.* (2011) 'The microenvironment patterns the pluripotent mouse epiblast through paracrine Furin and Pace4 proteolytic activities', *Genes & development*. Cold Spring Harbor Laboratory Press, 25(17), pp. 1871–1880. doi: 10.1101/gad.16738711.
- Montague, T. G., Gagnon, J. A. and Schier, A. F. (2018) 'Conserved regulation of Nodal-mediated left-right patterning in zebrafish and mouse', *Development*. The Company of Biologists Ltd. doi: 10.1242/dev.171090.
- Montague, T. G. and Schier, A. F. (2017) 'Vg1-Nodal heterodimers are the endogenous inducers of mesendoderm', *eLife*. Edited by E. Robertson. eLife Sciences Publications, Ltd, 6, p. e28183. doi: 10.7554/eLife.28183.
- Monteiro, R. *et al.* (2008) 'Two novel type II receptors mediate BMP signalling and are required to establish left-right asymmetry in zebrafish', *Developmental Biology*, 315(1), pp. 55–71. doi: <https://doi.org/10.1016/j.ydbio.2007.11.038>.
- Montero, J.-A. *et al.* (2005) 'Shield formation at the onset of zebrafish gastrulation', *Development*, 132(6), pp. 1187–1198. doi: 10.1242/dev.01667.
- Murata, K. and Kinoshita, M. (2015) 'Establishment of proprotein convertase, furinA knocked-out lines in medaka, *Oryzias latipes*, and unique form of medaka furin-like proprotein convertase (mfIPC).', *Comparative biochemistry and physiology. Toxicology & pharmacology : CBP*. United States, 178, pp. 169–180. doi: 10.1016/j.cbpc.2015.10.005.
- Niessen, K. and Karsan, A. (2008) 'Notch Signaling in Cardiac Development', *Circulation Research*. American Heart Association, 102(10), pp. 1169–1181. doi: 10.1161/CIRCRESAHA.108.174318.

- Noël, E. S. *et al.* (2013) ‘A Nodal-independent and tissue-intrinsic mechanism controls heart-looping chirality’, *Nature Communications*, 4(1), p. 2754. doi: 10.1038/ncomms3754.
- Passmore, L. A. and Collier, J. (2022) ‘Roles of mRNA poly(A) tails in regulation of eukaryotic gene expression’, *Nature Reviews Molecular Cell Biology*, 23(2), pp. 93–106. doi: 10.1038/s41580-021-00417-y.
- Prabhu, L. *et al.* (2015) ‘Role of post-translational modification of the Y box binding protein 1 in human cancers’, *Genes & Diseases*, 2(3), pp. 240–246. doi: <https://doi.org/10.1016/j.gendis.2015.05.001>.
- Prall, O. W. J. *et al.* (2007) ‘An Nkx2-5/Bmp2/Smad1 negative feedback loop controls heart progenitor specification and proliferation’, *Cell*, 128(5), pp. 947–959. doi: 10.1016/j.cell.2007.01.042.
- Ran, F. A. *et al.* (2013) ‘Genome engineering using the CRISPR-Cas9 system.’, *Nature protocols*, 8(11), pp. 2281–2308. doi: 10.1038/nprot.2013.143.
- Roebroek, A. J. *et al.* (1998) ‘Failure of ventral closure and axial rotation in embryos lacking the proprotein convertase Furin’, *Development*, 125(24), pp. 4863–4876. doi: 10.1242/dev.125.24.4863.
- Romaine, S. P. R. *et al.* (2015) ‘MicroRNAs in cardiovascular disease: an introduction for clinicians’, *Heart*, 101(12), pp. 921 LP – 928. doi: 10.1136/heartjnl-2013-305402.
- Ryan, A. K. *et al.* (1998) ‘Pitx2 determines left-right asymmetry of internal organs in vertebrates.’, *Nature*. England, 394(6693), pp. 545–551. doi: 10.1038/29004.
- Sampath, K. and Robertson, E. J. (2016) ‘Keeping a lid on nodal: transcriptional and translational repression of nodal signalling.’, *Open biology*. England, 6(1), p. 150200. doi: 10.1098/rsob.150200.
- Samsa, L. A. *et al.* (2015) ‘Cardiac contraction activates endocardial Notch signaling to modulate chamber maturation in zebrafish.’, *Development (Cambridge, England)*. England, 142(23), pp. 4080–4091. doi: 10.1242/dev.125724.
- Schier, A. F. (2009) ‘Nodal morphogens.’, *Cold Spring Harbor perspectives in biology*. United States, 1(5), p. a003459. doi: 10.1101/cshperspect.a003459.
- Schier, A. F. and Talbot, W. S. (2005) ‘Molecular Genetics of Axis Formation in Zebrafish’, *Annual Review of Genetics*. Annual Reviews, 39(1), pp. 561–613. doi: 10.1146/annurev.genet.37.110801.143752.
- Schweickert, A. *et al.* (2017) ‘Vertebrate Left-Right Asymmetry: What Can Nodal Cascade Gene Expression Patterns Tell Us?’, *Journal of cardiovascular development and disease*, 5(1). doi: 10.3390/jcdd5010001.
- Shav-Tal, Y. and Singer, R. H. (2005) ‘RNA localization.’, *Journal of cell science*, 118(Pt 18), pp. 4077–4081. doi: 10.1242/jcs.02543.
- Shen, M. M. (2007) ‘Nodal signaling: developmental roles and regulation’,

Development, 134(6), pp. 1023–1034. doi: 10.1242/dev.000166.

Shi, X. *et al.* (2021) ‘Zebrafish hhatla is involved in cardiac hypertrophy.’, *Journal of cellular physiology*. United States, 236(5), pp. 3700–3709. doi: 10.1002/jcp.30106.

Shinohara, K. and Hamada, H. (2017) ‘Cilia in Left-Right Symmetry Breaking’, *Cold Spring Harbor perspectives in biology*. Cold Spring Harbor Laboratory Press, 9(10), p. a028282. doi: 10.1101/cshperspect.a028282.

Shiratori, H. and Hamada, H. (2006) ‘The left-right axis in the mouse: from origin to morphology’, *Development*. The Company of Biologists Ltd, 133(11), pp. 2095–2104. doi: 10.1242/dev.02384.

Singleman, C. and Holtzman, N. G. (2014) ‘Growth and maturation in the zebrafish, *Danio rerio*: a staging tool for teaching and research’, *Zebrafish*. 2014/06/30. Mary Ann Liebert, Inc., 11(4), pp. 396–406. doi: 10.1089/zeb.2014.0976.

Smith, K. A. *et al.* (2011) ‘Bmp and Nodal Independently Regulate lefty1 Expression to Maintain Unilateral Nodal Activity during Left-Right Axis Specification in Zebrafish’, *PLoS Genetics*. Public Library of Science, 7(9), p. e1002289. Available at: <https://doi.org/10.1371/journal.pgen.1002289>.

Sun, J. *et al.* (2018) ‘Maternal Ybx1 safeguards zebrafish oocyte maturation and maternal-to-zygotic transition by repressing global translation.’, *Development (Cambridge, England)*. England, 145(19). doi: 10.1242/dev.166587.

Sun, X. *et al.* (2009) ‘Cardiac Hypertrophy Involves Both Myocyte Hypertrophy and Hyperplasia in Anemic Zebrafish’, *PLoS ONE*. Public Library of Science, 4(8), p. e6596. Available at: <https://doi.org/10.1371/journal.pone.0006596>.

Suresh, P. S., Tsutsumi, R. and Venkatesh, T. (2018) ‘YBX1 at the crossroads of non-coding transcriptome, exosomal, and cytoplasmic granular signaling.’, *European journal of cell biology*. Germany, 97(3), pp. 163–167. doi: 10.1016/j.ejcb.2018.02.003.

Svitkin, Y. V *et al.* (2009) ‘General RNA-binding proteins have a function in poly(A)-binding protein-dependent translation.’, *The EMBO journal*. England, 28(1), pp. 58–68. doi: 10.1038/emboj.2008.259.

Tanaka, C. *et al.* (2007) ‘Long-range action of Nodal requires interaction with GDF1’, *Genes & development*. Cold Spring Harbor Laboratory Press, 21(24), pp. 3272–3282. doi: 10.1101/gad.1623907.

Tessadori, F. *et al.* (2015) ‘Nodal signaling range is regulated by proprotein convertase-mediated maturation.’, *Developmental cell*. United States, 32(5), pp. 631–639. doi: 10.1016/j.devcel.2014.12.014.

Tessadori, F. *et al.* (2018) ‘Effective CRISPR/Cas9-based nucleotide editing in zebrafish to model human genetic cardiovascular disorders.’, *Disease models & mechanisms*. England, 11(10). doi: 10.1242/dmm.035469.

Thielicke, W. and Sonntag, R. (2021) ‘Particle Image Velocimetry for MATLAB:

Accuracy and enhanced algorithms in PIVlab’, *Journal of Open Research Software*, 9(1), p. 12.

Thomas, G. (2002) ‘Furin at the cutting edge: from protein traffic to embryogenesis and disease’, *Nature reviews. Molecular cell biology*, 3(10), pp. 753–766. doi: 10.1038/nrm934.

Thyme, S. B. *et al.* (2016) ‘Internal guide RNA interactions interfere with Cas9-mediated cleavage’, *Nature Communications*, 7(1), p. 11750. doi: 10.1038/ncomms11750.

Tian, T. and Meng, A. M. (2006) ‘Nodal signals pattern vertebrate embryos’, *Cellular and Molecular Life Sciences CMLS*, 63(6), pp. 672–685. doi: 10.1007/s00018-005-5503-7.

Uribe-Salazar, J. M. *et al.* (2022) ‘Evaluation of CRISPR gene-editing tools in zebrafish’, *BMC Genomics*, 23(1), p. 12. doi: 10.1186/s12864-021-08238-1.

van Boxtel, A. L. *et al.* (2015) ‘A Temporal Window for Signal Activation Dictates the Dimensions of a Nodal Signaling Domain’, *Developmental Cell*. Elsevier, 35(2), pp. 175–185. doi: 10.1016/j.devcel.2015.09.014.

Varlet, I. and Robertson, E. J. (1997) ‘Left-right asymmetry in vertebrates.’, *Current opinion in genetics & development*. England, 7(4), pp. 519–523.

Vastenhouw, N. L., Cao, W. X. and Lipshitz, H. D. (2019) ‘The maternal-to-zygotic transition revisited’, *Development*, 146(11), p. dev161471. doi: 10.1242/dev.161471.

Vermot, J. *et al.* (2009) ‘Reversing Blood Flows Act through klf2a to Ensure Normal Valvulogenesis in the Developing Heart’, *PLOS Biology*. Public Library of Science, 7(11), p. e1000246. Available at: <https://doi.org/10.1371/journal.pbio.1000246>.

Vey, M. *et al.* (1994) ‘Maturation of the trans-Golgi network protease furin: compartmentalization of propeptide removal, substrate cleavage, and COOH-terminal truncation.’, *The Journal of cell biology*, 127(6 Pt 2), pp. 1829–1842. doi: 10.1083/jcb.127.6.1829.

Vignes, H. *et al.* (2022) ‘Extracellular mechanical forces drive endocardial cell volume decrease during zebrafish cardiac valve morphogenesis’, *Developmental Cell*, 57(5), pp. 598-609.e5. doi: <https://doi.org/10.1016/j.devcel.2022.02.011>.

Wagner, D. S. *et al.* (2004) ‘Maternal Control of Development at the Midblastula Transition and beyond: Mutants from the Zebrafish II’, *Developmental Cell*, 6(6), pp. 781–790. doi: <https://doi.org/10.1016/j.devcel.2004.04.001>.

Wahlquist, C. *et al.* (2014) ‘Inhibition of miR-25 improves cardiac contractility in the failing heart’, *Nature*, 508(7497), pp. 531–535. doi: 10.1038/nature13073.

Walker, M. B. *et al.* (2006) ‘Zebrafish furin mutants reveal intricacies in regulating Endothelin1 signaling in craniofacial patterning.’, *Developmental biology*. United States, 295(1), pp. 194–205. doi: 10.1016/j.ydbio.2006.03.028.

Wang, Y. *et al.* (2016) ‘Extracellular interactions and ligand degradation shape the

nodal morphogen gradient', *eLife*. Edited by D. Y. R. Stainier. eLife Sciences Publications, Ltd, 5, p. e13879. doi: 10.7554/eLife.13879.

White, R. J. *et al.* (2017) 'A high-resolution mRNA expression time course of embryonic development in zebrafish', *eLife*. Edited by D. Y. R. Stainier. eLife Sciences Publications, Ltd, 6, p. e30860. doi: 10.7554/eLife.30860.

Williams, M. L. K. and Solnica-Krezel, L. (2020) 'Nodal and planar cell polarity signaling cooperate to regulate zebrafish convergence and extension gastrulation movements', *eLife*. Edited by P. Müller and D. Y. R. Stainier. eLife Sciences Publications, Ltd, 9, p. e54445. doi: 10.7554/eLife.54445.

WooJin, K. *et al.* (2012) 'Loss of Endothelial Furin Leads to Cardiac Malformation and Early Postnatal Death', *Molecular and Cellular Biology*. American Society for Microbiology, 32(17), pp. 3382–3391. doi: 10.1128/MCB.06331-11.

Yergert, K. M. *et al.* (2021) 'Identification of 3' UTR motifs required for mRNA localization to myelin sheaths in vivo', *PLOS Biology*. Public Library of Science, 19(1), p. e3001053. Available at: <https://doi.org/10.1371/journal.pbio.3001053>.

Yuan, S. *et al.* (2015) 'Intraciliary Calcium Oscillations Initiate Vertebrate Left-Right Asymmetry', *Current Biology*, 25(5), pp. 556–567. doi: <https://doi.org/10.1016/j.cub.2014.12.051>.

Zaucker, A. *et al.* (2017) 'Translational co-regulation of a ligand and inhibitor by a conserved RNA element', *Nucleic Acids Research*, 46(1), pp. 104–119. doi: 10.1093/nar/gkx938.

Zaucker, A., Kumari, P. and Sampath, K. (2019) 'Zebrafish embryogenesis - A framework to study regulatory RNA elements in development and disease.', *Developmental biology*. United States. doi: 10.1016/j.ydbio.2019.01.008.

Zhou, Q. *et al.* (2021) 'Proprotein convertase furina is required for heart development in zebrafish', *Journal of Cell Science*, 134(21). doi: 10.1242/jcs.258432.